AD-A151 000

TECHNICAL REPORT: NAVTRAEQUIPCEN 83-C-0068

SYNTHETIC APERTURE RADAR SIMULATION STUDY

Robert L. Peters
Link Flight Simulation Division, Singer Co.
1077 E. Arques Avenue
sunnyvale, California 94086

FINAL REPORT March 1984

DoD Distribution Statement

Approved for public release;
distribution unlimited

DTIC
ELECTE
MAR 8 1985

D

DTIC FILE COPY

85 02 26 051

GOVERNMENT RIGHTS IN DATA STATEMENT

Reproduction of this publication in whole
or in part is permitted for any purpose of
the United States Government.

DISCLAIMER NOTICE

**THIS DOCUMENT IS BEST QUALITY
PRACTICABLE. THE COPY FURNISHED
TO DTIC CONTAINED A SIGNIFICANT
NUMBER OF PAGES WHICH DO NOT
REPRODUCE LEGIBLY.**

SECURITY CLASSIFICATION OF THIS PAGE *(When Data Entered)*

REPORT DOCUMENTATION PAGE	READ INSTRUCTIONS BEFORE COMPLETING FORM

1. REPORT NUMBER NAVTRAEQUIPCEN 83-C-0068	2. GOVT ACCESSION NO. AD-A151 000	3. RECIPIENT'S CATALOG NUMBER

4. TITLE *(and Subtitle)* SYNTHETIC APERTURE RADAR SIMULATION STUDY	5. TYPE OF REPORT & PERIOD COVERED Final Report May '83 to March '84
	6. PERFORMING ORG. REPORT NUMBER

7. AUTHOR(s) Robert L. Peters	8. CONTRACT OR GRANT NUMBER(s) N61339-83-C0068

9. PERFORMING ORGANIZATION NAME AND ADDRESS The Singer Company Link Flight Simulation Division 1077 E. Arques Ave., Sunnyvale, Calf. 94088	10. PROGRAM ELEMENT, PROJECT, TASK AREA & WORK UNIT NUMBERS NAVTRAEQUIPCEN Task Number 3735

11. CONTROLLING OFFICE NAME AND ADDRESS Commanding Officer Naval Training Equipment Center Orlando, FL 32813	12. REPORT DATE March 1984
	13. NUMBER OF PAGES 185

14. MONITORING AGENCY NAME & ADDRESS*(If different from Controlling Office)*	15. SECURITY CLASS. *(of this report)* Unclassified
	15a. DECLASSIFICATION/DOWNGRADING SCHEDULE

16. DISTRIBUTION STATEMENT *(of this Report)*

Approved for Public Release;
Distribution Unlimited

17. DISTRIBUTION STATEMENT *(of the abstract entered in Block 20, if different from Report)*

18. SUPPLEMENTARY NOTES

"Original contains color plates: All DTIC reproductions will be in black and white"

19. KEY WORDS *(Continue on reverse side if necessary and identify by block number)*

Synthetic Aperture Radar (SAR) Simulation Study
Radar Simulation
Data Bases
Computer Image Generation Display

Synthetic aperture radar

20. ABSTRACT *(Continue on reverse side if necessary and identify by block number)*

This study develops the theory of the doppler effect and SAR. The similarity between SAR and a lens is made clear. The characteristics of SAR, such as isodoppler mapping, focused array, range walk and rotation are explored in this report. Algorithms for simulation are provided, SAR anomalies, such as moving targets, footprint, doppler elevation mapping, and multilook are discussed. A chapter is devoted to elevation and planimetric data bases. In addition, sixteen pictures of SAR images from Hughes Aircraft, as well as nineteen emulation SAR images are included in this publication.

DD FORM 1473 EDITION OF 1 NOV 65 IS OBSOLETE
1 JAN 73
S/N 0102-LF-014-6601

→ Additional keywords: computer graphics, high resolution radar, →

———> F-18 aircraft, F/A-18 aircraft.

CONTENTS

Accession For

NTIS GRA&I ☒
DTIC TAB ☐
Unannounced ☐
Justification

By
Distribution/
Availability Codes

Dist	Avail and/or Special
A-1	23

DTIC COPY INSPECTED 6

List of Figures

List of Figures (continued)

List of Figures (continued)

List ot Figures (continued)

List ot Tables

1.0 INTRODUCTION

This report prepared by the Link Flight Simulation Division of the Singer Company is in compliance with Contract N61339-83-0068 granted by the United States Navy, Naval Training Equipment Center (NTEC) in Orlando, Florida, to explore the implications of Doppler beam sharpened radar and synthetic aperture radar[1] in training requirements.

During the next decade, virtually all airborne radars will have Doppler beam sharpening/synthetic aperture capabilities. The new radars differ significantly from present real beam radar and perhaps the most striking difference is in the respective resolution capabilities. Rather than the 100 to 300 foot resolution available on real beam radar, synthetic aperture radar resolution capabilities are 10 feet or less. Within the next four years, it is anticipated that three-foot resolution will be attainable.

The impact that accompanies introduction of the new types of radar is not limited to resolution factors only, dramatic as that improvement is. In addition, synthetic aperture radar (SAR) uses principles that differ from current real beam sets and consequently the radar images exhibit different characteristics. In the following report, these differences will be explored, anomalies will be described, and the impact of the differences on simulation will be discussed. We call these image differences anomalies because a real beam radar system and a synthetic aperture radar system would generate images of differing appearance even if both systems had the same resolution.

Apart from the resolution improvement and the anomalies, the new radar systems differ significantly from present ones in implementation methodology. While

---

1. There is no universally accepted distinction between Doppler beam sharpened radar and synthetic aperture radar. In this report the two technologies will be used interchangeably.

current real beam radars make use of some digital processing techniques, the new generation of radars are controlled by very powerful computers with capabilities for executing several million instructions per second. These advanced computers control the digital signal processing devices used for the implementation of synthetic aperture calculations and also control all modes of the radar. The resident program in such a general purpose computer may typically consist of several hundred thousand instructions.

Another important difference between real beam and synthetic aperture radars are the failure modes. Aircrews must be trained to recognize these failure modes and make appropriate adjustments to restore radar system functioning.

The introduction of synthetic aperture radar will have yet another major impact: new air-to-ground tactics will be needed because the resolution of SAR images in the vicinity of the flight vector degenerates to that of real beam radars. Current tactics do not take full advantage of some of the capabilities of SAR because of this "notch" in resolution. There is no doubt that new military tactics will be developed which use this high resolution capability to increase mission effectiveness.

In presenting the current SAR Simulation Study, a beginning short section is devoted to current radar training on the F-18 aircraft, followed by a discussion of SAR theory, radar simulation, and relevant discussions of anomalies and malfunctions. The report includes photographs of actual SAR images to illustrate various effects and characteristics. These images are reproduced by courtesy of Hughes Aircraft and were made on the F-15 radar system manufactured by Hughes Aircraft. The report also contains SAR images made by the Link Emulation Laboratory from an enhanced Defense Mapping Agency (DMA) map of the China Lake area.

As will be explained in this report, radars relying on the Doppler effect have limitations in resolution along, and in the vicinity of, the flight vector. This area, designated as the "notch," is typically a few degrees in width where Doppler images can be generated. For this reason, the straight-in approach toward the target is not optimal because SAR resolution in this area

does not differ from that of a real beam radar. Neither does the straight-in approach make use of one of the unique features of the F/A-18 radar; that is, rotating the display in such a manner that the display area is always correctly oriented with respect to the aircraft heading. Because of these facts, it is expected that tactics developed for the aircraft will be significantly different from those in present use.

Because synthetic aperture radar simulators are likely to be substantially different from present ones, Link recommends that NTEC procure a research synthetic aperture radar simulator. The procurement of such a simulator would allow the U.S. Government to accurately determine and specify requirements of future simulators and also assist in development of new tactics for use of the high resolution radar systems. The research simulator should be highly programmable to allow the government to easily perform experiments in the selection of special effects, modes, and types of radar.

2.0 HIGH RESOLUTION RADAR TRAINING

At present the F/A-18 is the only operational aircraft with high resolution Doppler beam sharpening/synthetic aperture radar capability. To determine the status of radar training on this aircraft, Link personnel visited both LeMoore Naval Air Station and El Toro Marine Corps Air Station in California. LeMoore NAS is the home base of an F/A-18 Replacement Air Group (RAG) and El Toro MCAS is the base for an F/A-18 Marine Corps squadron. In addition, Link has met with personnel from Hughes Aircraft and McDonnell Douglas Corporation and discussed the technical aspects of radar training requirements for this aircraft.

At present the F/A-18 squadrons are in the early stages of combat readiness; their principle missions are defense of the fleet rather than close air support. As a result, training is primarily concentrated on interceptor activities. The existing F/A-18 simulator has radar simulation capabilities but only for air-to-air engagements; no high resolution radar landmass simulation currently exists. To train pilots in the use of F/A-18 ground mapping radar, there is a ground school program followed by two training flights to teach students use of the radar in navigation and weapon delivery. Considering the fact that most students have had no previous experience with SAR radar, this limited amount of training is insufficient for pilots to achieve proficiency in the numerous ground mapping modes and capabilities of the F/A-18 radar.

It appears at the present time that the primary training requirement for pilots is for interception modes, with a secondary goal being ground support under visual conditions, and only a tertiary requirement for pilot training in close air support under limited visibility conditions. Because the F/A-18 aircraft is presently only a single-seat configuration, Navy personnel feel that close air support under limited visibility conditions is feasible only when coordinates of the target are accurately known. Because of the task loading on the pilot, a significant amount of radar interpretation during flight is not feasible and hence the target location must be known ahead of time.

Because of the relatively low priority of the close air support mission, tactics for this task have not yet been fully developed. Squadron VX-5 at China Lake is now tasked to develop these tactics. It is clear, however, that these tactics must differ from those of current aircraft if the full capabilities of the radar are to be used to support the attack mission.

3.0 PRINCIPLES OF DOPPLER BEAM SHARPENING AND SAR

Numerous articles and books have been written expressly on the subject of synthetic aperture radar (SAR) and collectively they cover many facets of this emerging field of radar technology. In a search of this literature, however, no single article would lead a person not in the field through the theoretical aspects of SAR. SAR theory is founded on mathematical concepts and consequently the design of a SAR system requires rigorous analysis and understanding of fundamental mathematics. When highly advanced mathematics are required, a solution is available from accepted and traditional sources. For simulation purposes, comprehension of SAR technology is essential for discriminating selection of important factors and characteristics, and also for recognizing traits that are irrelevant in radar simulation.

In this SAR study, theory development progresses by using basic mathematics and physics laws and supplemental sources, as required. Reference sources are listed and identified in Appendix A. Subjects in the study include Doppler theory, synthetic aperture radar theory, equations, simulation algorithms, and radar simulation algorithms. A list of mathematical signs, definitions, and symbols is included in Appendix B.

3.1 DOPPLER EFFECT

Doppler shift, the change in frequency of a wave reaching an observer or system, is the basic concept for synthetic aperture radar and a logical starting point for the SAR study. Doppler equations are derived from two postulations. The first approach is classically derived and the second is distinguished by use of the Doppler shift in SAR applications. In both derivations, an aircraft will be assumed to be heading directly toward a reflecting surface.

In the classical approach, a vehicle transmitting at a frequency F_T and moving in the direction of transmission will produce F_T cycles in a length $[C-V_{AC}]$ where C is the speed of light and V_{AC} the velocity of the aircraft. The wavelength of this signal will be $[(C-V_{AC})/F_T]$. To an observer on the ground, the received frequency will be $[C/(C-V_{AC})/F_T]$ or

$(C \cdot F_T/(C-V_{AC}))$. This frequency is that of a reflected signal from a vehicle approaching a reflecting surface. Assume that the transmitted signal is ahead of the vehicle. The velocity of the passing signal is $C+V_{AC}$. The number of wavelengths passing per second is $((C+V_{AC})/C)$, hence the received frequency will be $(F_T(C+V_{AC})/C)$. If we summarize the above equations and combine them, the equation for the transmitter moving toward a stationary observer is:

$$F_R = \frac{C \cdot F_T}{C - V_{AC}} \qquad (3.1.1)$$

Where

F_T = transmitted frequency

F_R = received frequency

C = velocity of light

V_{AC} = aircraft velocity

If the transmitter is stationary and the observer is moving toward it, the equation is:

$$F_R = \frac{F_T \cdot (C+V_{AC})}{C} \qquad (3.1.2)$$

The equation for a Doppler frequency if the transmitter is moving and the signal is reflected back to the transmitter is obtained by substituting the received frequency of Equation 3.1.1 for the transmitted frequency in Equation 3.1.2.

$$F_R = F_T \frac{(C+V_{AC})}{(C-V_{AC})} \qquad (3.1.3)$$

The Doppler shift is obtained by subtracting the transmitted frequency from Equation 3.1.3:

$$F_{DS} = 2 \cdot V_{AC} \cdot F_T/(C-V_{AC}) \qquad (3.1.4)$$

Where

F_{DS} = Doppler frequency

Note Equations 3.1.1 and 3.1.2 give a slightly different frequency shift.

The SAR approach does not differentiate between the outward path and the return path of the signal. Consider the signal of the transmitter to be represented by the signal:

$$S_T = exp\left[j \cdot 2 \cdot \pi \cdot F_T \cdot t\right]$$ (3.1.5)

Where

exp = exponential to the base e

j   = square root of -1

π = 3.14159

t   = time

S_T = transmitted signal

The range from the transmitter to the reflector can be given by:

$$R = R_{t1} + R_R \cdot t$$ (3.1.6)

Where

R   = range

R_{t1} = range at time t1

R_R = range rate

The elapsed time for the signal to reach the reflector and return is:

$$t_D = 2 \cdot R / C = 2 \cdot \frac{(R_{t1} + R_R \cdot t)}{C}$$ (3.1.7)

Where

t_D = delta time

In Equation 3.1.5 substitute $t+t_D$ for t to give:

$$S_R = exp\left[j \cdot 2 \cdot \pi \cdot F_T \cdot t + \frac{j \cdot 4 \cdot \pi \cdot F_T \cdot R_R \cdot t}{C} + \frac{j \cdot 4 \cdot \pi \cdot F_T \cdot R_{t1}}{C}\right]$$ (3.1.8)

Where

S_R = received signal

The term $j \cdot 4 \cdot \pi \cdot F_T \cdot R_{t1}/C$ is a constant phase shift and can be dropped out to give:

$$S_T = exp\left[j \cdot t \cdot \left(2 \cdot \pi \cdot F_T + \frac{4 \cdot \pi \cdot F_T \cdot R_R)}{C}\right)\right]$$ (3.1.9)

Equation 3.1.9 can be divided into two parts by using Equation 3.1.10:

$$exp(jx) = cos(x) + j \cdot sin(x)$$ (3.1.10)

Where

cos = cosine

sin = sine

X = variable

$$S_R = \cos\left[2\cdot\pi\cdot F_T\cdot t + \frac{4\cdot\pi\cdot F_T\cdot R_R\cdot t}{C}\right] + j\cdot\sin\left[2\cdot\pi\cdot F_T\cdot t + \frac{4\cdot\pi\cdot F_T\cdot R_R\cdot t}{C}\right] \qquad (3.1.11)$$

Subtracting the transmitted signal from Equation 3.1.11 and substituting the velocity of light divided by wavelength for transmitted frequency gives:

$$S_R = \cos\left[\frac{4\cdot\pi\cdot R_R\cdot t}{\lambda}\right] + j\cdot\sin\left[\frac{4\cdot\pi\cdot R_R\cdot t}{\lambda}\right] \qquad (3.1.12)$$

Where

λ = wavelength of the signal

The received signal is in units of radius per second and range rate (R_R) is the aircraft velocity. The signal can be expressed in cycles per second by removing $2\cdot\pi$. This simplification is given:

$$S_{RF} = \cos\left[\frac{2 V_{AC}\cdot t}{\lambda}\right] + j\cdot\sin\left[\frac{2 V_{AC}\cdot t}{\lambda}\right] \qquad (3.1.13)$$

Where

S_{RF} = received signal in frequency

When the in phase and quadrature phase are sampled at twice the frequency of the received signal frequency or higher, the complete description of the reflected signal is known. The amplitude of the reflected signal is given:

$$S_{AMT} = \sqrt{S_{IP}^2 + S_Q^2} \qquad (3.1.14)$$

Where

S_{AMT} = received signal amplitude
S_{IP} = in phase component of the received signal
S_Q = quadrature component of the received signal

The phase shift of the reflected signal is given:

$$P = \tan\left(\frac{S_Q}{S_{IP}}\right)$$

(3.1.15)

Where

tan = tangent

In operational SAR, the reflected signal is converted to digital signals by sampling the reflected signal. This sampling is normally performed at a rate that is higher than the Nyquist sampling rate. The number of levels in the analog-to-digital converter determines the dynamic range of the received signal. When the digital-to-analog converter saturates, information is lost and ghost signals can be generated. Dynamic range and saturation factors are discussed in other sections of this study.

In our reviews, it has been shown that by sampling the in phase and quadrature phase of a reflected signal at a sampling rate of at least twice the reflected signal frequency, all characteristics of an image point can be recorded. Recording of the reflected signal to allow signal processing to be performed in non-real time is the basis of modern synthetic aperture radar.

3.2 SAR THEORY

The theory of Doppler shift has been briefly introduced. The theory of synthetic aperture radar is developed using the Doppler equation. Rather than straight ahead, the reflector will be 90 degrees from the velocity vector. Results when the target is not 90 degrees from the velocity vector will be developed in later text. Figure 3.2-1 is a diagram used to develop SAR formulations.

The line D_{PPT} (distance from point PT) is perpendicular to the velocity vector and connects the velocity vector to point $P_T(X_{(n)}, Y_{(m)})$. This line is the reference line of the SAR equation. The signal that is received after being reflected from the ground is given by:
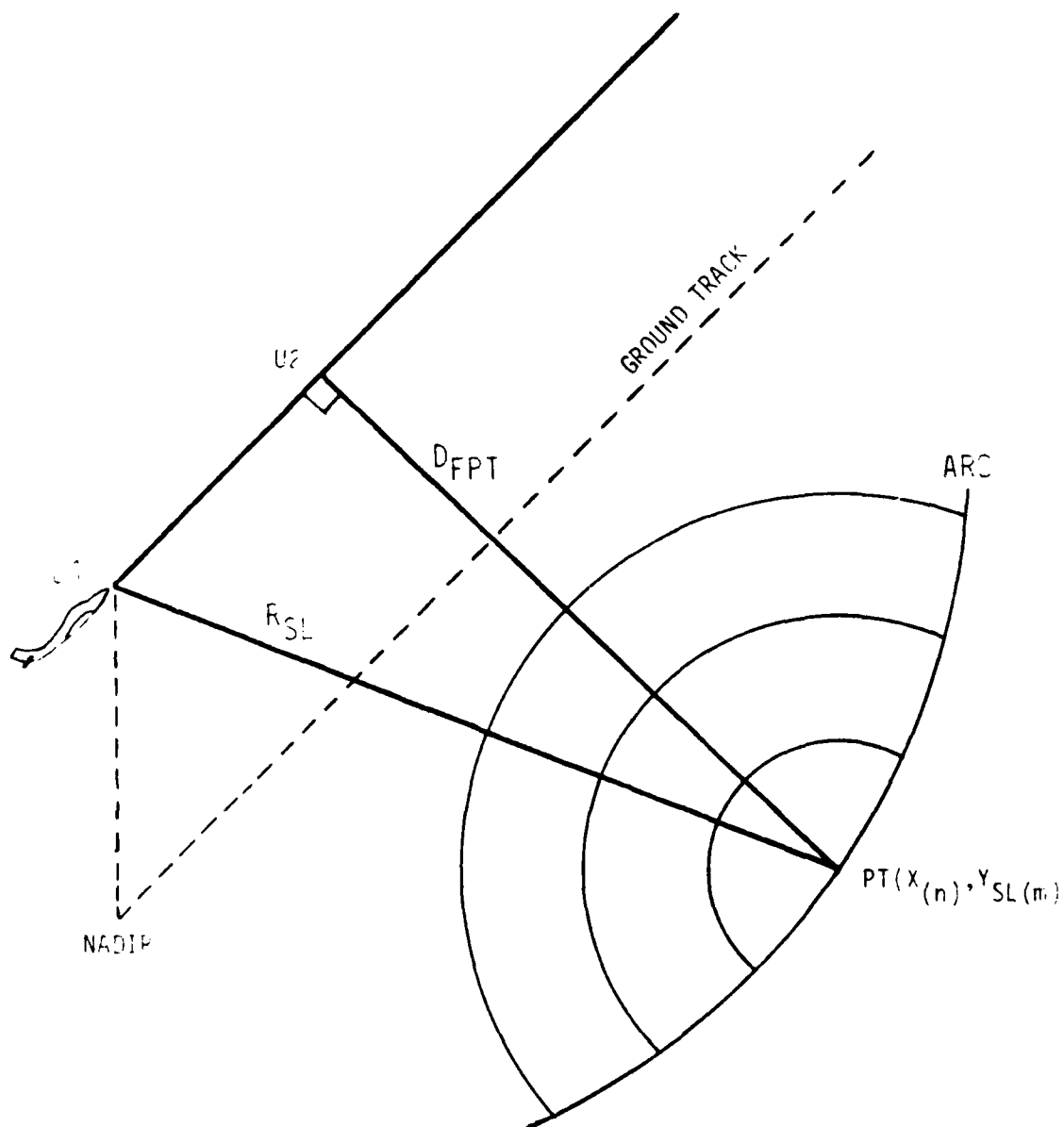
Figure 3.2-1 SAR EQUATION DIAGRAM

$$S_R = S_T \cdot T_{REF}\left(x_{(n)}, R_{SL(m)}\right) \cdot exp\left[j \cdot 2 \cdot \pi \cdot F \cdot \left(t - \frac{2R_{SL}}{C}\right)\right] \qquad (3.2.1)$$

Where

T_{REF} = target reflectance coefficient

$X_{(n)}$ = azimuth coordinate

$R_{SL(m)}$ = range coordinate

F = frequency

R_{SL} = slant range

The slant range (R_{SL}) can be derived from the distance (D_{FPT}) and the distance $(Y-Y_{(m)})$:

$$R_{SL} = \sqrt{\left(D_{FPT}\right)^2 + \left(Y - Y_{(m)}\right)^2} \qquad (3.2.2)$$

Where

D_{FPT} = distance from point PT

Y = reference along the flight path

$Y_{(m)}$ = point along the flight path

Since the term $(Y-Y_{(m)})$ is much less than D_{FPT}, the binomial expansion can be used to get a simpler expression:

$$R_{SL} = D_{FPT} + \frac{[Y - Y_{(m)}]^2}{2 \cdot D_{FPT}} \qquad (3.2.3)$$

Equation 3.2.4 is obtained by substituting Equation 3.2.3 into Equation 3.2.1:

$$S_{R(n,m)} = S_T \cdot T_{REF}\left[x_{(n)}, R_{SL(m)}\right] \cdot exp\left\{j \cdot 2 \cdot \pi \cdot F(t - 2 \cdot D_{FPT}/C - [Y - Y_{(m)}]^2/C \cdot D_{FPT})\right\} \qquad (3.2.4)$$

Collecting the terms in Equation 3.2.4 gives:

$$S_{R(n,m)} = S_T \cdot T_{REF} \left[\left(z_{(n)}, R_{SL(m)} \right) \right] \cdot exp \left[j \cdot 2 \cdot \pi \cdot F \cdot t - 4 \cdot \pi \cdot D_{FPT} \, F/C - 2 \cdot \pi \cdot F \cdot \left(Y - Y_{(m)} \right)^2 /C \cdot D_{FPT} \right] \qquad (3.2.5)$$

Substituting the velocity of light divided by wavelength for frequency and separating the exponent gives:

$$S_{R(n,m)} = S_T \cdot T_{REF} \left(X_{(n)}, R_{SL(m)} \right) \cdot exp \left[j \cdot 2 \cdot \pi \cdot F \cdot t \right] \cdot \qquad (3.2.6)$$
$$exp \left[-j \cdot 4 \cdot \pi \cdot D_{FPT}/\lambda \right] \cdot exp \left[-j \cdot \left(2 \cdot \pi \cdot \left(Y - Y_{(m)} \right)^2 /\lambda \cdot D_{FPT} \right) \right]$$

The first exponent is the transmitted signal and contains no information. The second exponent is a constant phase shift and contains no information. By demodulating the signal, the first and second exponent can be removed:

$$S_{R(n,m)} = S_T \cdot T_{REF} \left[X_{(n)}, R_{SL(m)} \right] \cdot exp \left[-j \cdot 2 \cdot \pi \cdot \left(Y - Y_{(m)} \right)^2 /\lambda \cdot D_{FPT} \right] \qquad (3.2.7)$$

If the factor 2 is removed, Equation 3.2.7 would be the equation of a positive cylindrical lens centered at $Y_{(m)}$. Because the SAR antenna transmits and receives the signal, there is a two-way path for phase shift occurrence; whereas, a lens has an external source of illumination and there is only a one-way path for phase shift occurrence. Equation 3.2.7 can be simplified to in phase and quadrature components.

This simplification would be a SAR function. For this treatise, the equation as given is more meaningful.

In Equation 3.2.7 each signal $(S_{R(n)})$ is composed of the sum of all the reflected energy from the points on the arc. When the sample of the arc from points U1 to U2 is made, the reflectance of the arc becomes known. Information is in a coded format, and to be useful it must be decoded. In optics, this coded information is referred to as a holograph. The first SAR processors made use of holographic principles to decode SAR images. To obtain SAR images, azimuth and slant range must be scanned.

To store SAR image information, two memories are required. One memory is used to record the in-phase (cos) signals and the other memory is used for recording the quadrature signal (j·sin). The memories can be considered to be two-dimensional. Loading takes place along the slant range, a single scanline at a time. When data is decoded, access is at a constant slant range. This type of memory is often called a corner memory. This theoretical account has identified none of the second order effects which later will be defined individually. The report now equates synthetic aperture radar with the nature and properties of optics.

A valid reason for analyzing SAR and its relationship to optics is that a lens is a commonly known device familiar to most everyone. Figure 3.2-2 is a diagram of a 1:1 cylindrical lens. The cylindrical lens collects rays from point 0 from the object and redirects them to form point P at the image plane. In the center of the lens, rays from a number of points in the object plane meet at a single point in plane L of the lens. This happens along all points in plane L. A SAR system duplicates the refraction of the cylindrical lens from the object to plane L. SAR stores information as it appears at plane L and processes it later; a lens system performs real-time processing.

Some of the first SAR processors used an optical system for processing SAR images; this type of processing is still continued. A good discussion of processing SAR data by optical methods can be found in "Introduction to Fourier Optics" by J.W. Goodman (page 184). Modern SAR systems in aircraft process by high speed signal processing. Some of the problems evident in SAR can be observed by using a lens. By blocking a part of the lens, the image dims and is less sharp, causing lens aberrations. In SAR, acceleration errors do the same thing to a SAR image. When a prism is put between the object and the lens, the image is shifted. In SAR a velocity error will cause the SAR
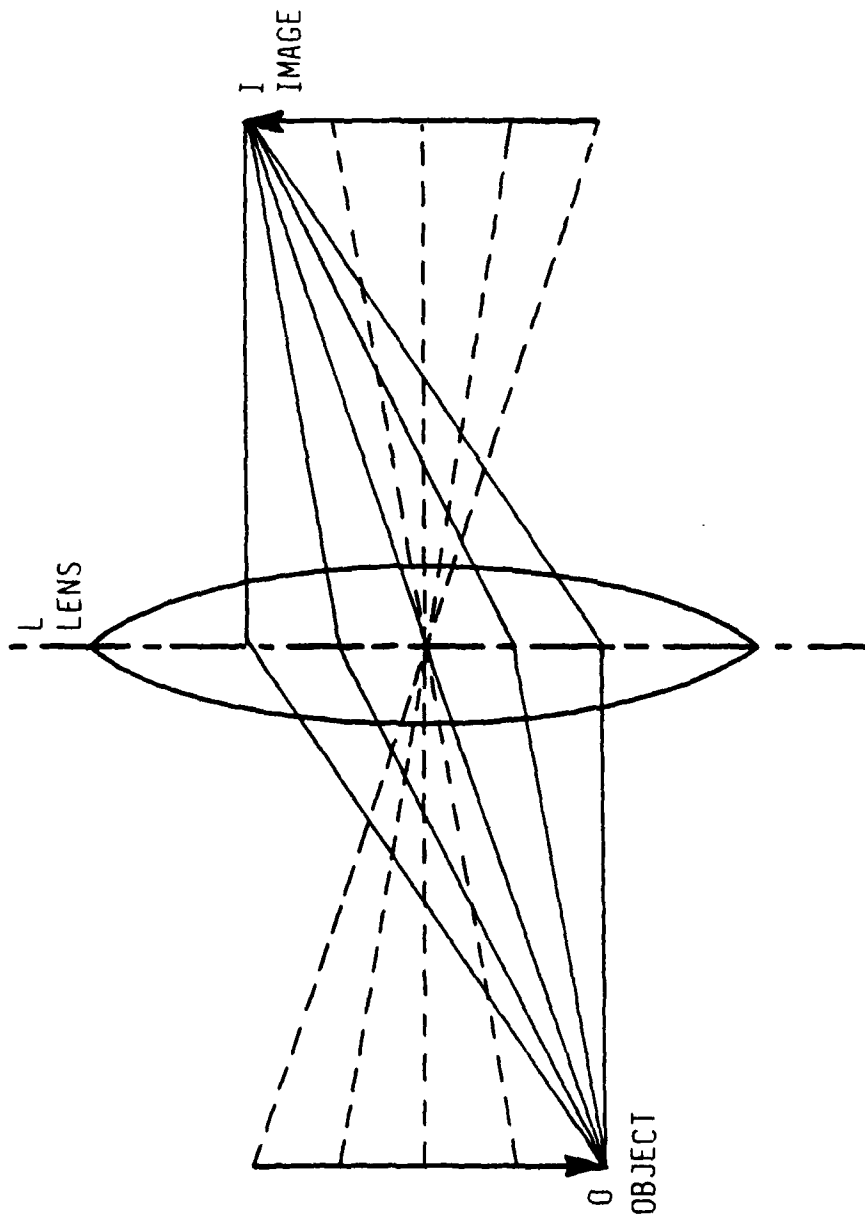
Figure 3.2-2 ONE-TO-ONE OPTICS DIAGRAM (CYLINDRICAL LENS)

image to shift in the same way as the prism in the optical system. From this explanation, it can be seen that there is nothing mysterious about SAR.

The next step in understanding synthetic aperture radar is more complex. The book "Introduction to Statistical Optics," by Edward L. O'Neill has a chapter on Diffraction Theory of Image Formation (page 70). In this chapter, four equations are developed for a cylindrical lens and the example of a cylindrical lens can be related to the equations of SAR for better understanding. The first equation is the complex amplitude distribution in the exit pupil. The information from this equation reflects what is stored in SAR memory. This equation is:

$$F(\beta) = \left|F(\beta)\right|e^{-ik\Delta(\beta)}, \qquad \beta \subset \Sigma \quad \textit{(inside the aperature)} \tag{3.2.8}$$

$$= 0, \qquad \beta \not\subset \Sigma \quad \textit{(outside the aperature)}$$

$$\beta = \frac{ku}{R} \qquad k = \frac{2\pi}{\lambda}$$

Where

k   = wave number

Δ   = lens aberration

F(ß)   = aperture function

i   = square root of -1   (physics usage)

K   = selectable constant

The second equation is the complex amplitude distribution in the point (line) image:

$$u_{(s)} = A\int_{-\infty}^{\infty} F(\beta)e^{-i\beta z}\,d\beta \tag{3.2.9}$$

Where

u   = dimension in the aperture

A   = amplitude

u$_{(X)}$ = complex amplitude distribution of the point image

Equation 3.2.9 describes the distribution of light from a point source after going through a lens. If the lens were perfect, a point would remain a point. This equation is very important and it will be used to derive the SAR resolution equation.

The third equation is the intensity spread function:

$$S_{(x)} = \left| u(x) \right|^2 \tag{3.2.10}$$

Where

$S(x)$ = intensity spread function

Equation 3.2.10 is a description of the energy distribution of a point source after going through a lens.

The fourth equation is the normalized transfer function. These equations are 3.2.11 and 3.2.12:

$$\tau(\omega_x) = \frac{\int\limits_{-\infty}^{\infty} s(x) e^{i\omega x'} \, dx}{\int\limits_{-\infty}^{\infty} s(x) \, dx} \tag{3.2.11}$$

Where

$\tau_{(\omega x)}$ = normalized transfer function

$$\tau(\omega_x) = \frac{\int\limits_{-\infty}^{\infty} F(\beta) F^*(\beta - \omega_x) \, d\beta}{\int\limits_{-\infty}^{\infty} |F(\beta)|^2 d\beta} \tag{3.2.12}$$

Where

β = $K \cdot \mu / R$

ω = $2 \cdot \pi$ times frequency

R = distance from aperture to image plane

The derivation of the characteristics of a cylindrical lens can be found on page 79 of "Introduction to Statistical Optics." The response distribution of a point is given:

$$u(x) = 2A\beta_0 \frac{\sin(\beta_0 x)}{\beta_0 x} \tag{3.2.13}$$

$$\beta_0 = \frac{ka}{R} \qquad k = \frac{2\pi}{\lambda}$$

Where

$u_{(X)}$ = response distribution of a point

a = one-half of the aperture width

A = amplitude

The normalized spread function is:

$$s(x) = \left[\frac{\sin(\beta_0 x)}{\beta_0 x}\right]^2 \tag{3.2.14}$$

The transfer function is given:

$$\tau(\omega_x) = \left[1 - \frac{\omega_x}{2\beta_0}\right] \qquad |\omega_x| \leq 2\beta_0 \tag{3.2.15}$$

$$= 0 \qquad\qquad |\omega_x| > 2\beta_0$$

Figure 3.2-3 is a plot of these functions. The equations of the lens can now be used to derive the equations of SAR.

The resolution will be derived from Equations 3.2.13 and 3.2.15. By inspection it can be seen that Equation 3.2.13 is zero at π, 2π ...$n\pi$.

$$X = \frac{\pi}{\beta_0} = \frac{\pi}{2\cdot\pi\cdot a/R\cdot\lambda} \tag{3.2.16}$$

$$X = \frac{R\lambda}{2a} = \frac{R\cdot\lambda}{A_L} \tag{3.2.17}$$
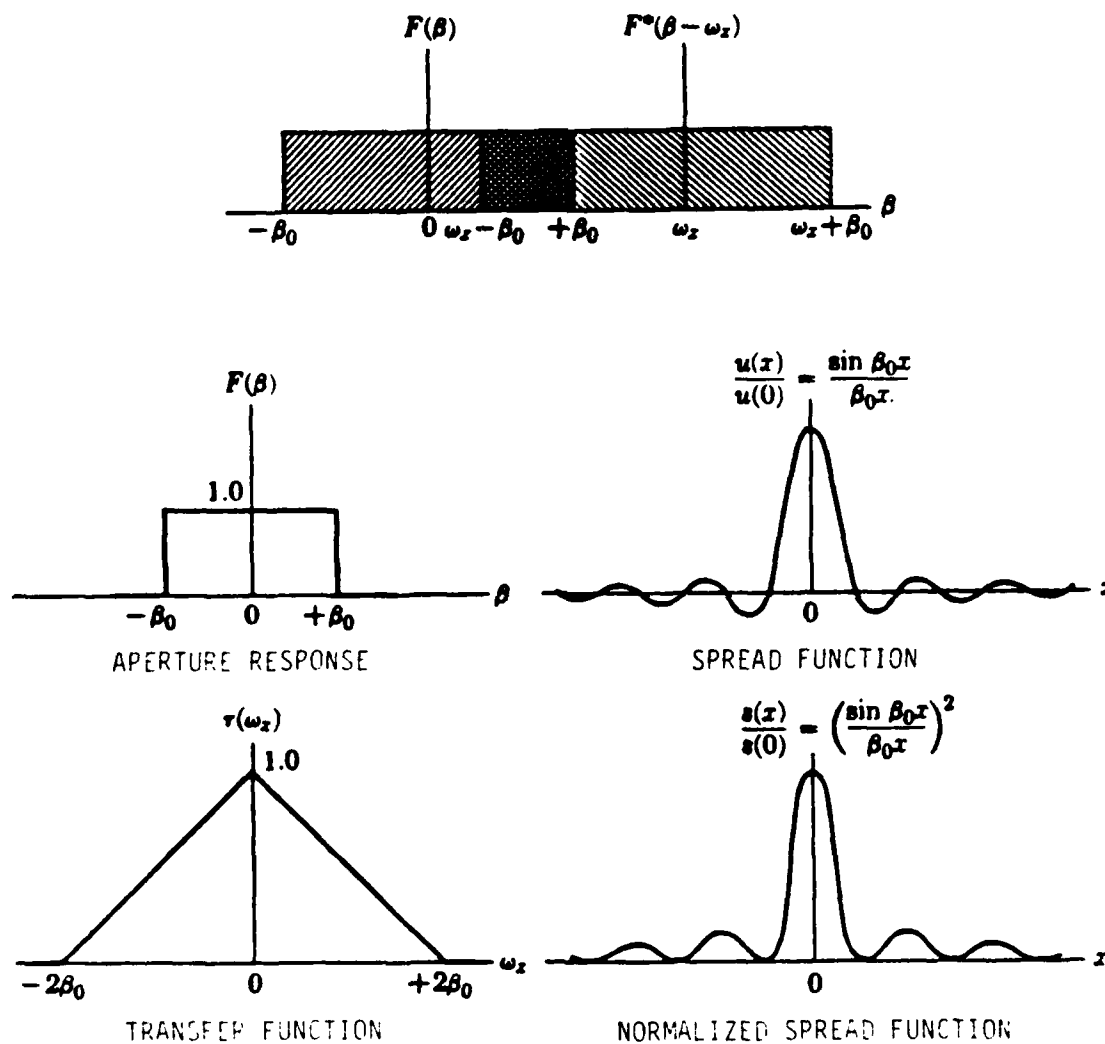
Figure 3.2-3   SUMMARY OF ONE-DIMENSIONAL PROBLEM

Where

A_L = aperture

An interpretation of Equation 3.2.17 shows that a point's main intensity area is spread over a distance of $2R\lambda/A$. In Equation 3.2.15 let $\tau(\omega_x)$ be zero and solve for ω_x.

$$\omega_z = \frac{2\cdot\pi\cdot A_L}{R\cdot\lambda}$$
(3.2.18)

The wavelength in the transfer function that has zero amplitude in Equation 3.2.18 is indicated in Equation 3.2.19, the resolution for a lens. It has already been mentioned that range would be divided by two (the two-way path). Hence the resolution for SAR can be written as:

$$RES = \frac{R\cdot\lambda}{A_L}$$
(for a lens)   (3.2.19)

$$RES = \frac{R\cdot\lambda}{2\cdot A_L}$$
(for SAR)   (3.2.20)

Where

RES = resolution in length

This resolution occurs when the modulation transfer function has zero modulation. Two pixels are required for each cycle by the Nyquist criteria.

Equation 3.2.20 is the resolution equation of a SAR that is looking at the ground 90 degrees from the velocity vector and "A" is the data collection distance along the flight path. Figure 3.2-4 is a diagram indicating what happens when data for SAR processing is not collected at 90 degrees from the velocity vector. "A" is the data collection distance but the effective data collection distance along the velocity vector is $A\cdot\sin(\phi)$. SAR processing is most efficient at 90 degrees and is zero straight ahead.
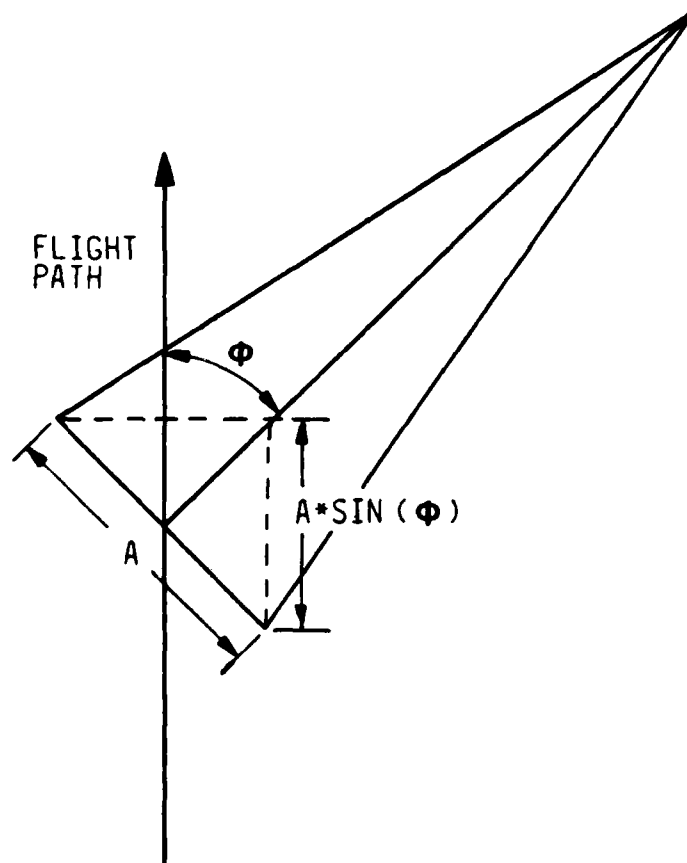
Figure 3.2-4   APERTURE VS SQUINT ANGLE DIAGRAM

Equation 3.2.20 can now be written as:

$$RES = \frac{R_{SL} \cdot \lambda}{2 \cdot D_C \cdot \sin(\phi)}$$

(3.2.21)

Where

D_C = distance along the flight path where data is collected

ϕ = squint angle

Equation 3.2.20 can be derived in other ways. Another way is to differentiate the Doppler frequency with respect to the squint angle:

$$F_R = F_T \cdot \cos(\phi)$$

(3.2.22)

$$\frac{dF_R}{d\phi} = F_T \cdot \sin(\phi)$$

(3.2.23)

Equation 3.2.23 shows that SAR processing is most efficient at 90 degrees from the velocity vector and the resolution is a function of the sine of the squint angle.

Information and equations for SAR simulation requirements are now stated. Equation 3.2.9 shows that the designer of a SAR system has a powerful tool with which to control the side lobes of the radar. Note that response of a point is a function of the aperture ($F(\beta)$). When the samples are multiplied by a weighting function, the response of a point can be modified. Figure 3.2-5 is a plot of uniform aperture and a weighted aperture. By accepting a wider main lobe, the side lobes can be decreased.

There are many functions that can be used to modify the aperture. One such function is the cosine raised to the k power. Figure 3.2-6 is a plot of the point response as a function of k in which the function is $\cos \cdot^k$. Modifying the aperture with the function $\cos^k$ attenuates the higher frequencies of the normalized transfer function.
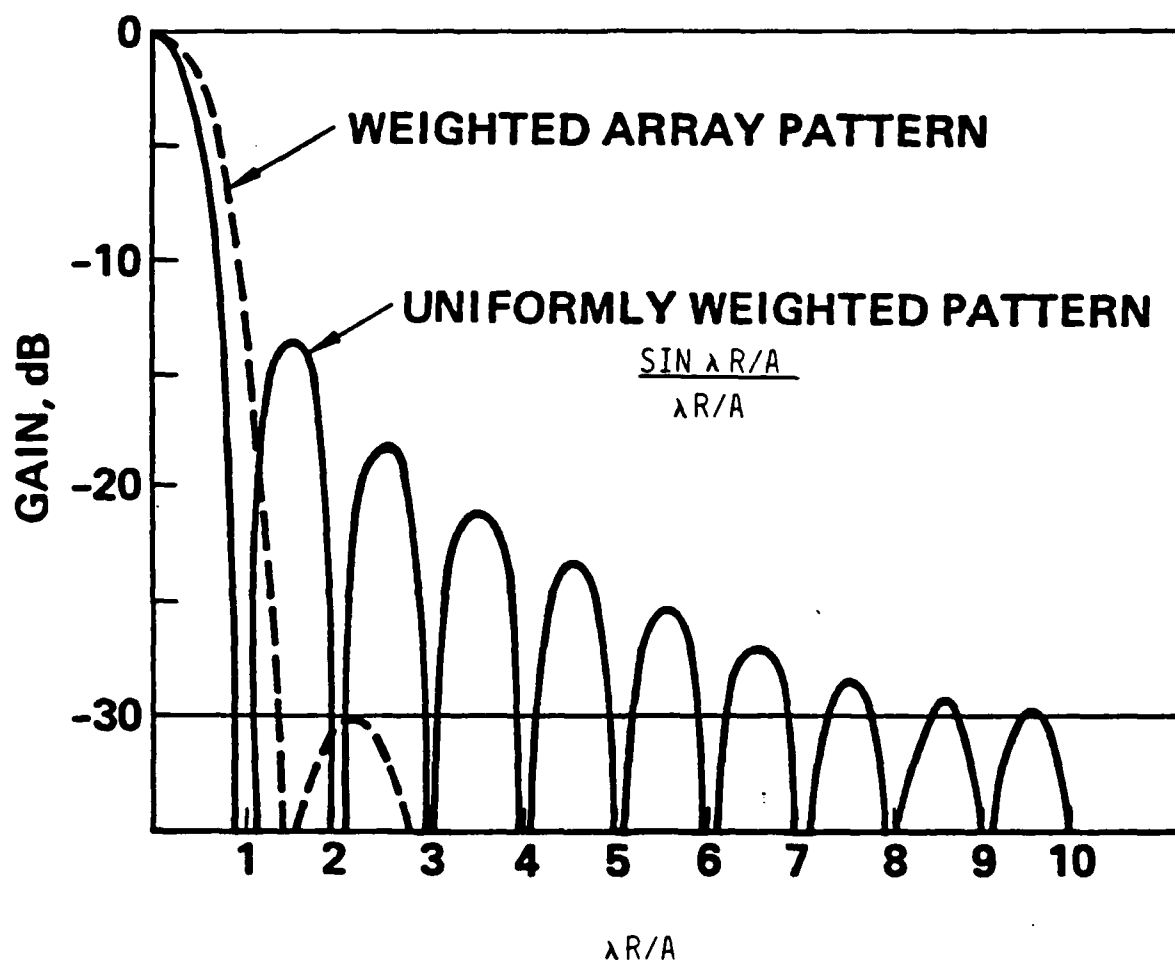
Figure 3.2-5   RESPONSE OF A POINT IMAGE
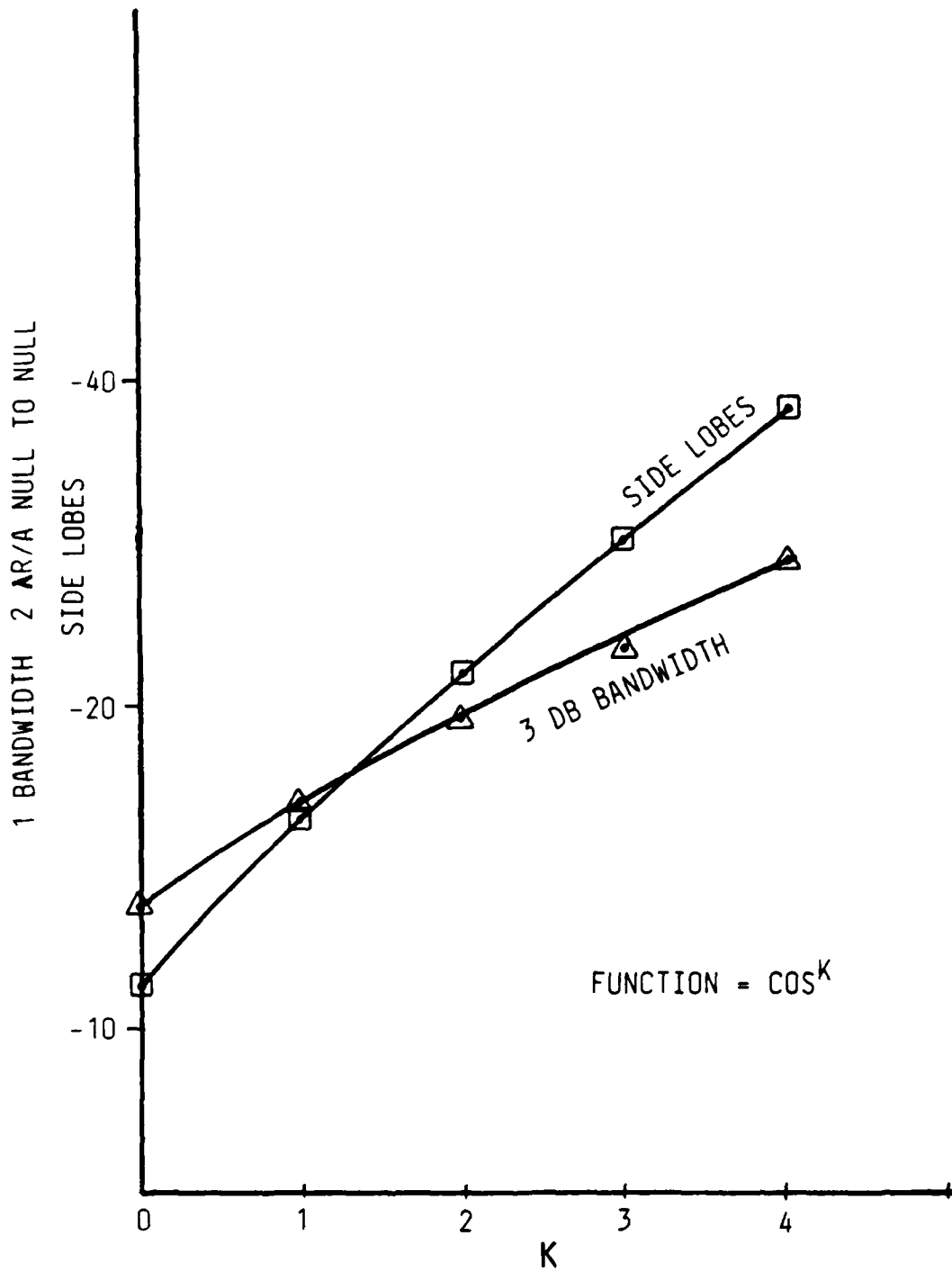
Figure 3.2-6   ANTENNA PARAMETERS AS A FUNCTION OF $(\cos)^K$

Since the aperture function is being modified to control the side lobes, there should be a better method of specifying resolution. One way to do this is to take into account the 3 dB bandwidth. Equation 3.2.21 can be rewritten to accomplish this, as indicated in:

$$RES = \frac{R_{SL} \cdot \lambda \cdot K_F}{2 \cdot D_C \cdot \sin(\phi)}$$

(3.2.24)

Where

K_F = aperture modification factor

When the aperture function is $\cos^4$, then k_F would be 1.94. This value is twice as much as the limit of the normalized transfer function. Table 3.2-1 is a comparison of real aperture radar, SAR, and a lens function.

3.3 ISODOPPLER MAPPING

Theoretically, SAR was developed by considering only one arc. This is correct for SAR processing for each arc contains all data necessary to recover the azimuth information. Unfortunately, arcs are not linear with range. Figure 3.3-1 is an exaggerated example of isodoppler nonlinear mapping. This figure shows a 20 degree sector scan that is centered at an azimuth of 30 degrees. At mid-range the isodoppler filters were set to match the sector scan. The shaded area is mapped with constant isodoppler filters. This phenomenon distinguishes synthetic aperture radar from real aperture radar.

To understand isodoppler mapping, an error equation is derived and examples are given. Let $K_R = \cos(\theta_R) \cdot \cos(\Psi_R)$ where θ_R and Ψ_R are reference angles and the isodoppler filters match the width of the sector scan. The equation for azimuth error mapping is:

$$\Theta_{DE} = \Theta_R - \cos^{-1}\left[\frac{k \cdot R}{\cos(\psi)}\right]$$

(3.3.1)

Table 3.2-1   GROUND MAPPING TABLE

CHARACTERISTIC	LENS	RAR	SAR
ILLUMINATION	EXTERNAL	SELF	SELF
SIDE LOBE CONTROL	NONE	ANTENNA DESIGN	SIGNAL PROCESSING
RESOLUTION	L/RA	NO EXACT EQUATION	$2*A*SIN(SQA)/RA *KF$
PHASE SHIFT	$EXP[-J2\pi (d\gamma)/A]$	NOT APPLICABLE	$EXP[-J2\pi (2d\gamma)/A]$
PROCESSING TIME	REAL TIME	SCANLINE BY SCANLINE	NON REAL TIME (SECONDS)
OVERLOAD CHARACTERISTICS	NONE	BAD	VERY BAD
PICTURE QUALITY	VERY GOOD	POOR	GOOD
MAPPING	PROJECTION CENTERED AT POINT OF INTEREST	AZIMUTH SLANT RANGE	ISODOPPLER LINES SLANT RANGE
FOCUS		AT INFINITY	CAN BE FOCUSED AT EACH RANGE CELL
DISADVANTAGES	EXTERNAL ILLUMINATION WILL NOT PENETRATE CLOUD DEPTH OF FIELD	POOR RESOLUTION ANTENNA MUST SCAN	LARGE AMOUNT OF SIGNAL PROCESSING
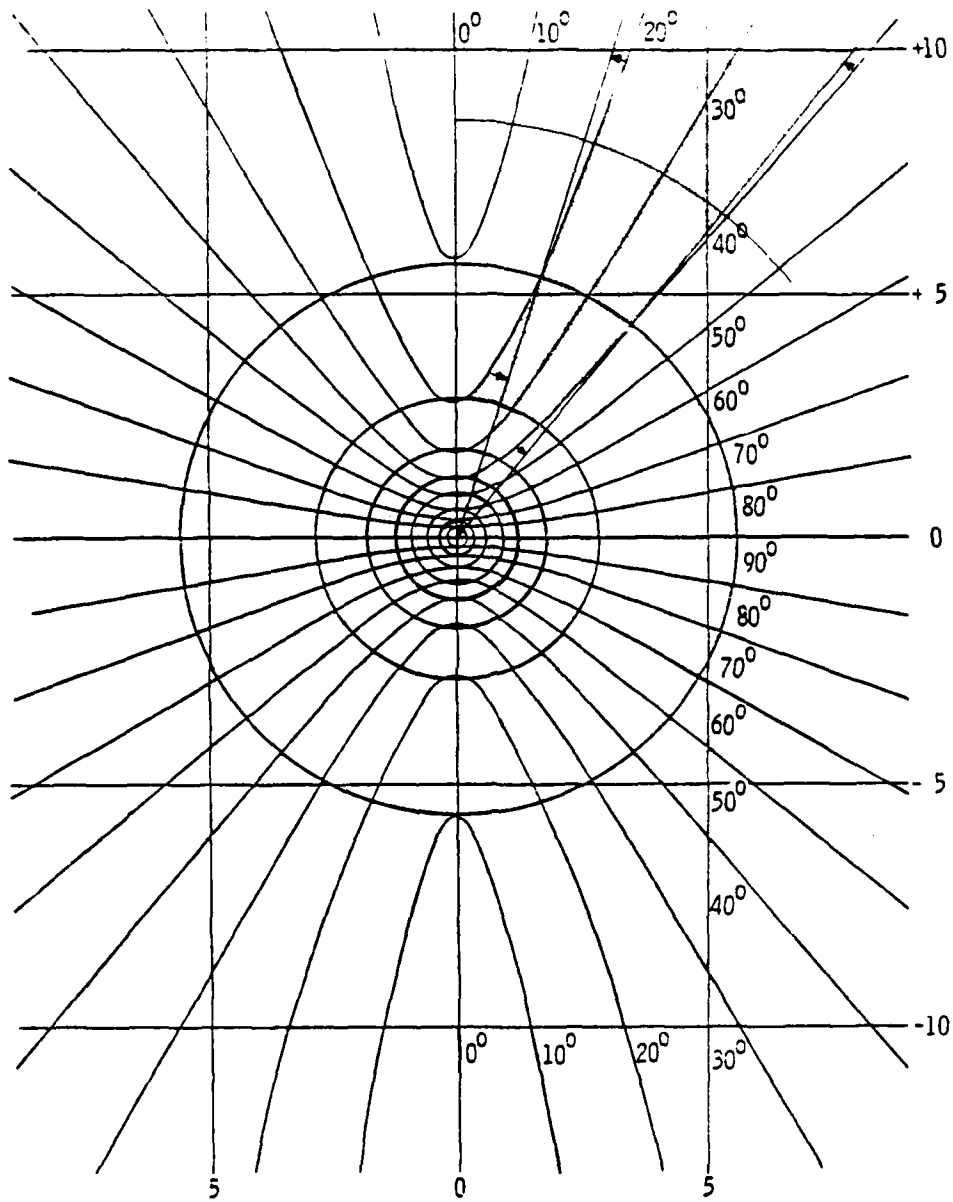
Figure 3.3-1   NORMALIZED ISODOPPLER AND ISORANGE

Where

θ_R = azimuth reference angle

$k_R = \cos(\theta_R) \cdot \cos(\Psi_R)$

Ψ_R = depression angle reference

Ψ = depression angle

θ_{DE} = azimuth Doppler error

Differentiating Equation 3.3.1 with respect to depression angle gives equation 3.3.2:

$$\frac{d\Theta_{DE}}{d\psi} = \frac{k_R \cdot \sin(\psi)}{\cos(\psi)} \cdot \sqrt{\cos^2(\psi) - k_R^2} \qquad (3.3.2)$$

Equation 3.3.2 can then be simplified:

$$\frac{d\Theta_{DE}}{d\psi} \approx \frac{\tan(\psi_R)}{\tan(\Theta_R)} \qquad (3.3.3)$$

Figure 3.3-1 confirms what Equation 3.3.3 implies. General mapping errors occur at large depression angles and near the velocity vector. Examples are given:

Example One: Isodoppler Mapping
Center of scan is 30 degrees
Depression angle reference is 3 degrees
Depression angle offset is 1 degree and 3 degrees

1 degree offset causes -0.120688 degree error in azimuth

3 degree offset causes +0.243451 degree error in azimuth

Example Two: Isodoppler Mapping

Center of scan is 30 degrees

Depression angle reference is 10 degrees

Depression angle offset is 5 degrees and 15 degrees

5 degree offset causes -1.115607 degrees error in azimuth

15 degree offset causes +2.000800 degrees error in azimuth

In the design of a SAR simulator, it is necessary to make a determination of isodoppler frequency in the aircraft SAR system. In radar simulators, for either synthetic or real aperture systems, aspect, shadow, and slant range processing must be performed along scanlines. This is an important consideration when designing for isodoppler mapping. The fact that isodoppler mapping is nonlinear with range requires interrogation of more scanlines in synthetic aperture radar than in real aperture radar because some of the data generated in SAR will not be used. Figure 3.3-2 is an example of SAR simulation overscan. The shaded area represents data that will not be used in the display.

The method of data display is determined by the aircraft SAR system. When the aircraft correctly maps data, simulator data is already correctly mapped. There is a problem in correctly determining what data is in the shaded area and assuring that this data is not displayed. If the aircraft does not correct for isodoppler mapping, the simulated isodoppler mapping becomes more complex[1]. The nonlinear isodoppler scan must now be mapped into the linear sector scan. Figure 3.3-3 is a diagram of this mapping.

1. F/A-18 radar isodoppler mapping errors are corrected when data is written on the display. This means that the display is a distorted sector scan.
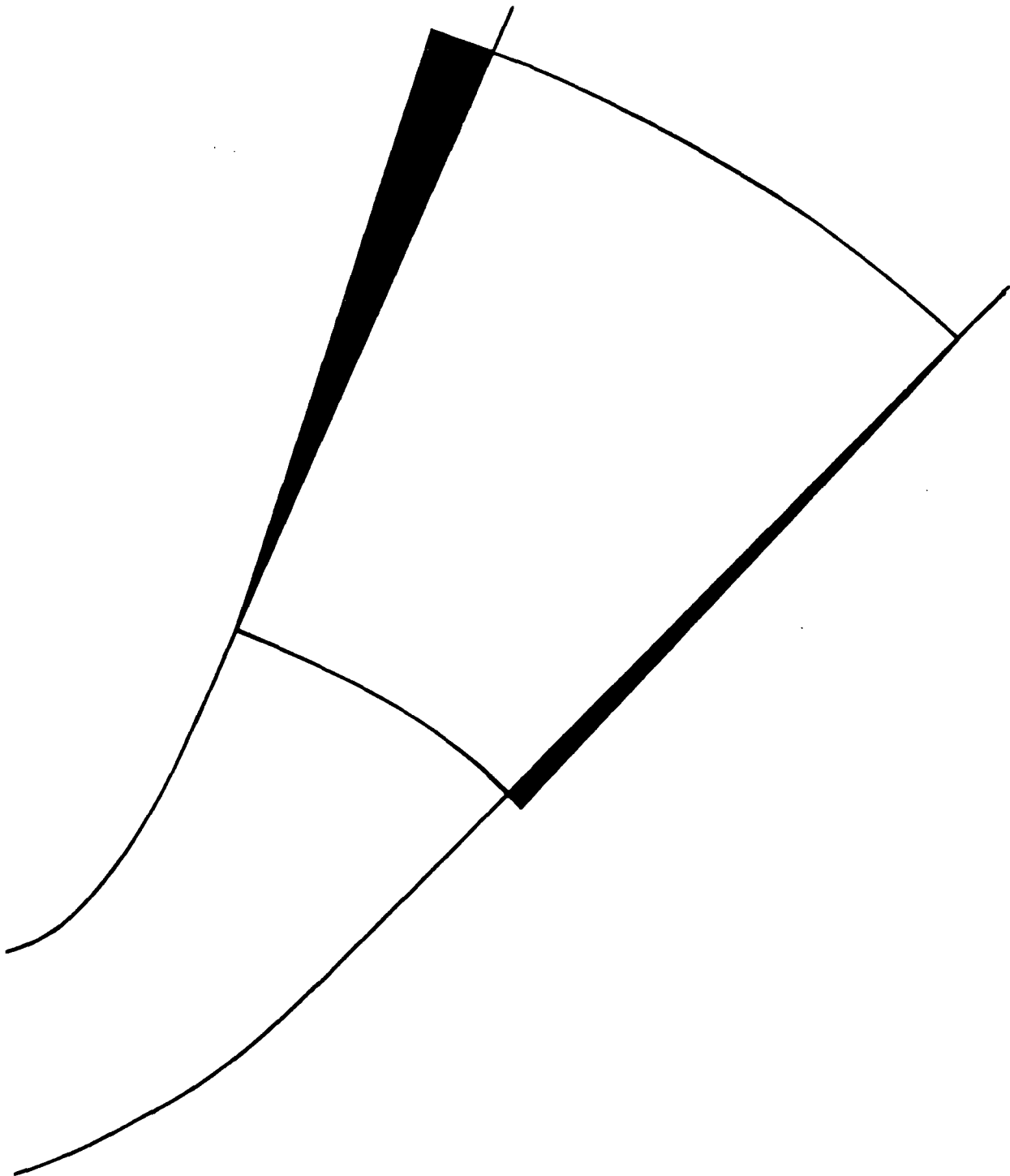
Figure 3.3-2   ISODOPPLER SCAN RELATIVE TO SECTOR SCAN
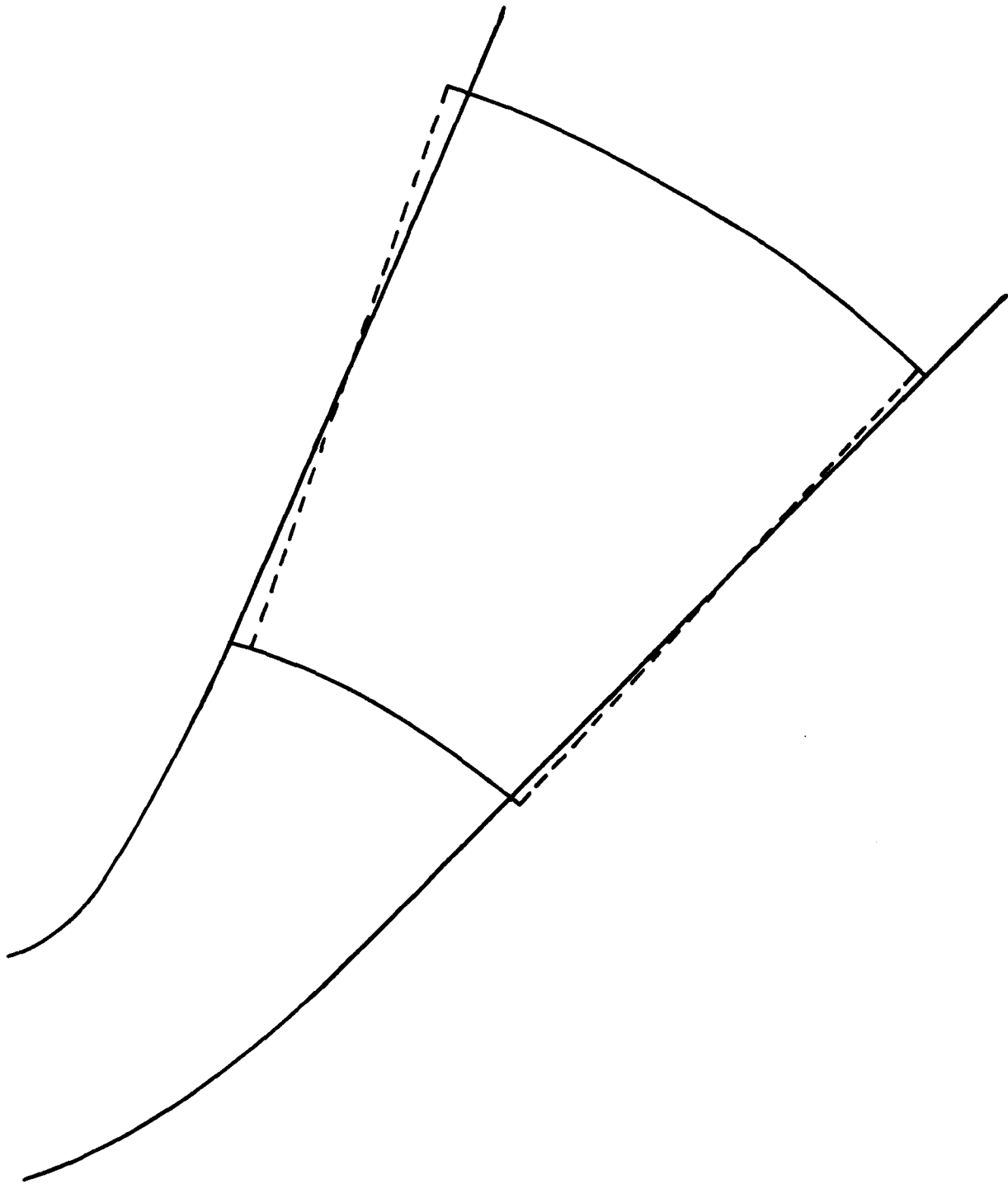
Figure 3.3-3   ISODOPPLER SCAN MAPPED INTO SECTOR SCAN

From a theoretical point of view, there is no reason which prevents generation of a frequency (a function of range) to correct for isodoppler frequencies. This generated frequency could be used as the local oscillator frequency to bring Doppler frequencies to SAR processing frequency. If the aircraft SAR system performed in this way, simulator isodoppler mapping would no longer be a design problem. At the current time, limited data on isodoppler mapping prevents a detailed analysis and satisfactory solution to design of simulator isodoppler mapping. Items of consideration in designing a simulator SAR isodoppler module include:

1) Performance characteristics of the aircraft SAR system
2) Accuracy versus training value
3) Cost

3.4 SQUINT ANGLE DEPENDENCE

Squint angle, the angle between the physical axis of the antenna and the axis of the radiated beam, enters into many SAR calculations and is a good beginning for deriving SAR equations for simulation purposes. Figure 3.4-1 is a diagram of the squint angle (ϕ), the azimuth angle (Θ_{VV}), the depression angle (Ψ), the altitude (A), the ground range (R_{GR}), and the slant range (R_{SL}). Appendix B contains a definition of the above mentioned terms. Using trigonometric functions, the following relationships can be derived relative to Figure 3.4-1:

$$X = R_G \cdot \sin(\Theta_{VV}) \tag{3.4.1}$$

$$Y = R_G \cdot \cos(\Theta_{VV}) \tag{3.4.2}$$

$$R_{SL} = \frac{R_{GR}}{\cos(\Psi)} \tag{3.4.3}$$

$$\cos(\Theta_{VV}) = \frac{Y}{\sqrt{X^2 + Y^2}} \tag{3.4.4}$$
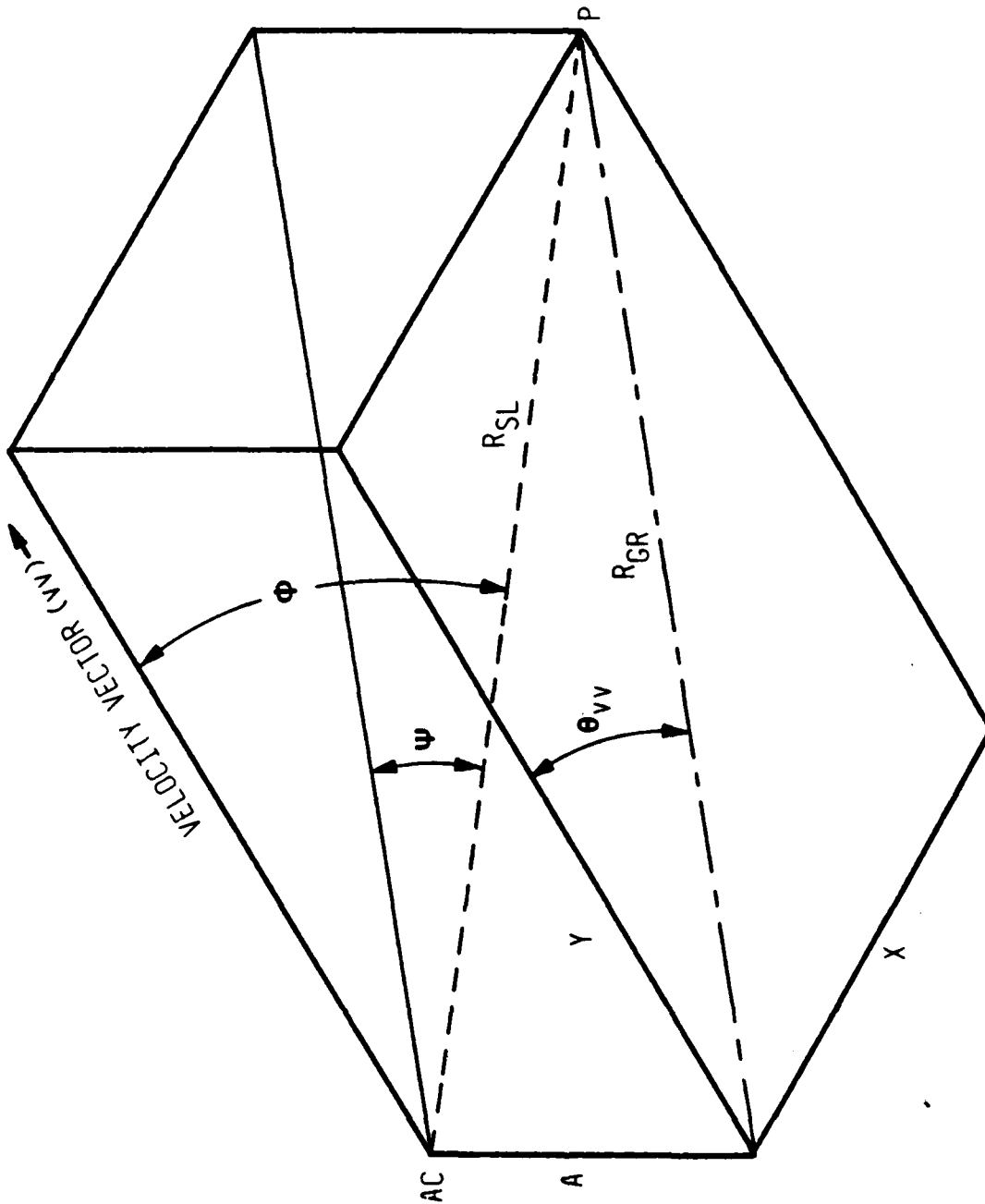
Figure 3.4-1 SQUINT ANGLE DIAGRAM

$$\cos(\psi) = \frac{\sqrt{z^2 + Y^2}}{\sqrt{X^2 + Y^2 + A^2}} \tag{3.4.5}$$

$$\cos(\Theta) = \frac{Y}{\sqrt{X^2 + Y^2 + A^2}} \tag{3.4.6}$$

$$\cos(\phi) = \cos(\Theta_{VV}) \cdot \cos(\Psi) \tag{3.4.7}$$

Where

Θ_{VV} = azimuth angle

A   = altitude

R_G = ground range

Equation 3.4.7 is derived by multiplying Equation 3.4.5 and Equation 3.4.6.

Figure 3.4-2 is derived by passing a plane through the velocity vector (V_V) and the slant range (R_{SL}). Velocity vector dimensions are length/time, and slant range dimension is length. Only directions of the vectors were used to derive the plane. The closing velocity is defined as:

$$V_C = V_V \cdot \cos(\phi) \tag{3.4.8}$$

Where

V_C = closing velocity

V_V = velocity vector

In Figure 3.4-2 V_V is the closing velocity of the point (P) and the aircraft (AC). When P is straight ahead of the flight path, the closing velocity (V_C) is equal to the velocity vector; when the point is abreast, the closing velocity is zero. The Doppler frequency and the closing velocity are directly related and thus the solution for the closing velocity is also the solution for the Doppler frequency.

POINT P

V_V

ϕ

V_C
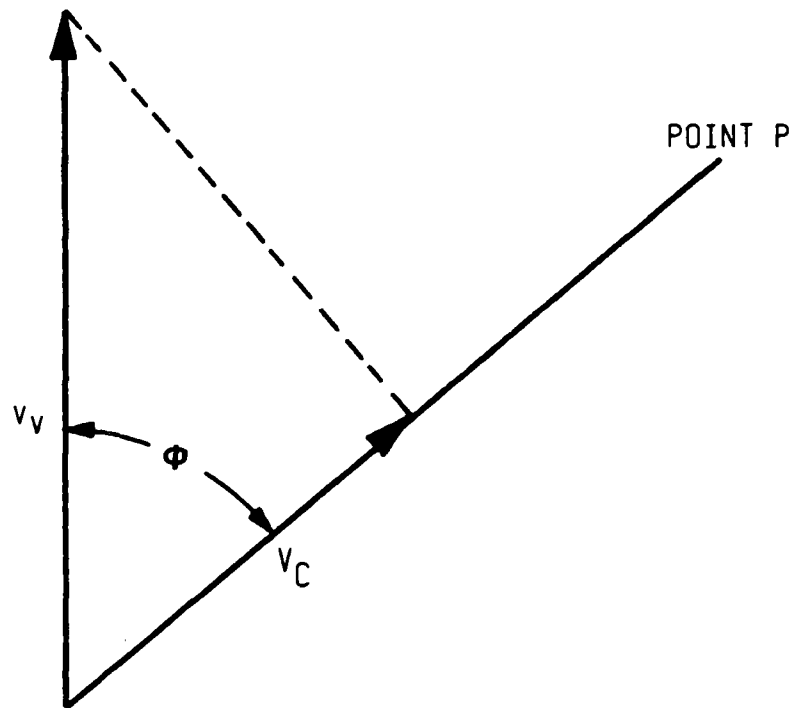
Figure 3.4-2   CLOSING VELOCITY DIAGRAM

In synthetic aperture radar, a point on the ground Doppler frequency changes as the aircraft flies along the data collecting path. In analyzing SAR for simulation purposes, the Doppler frequency of a point halfway along the data gathering path is called the Doppler frequency signature. If we return to Figure 3.4-1 and the associated equations and combine Equations 3.4.6 and 3.4.8, the resulting equation is:

$$V_C = \frac{V_V \cdot Y}{\sqrt{X^2 + Y^2 + A^2}}$$
(3.4.9)

Equation 3.4.9 can be normalized by setting V_V and A to 1.

$$V_C = \frac{Y}{\sqrt{X^2 + Y^2 + 1}}$$
(3.4.10)

Equation 3.4.10 can be written in the form:

$$-X^2 + \left[\frac{1}{V_c^2} - 1\right] \cdot Y^2 = 1$$
(3.4.11)

Equation 3.4.11 is the equation of a hyperbola symmetric to the Y axis. By setting V_c to different values, a family of hyperbolas can be generated. When Y is positive, Doppler frequencies are for a closing object and when Y is negative, Doppler frequencies are for an opening object. Figure 3.4-3 is a diagram of isodoppler and isorange lines.

A summarization of SAR derivations and implied results is given here. First, isodoppler lines and isorange lines are drawn for a flat surface. If the surface includes hills, isodoppler lines move toward the Y axis and isorange
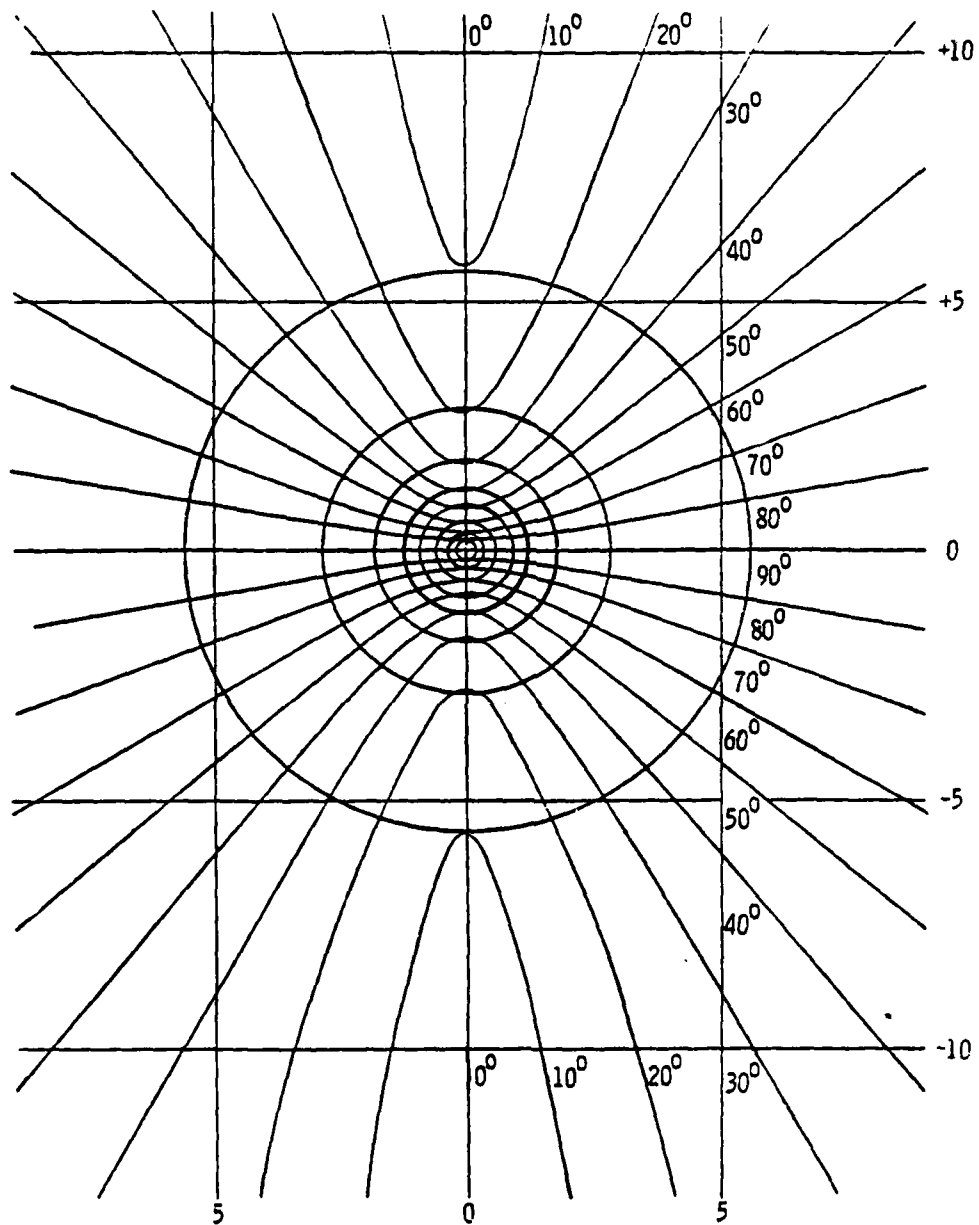
Figure 3.4-3 NORMALIZED ISODOPPLER AND ISORANGE

lines move toward the origin. A depression in the surface causes isodoppler lines to move toward the Y axis and isorange lines to move from the origin. Conventional radar range changes as a function of terrain elevation, although azimuth mapping is not affected. In synthetic aperture radar, range and azimuth mapping is a function of terrain elevation. SAR mapping is discussed in later text. Another important function that requires emphasis is nonlinear azimuth mapping in SAR. The isodoppler lines are hyperbolas.

If SAR processing is performed without correction for nonlinear factors, a nonlinear sweep must be used for the SAR display. An example of nonlinear mapping is shown in Figure 3.4-4, where the shaded area is bounded by two isorange lines and by two isodoppler lines. One isodoppler line azimuth varies from 0 to 19 degrees and the other isodoppler line varies from 23 to 28 degrees.

3.5 FOCUSED ARRAY

The theory of focused array is included as a means of understanding simulation considerations. In early SAR systems, the angle of view was unfocused and 90 degrees from the velocity vector. An unfocused SAR is equivalent to a pinhole camera in optics. Figure 3.5-1 is a diagram of an unfocused array. Point P is the reference point (the azimuth center of a picture), line C is the path length at the start of data collection, and line A is the path length at the end of data collection. Line B is the entire length of data collection (the aperture width). The law of cosines is used to derive the equation for an unfocused array. This relationship is given in equation 3.5-1.

$$A_A^2 = B_B^2 + C_C^2 - 2 \cdot B_B \cdot C_C \cdot \cos \phi \qquad (3.5.1)$$

Where

A_A = $R - \lambda K_p$

B_B = data collection distance

K_p = phase shift limit
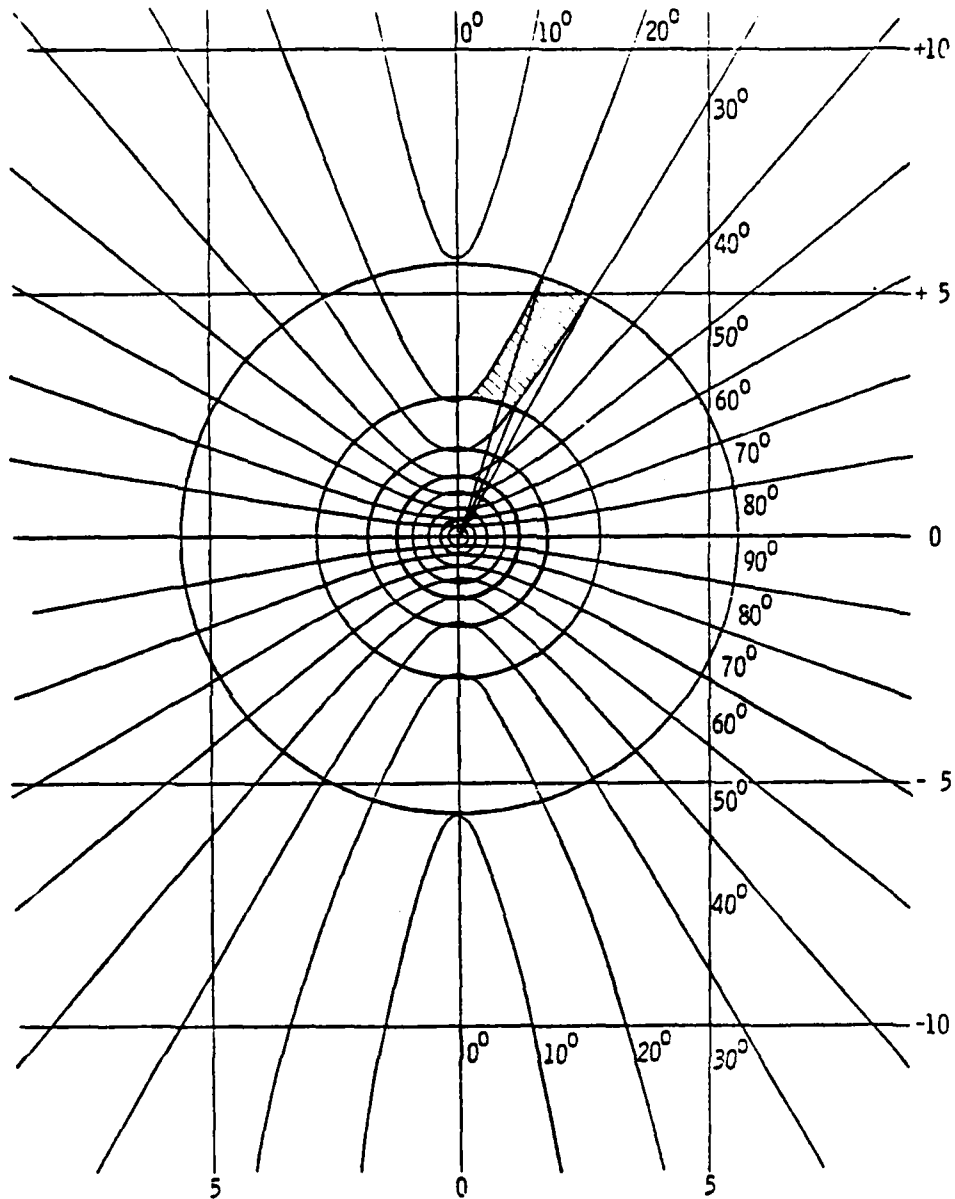
Figure 3.4-4 SAR ISODOPPLER MAPPING
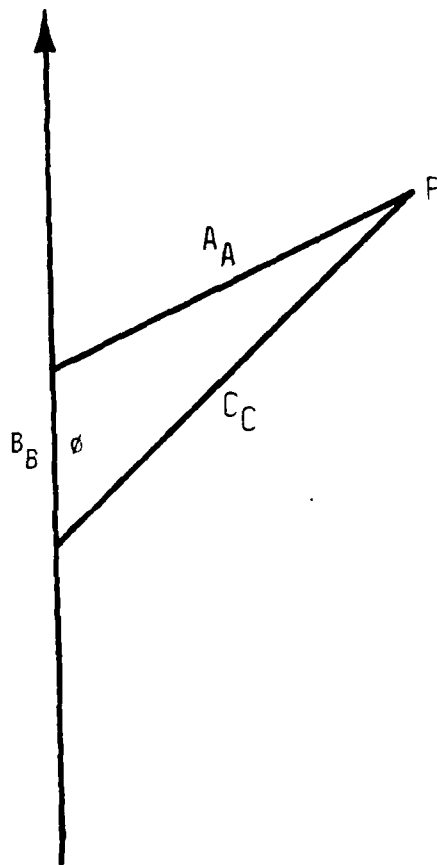
Figure 3.5-1   UNFOCUSED ARRAY DIAGRAM

Angle ϕ is the squint angle.

Let $A_A = R - \lambda \cdot K_p$ and $C_C = R$ in Equation 3.5.1 to give:

$$R^2 - 2 \cdot R \cdot \lambda \cdot K_p + \left(\lambda \cdot K_p\right)^2 = B_B^2 + R^2 - 2 \cdot B_B \cdot R \cdot \cos(\phi) \tag{3.5.2}$$

The solution of B_B (the unfocused path distance) is given:

$$B_B = R \cdot \cos(\phi) + R \left[\cos^2(\phi) - 2 \cdot \lambda \cdot K_P / R + (\lambda \cdot K_P / R)^2\right]^{1/2} \tag{3.5.3}$$

For verification, let the squint angle (ϕ) be 90 degrees and delete the term Equation 3.5.3 now becomes: $(\lambda \cdot K/R)/2$.

$$B_B = \sqrt{2 \cdot \lambda \cdot K_P \cdot R} \tag{3.5.4}$$

K_p represents the amount of phase shift that can be tolerated. Forty-five degrees phase shift is represented by a K_p of one-eighth. At 90 degrees the unfocused distance is doubled because of the symmetry around 90 degrees. Putting these values in Equation 3.5.4 gives the equation of an unfocused array at 90 degrees:

$$B_B = \sqrt{\lambda \cdot R} \tag{3.5.5}$$

This equation is given in "Introduction to Synthetic Array and Imaging Radars" by S.A. Hovanessin (page 23).

By establishing a certain confidence in Equation 3.3.3, we turn to the implications when the squint angle is not 90 degrees. A realistic value for $2 \cdot \lambda \cdot K_p / R$ is 0.0000004. After the cosine of ϕ exceeds this value, the unfocused distance approaches zero. SAR will not function in an unfocused mode when the squint angle is not 90 degrees.

Let angle ϕ be zero degrees and solve for B_B in Equation 3.5.3. Travel distance for an unfocused array is $\lambda \cdot K_p$. This distance gives a SAR aperture of approximately one-eighth of an inch. An unfocused array varies from zero at zero degrees to $(\lambda \cdot K_p \cdot R)^{1/2}$ at 90 degrees.

An important question for the simulation design engineer is a satisfactory solution if focusing fails.

3.6 SAR AZIMUTH RESOLUTION

There are actually three resolutions to consider in simulating SAR azimuth resolution. These resolutions are: 1) aircraft display pixel resolution, 2) aircraft SAR resolution, and 3) data base resolution. To make use of the SAR resolution, the pixel resolution should be at least twice that of the SAR resolution. This relationship is from the Nyquist Sampling Theorem. Since simulation is to be performed digitally an equation is needed to relate the three resolutions. This equation will not be an exact equation but a preferred or "best fit" solution. Pixel resolution will be the pixel resolution of the aircraft. The SAR resolution will then be modified to be compatible with the pixel resolution. The data base resolution will be made to fit the above resolutions. The equation relating the three resolutions:

$$\frac{R_{DS}}{K_K} = \frac{N1 \cdot R_{SAR}}{K_K} = \frac{N2 \cdot R_{DB}}{K_K} \qquad (3.6.1)$$

$$N1 \geq 1 \qquad N2 \geq 2$$

Where

R_{DS} = aircraft display resolution

R_{SAR} = synthetic aperture radar resolution

R_{DB} = data base resolution

K_K

= selectable constant for SAR resolution

N = integers

The factor K_K is directly related to the computing required. The ideal value of K_K would be equal to one to keep the computing load down, but it should be higher if the response distribution of a point is to be simulated with greater detail when N1 = 2. The data base should be equal to the SAR resolution for high quality simulation. In the first example, resolution is considered to be the size of one pixel, but aircraft SAR resolution and data base resolution are considered as two pixels. The minimum value of K_K is one and N1 and N2 have minimum values of two. Assume that the antenna 6 dB beamwidth is two pixels, the antenna null to null is four pixels, and the first side lobes are down 20 dB and spaced three pixels from the center of the main lobe. Figure 3.6-1 is a plot of the response of a corner reflector (point). Figure 3.6-2 shows two corner reflectors spaced at a distance of eight pixels. Figures 3.6-3, 3.6-4, 3.6-5, and 3.6-6 illustrate what happens as the two corner reflectors (points) move together to the limit of resolution. The numbers chosen for this example are the minimum numbers that can be used to simulate the amplitude distribution of a point. The above example maps the point response into five locations in azimuth, at the same slant range.

Resolution in a SAR system can be greater than two pixels. The two-pixel example is the ideal. Figure 3.6-7 is an example of the amplitude distribution of a point when the SAR resolution is six pixels. The point now maps into 23 pixel locations. This should not happen in actuality as the optimum SAR resolution in an aircraft is two pixels. Refer to Figures 3.6-8 and 3.6-9 for examples.
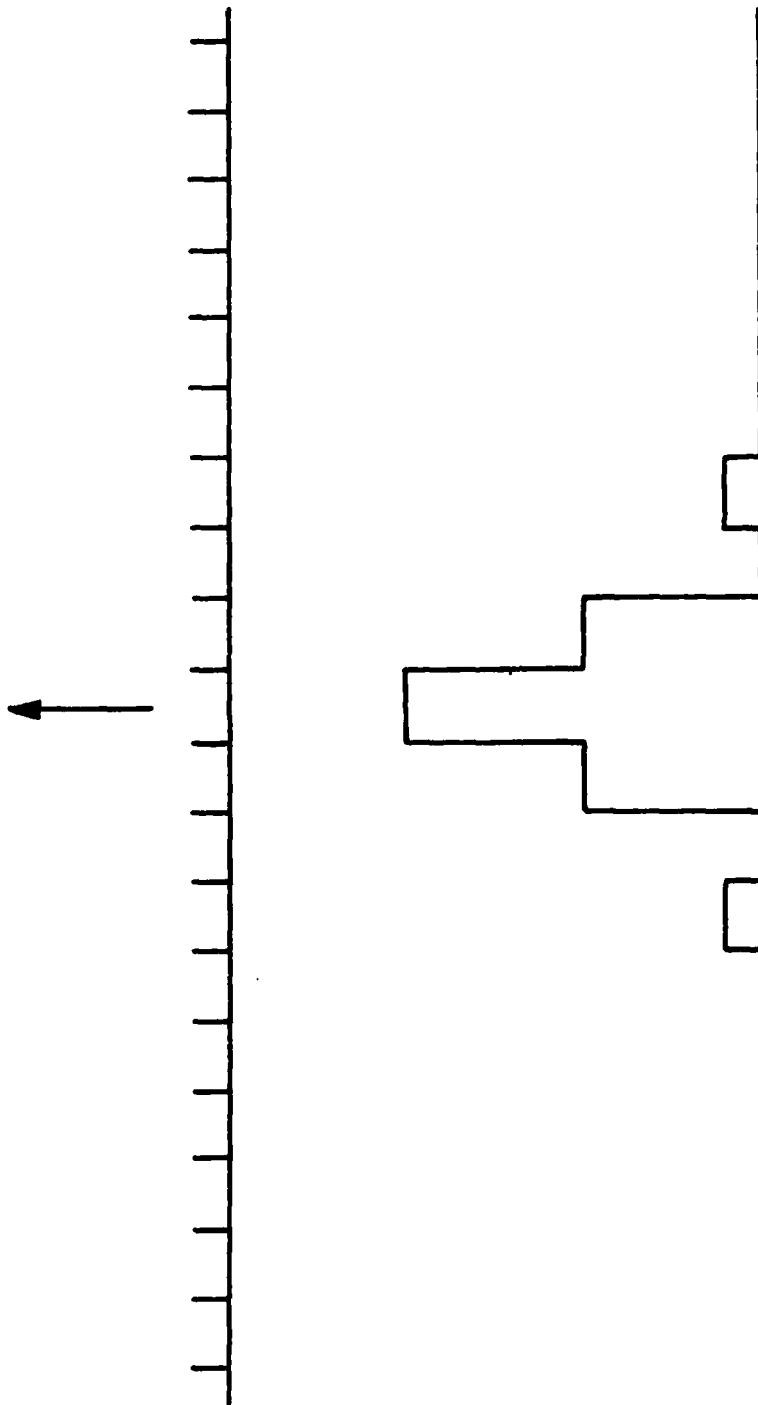
Figure 3.6-1 SIMULATED POINT RESPONSE
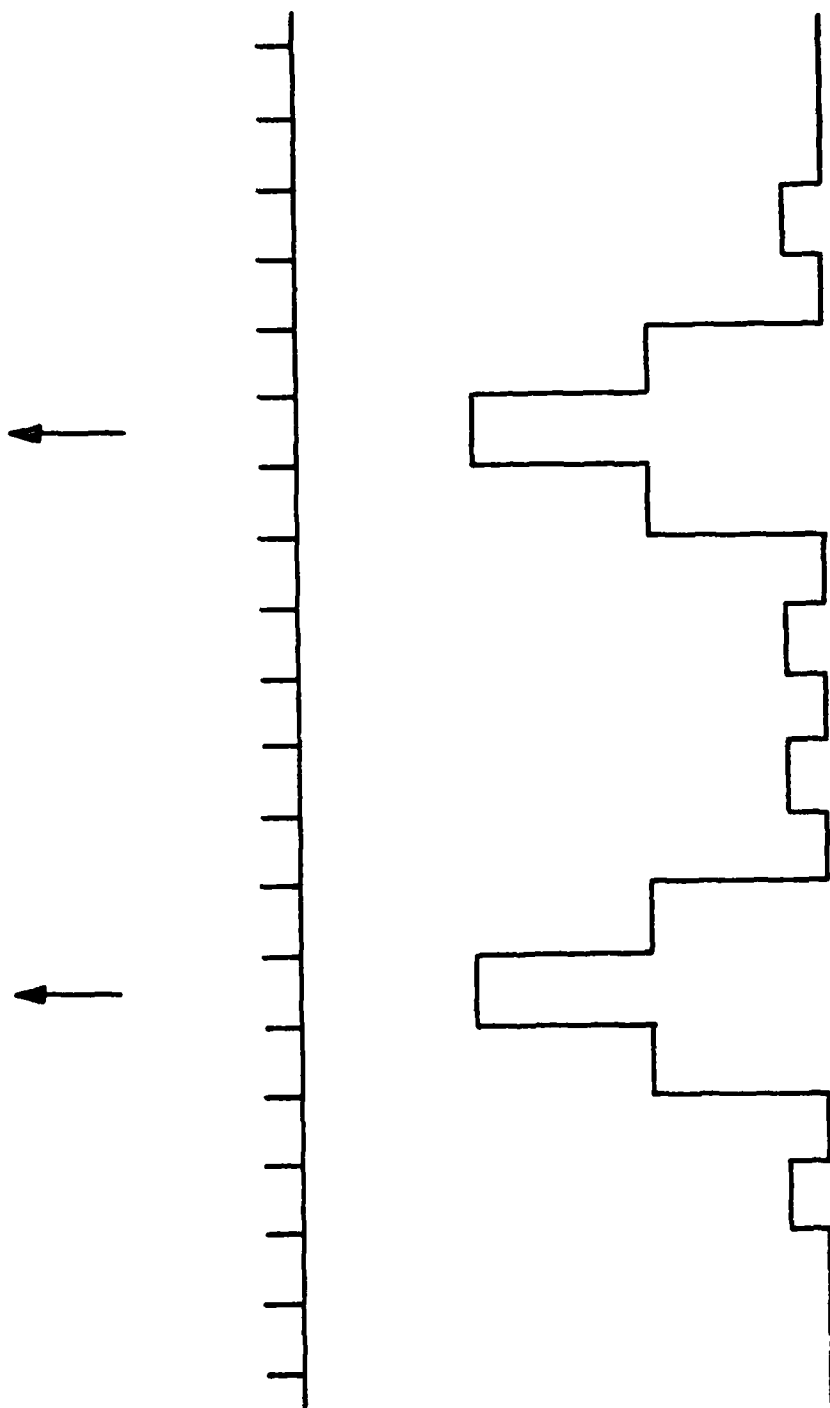
Figure 3.6-2 8-PIXEL SPACE SIMULATED TWO-POINT RESPONSE
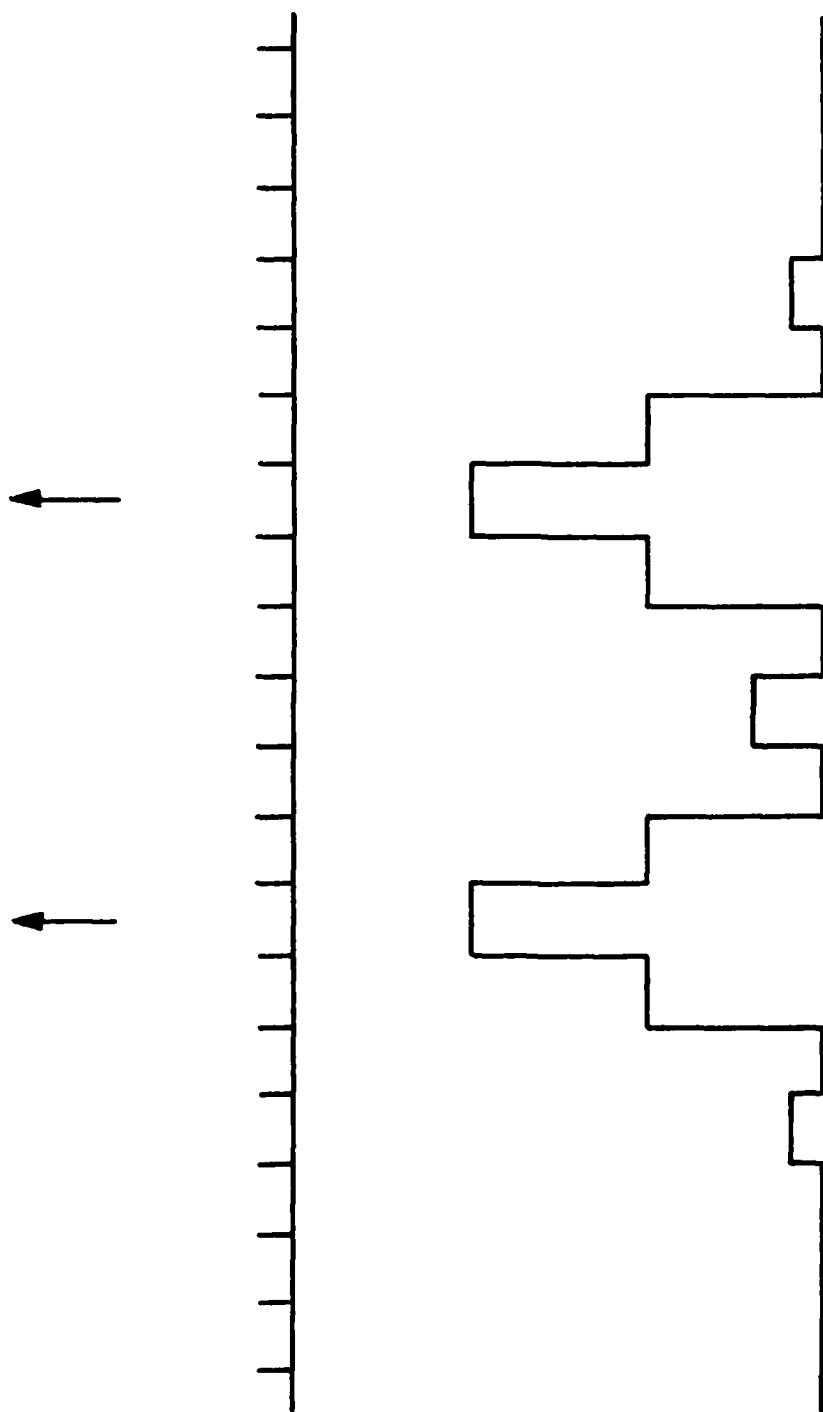
Figure 3.6-3 6-PIXEL SPACE SIMULATED TWO-POINT RESPONSE
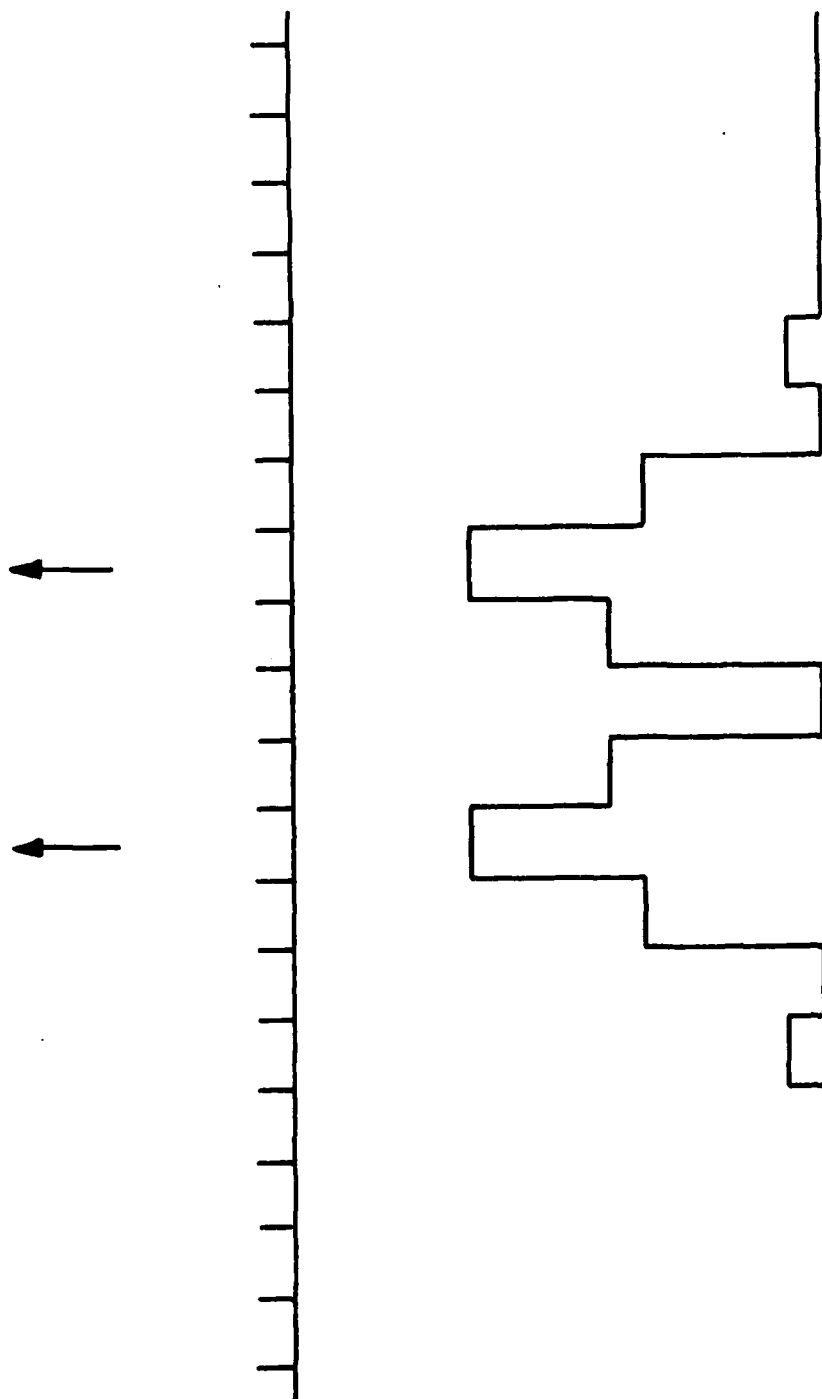
Figure 3.6-4 4-PIXEL SPACE SIMULATED TWO-POINT RESPONSE
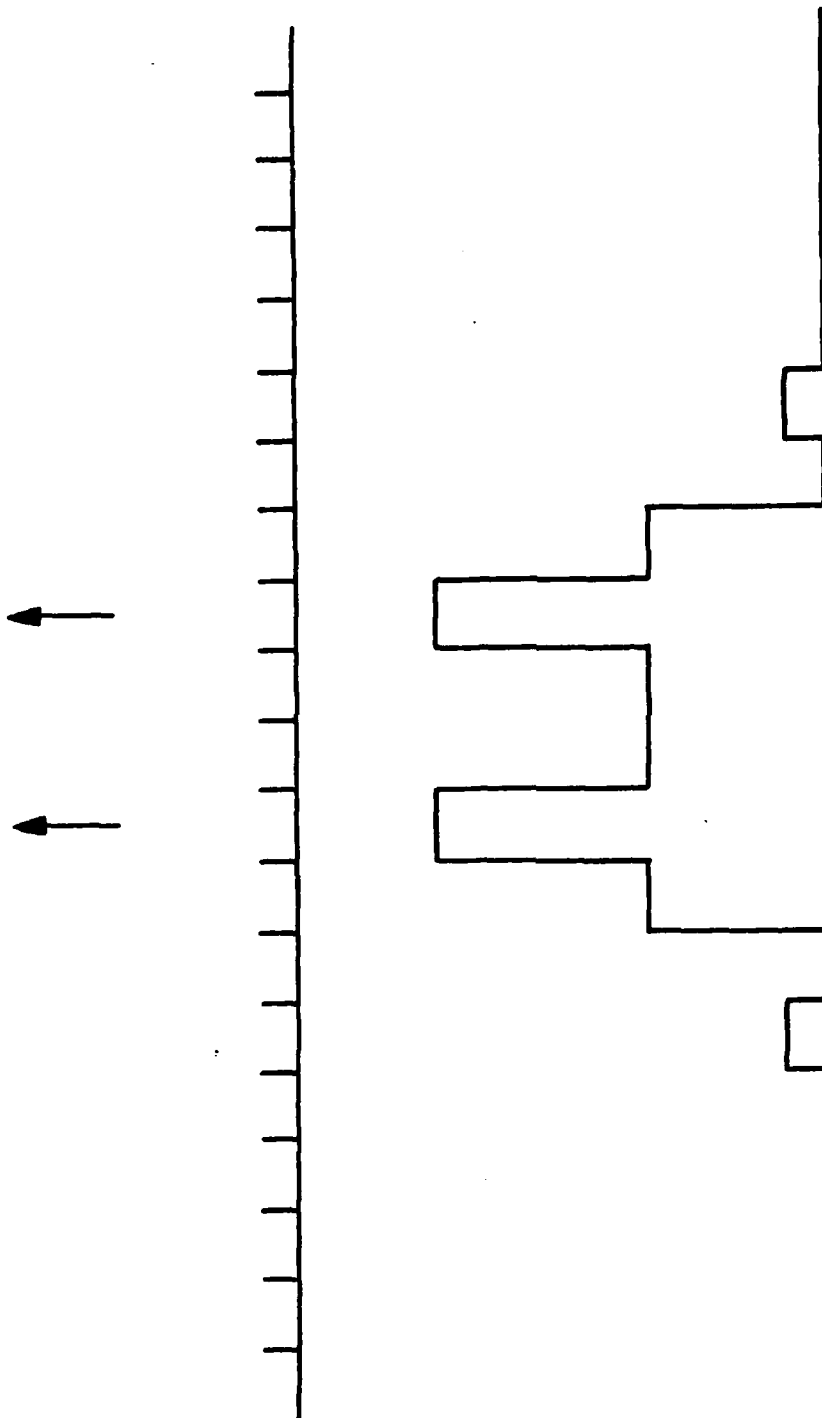
Figure 3.6-5 3-PIXEL SPACE SIMULATED TWO-POINT RESPONSE
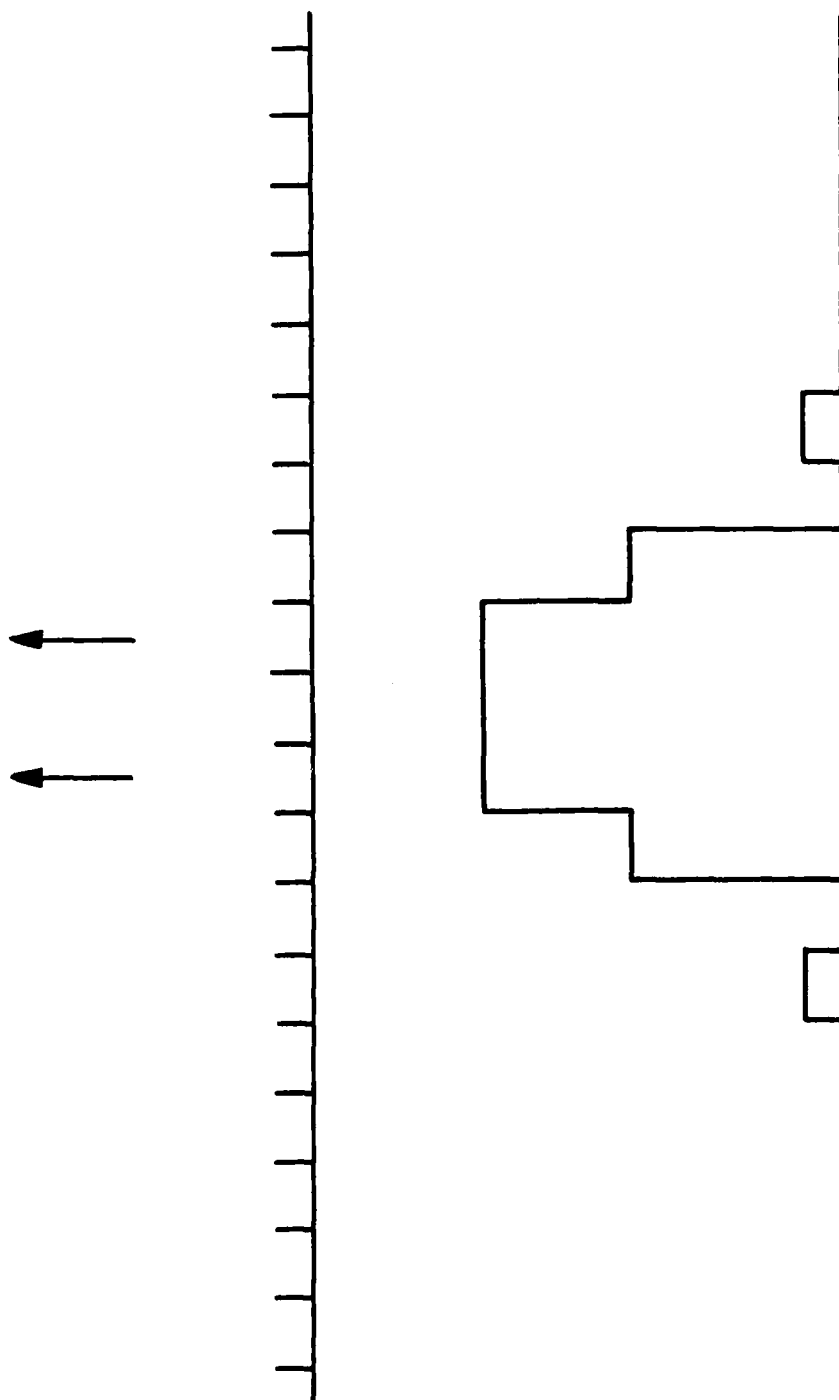
Figure 3.6-6 2-PIXEL SPACE SIMULATED TWO-POINT RESPONSE
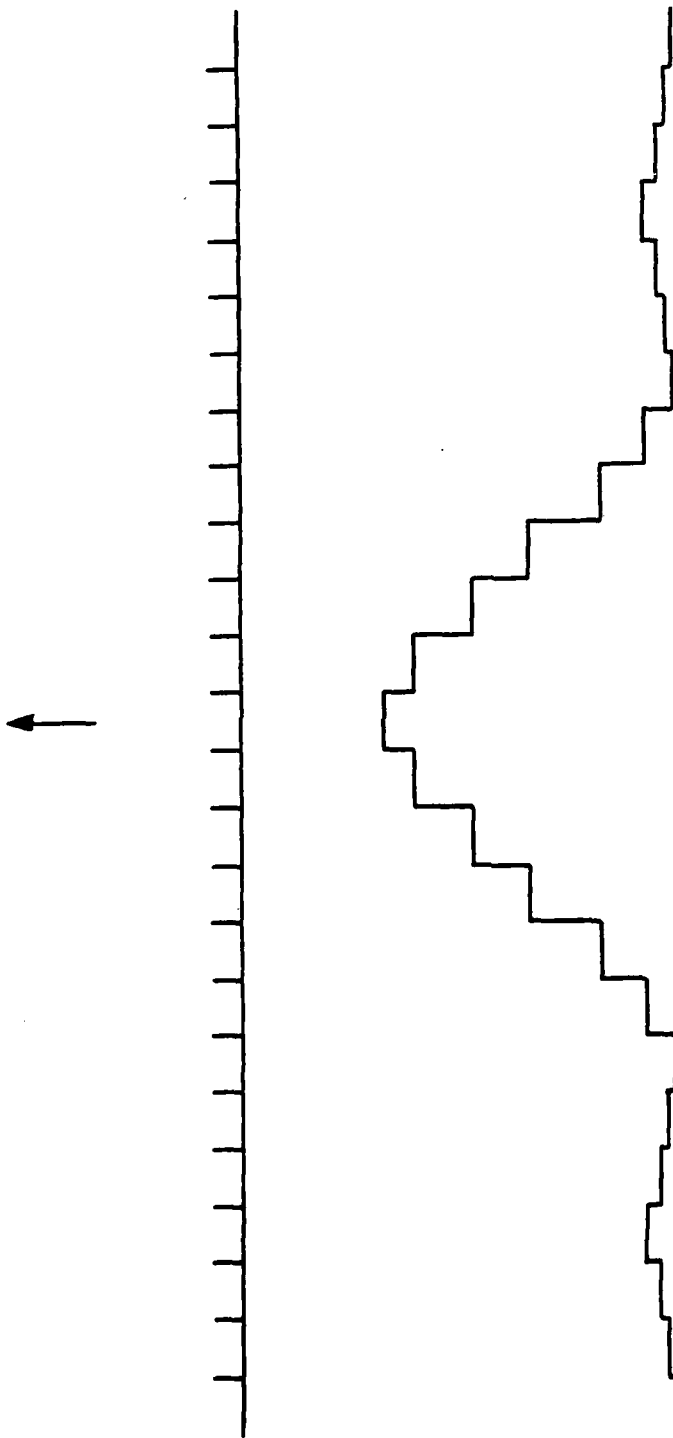
Figure 3.6-7 SIMULATED RESPONSE SAR RESOLUTION 6 PIXELS

RADAR RESOLUTION

"To quantify the HRR resolution in range and azimuth" was an important objective for the evaluation flight test. An array of nine corner reflectors was erected on Edwards AFB range PB-4 to support these measurements. The final configuration of the array is shown below.

This array was mapped for 8.5 and 17 foot resolution capability at squint angles from 15° to 20° and at grazing angles from 1° to 5° while varying aircraft velocity, range to map center, and number of looks. The aircrew reported that three reflectors could be discerned in range and azimuth, and the fourth reflector was visible from time to time.

A typical map is selected from flight No. 45 which was flown on January 20. The L-shaped array is distinctly visible in the center of map D45C04. The picture at the right is the array pixels magnified 16 times. The smallest reflector spacing is seen as two 8.5 foot resolution elements positioned in adjacent high-intensity pixels. Note that the 8.5 foot pixel width can be used to scale the separation between all of the reflectors in the array.

In the lower portion of the page above is a ground-level photograph showing the installation of the corner reflectors on range PB-4.
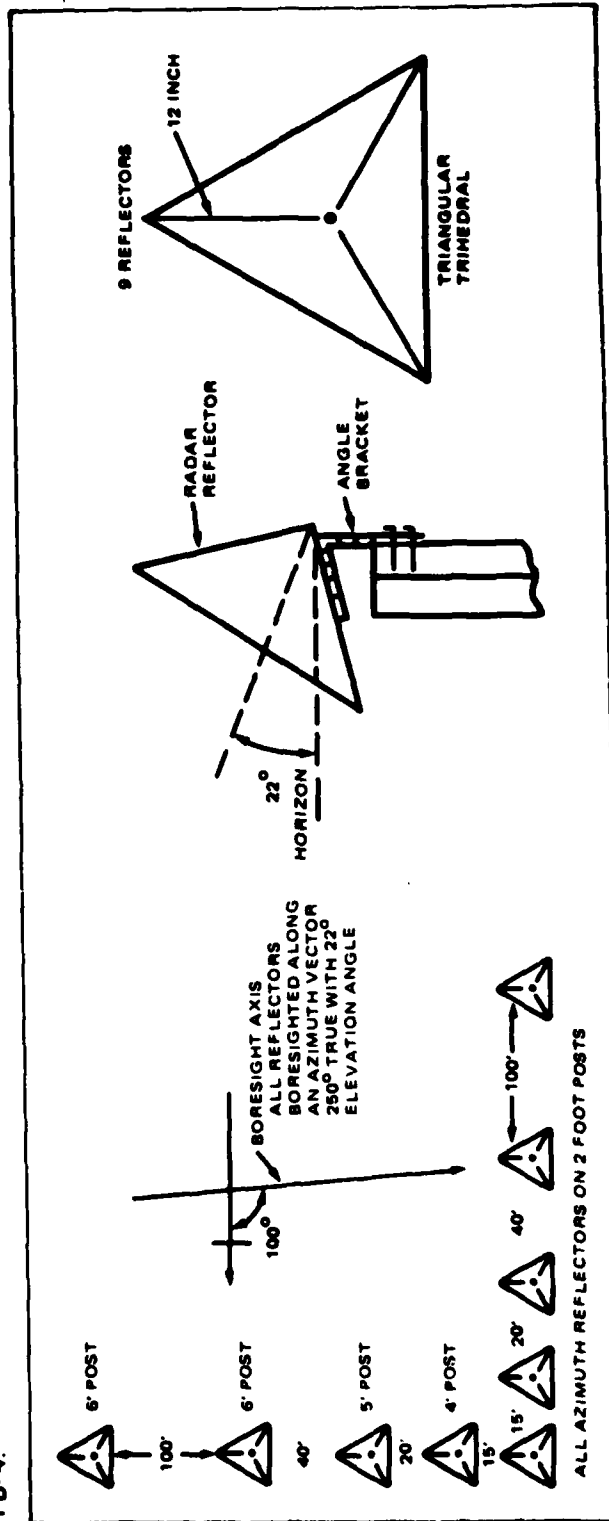
Figure 3.6-8   HUGHES PHOTO

3-47

16X Zoom of the Map on the Left
Showing the Resolution Array
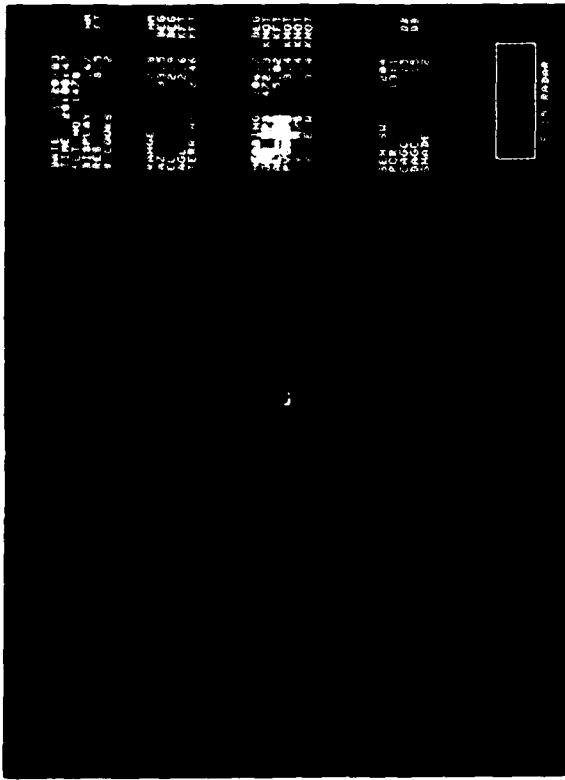
8.5 Resolution Map of the Resolution Array

Ground Photograph of the 12 Inch Corner Reflectors

43

Figure 3.6-9 shows the setup used in evaluating the F-15 SAR. Figure 3.6-9 is a photograph of the SAR display when viewing test targets. In the 16-X zoom of the SAR map, the two targets that are spaced 15 feet apart cannot be separated, but the targets that are spaced 20 feet apart can be identified as two separate targets. Also note that azimuth resolution and range resolution seem to track.

3.7 RANGE WALK AND ROTATION

In the theoretical evaluation of SAR, it was assumed that data would be collected along an arc and processed. Upon closer examination of the details of SAR functioning, SAR processing becomes more complex. Two processes, range walk and rotation, tend to make SAR processing more complex. Figures 3.7-1 and 3.7-2 are diagrams of the two processes and from Figure 3.7-2, equations for range walk and rotation can be developed. The equation for range walk is the trigonometric cosine law.

$$R_W = R_1 - \sqrt{R_1^2 + P_C^2 - 2 \cdot R_1 \cdot P_C \cdot \cos(\Phi)} \qquad (3.7.1)$$

Where

R_w = range walk

R_1 = range at position one

The equation for rotation is the trigonometric cosine law and the sine law.

$$R_2 = \sqrt{R_1^2 + P_C^2 - 2 \cdot R_1 \cdot P_C \cdot \cos(\Phi)} \qquad (3.7.2)$$

$$\Phi_2 = \sin^{-1}\left[\frac{R_2 \cdot \sin(\Phi)}{R_1}\right] \qquad (3.7.3)$$

Where

R_2 = range at position two

Φ_2 = squint angle at position two
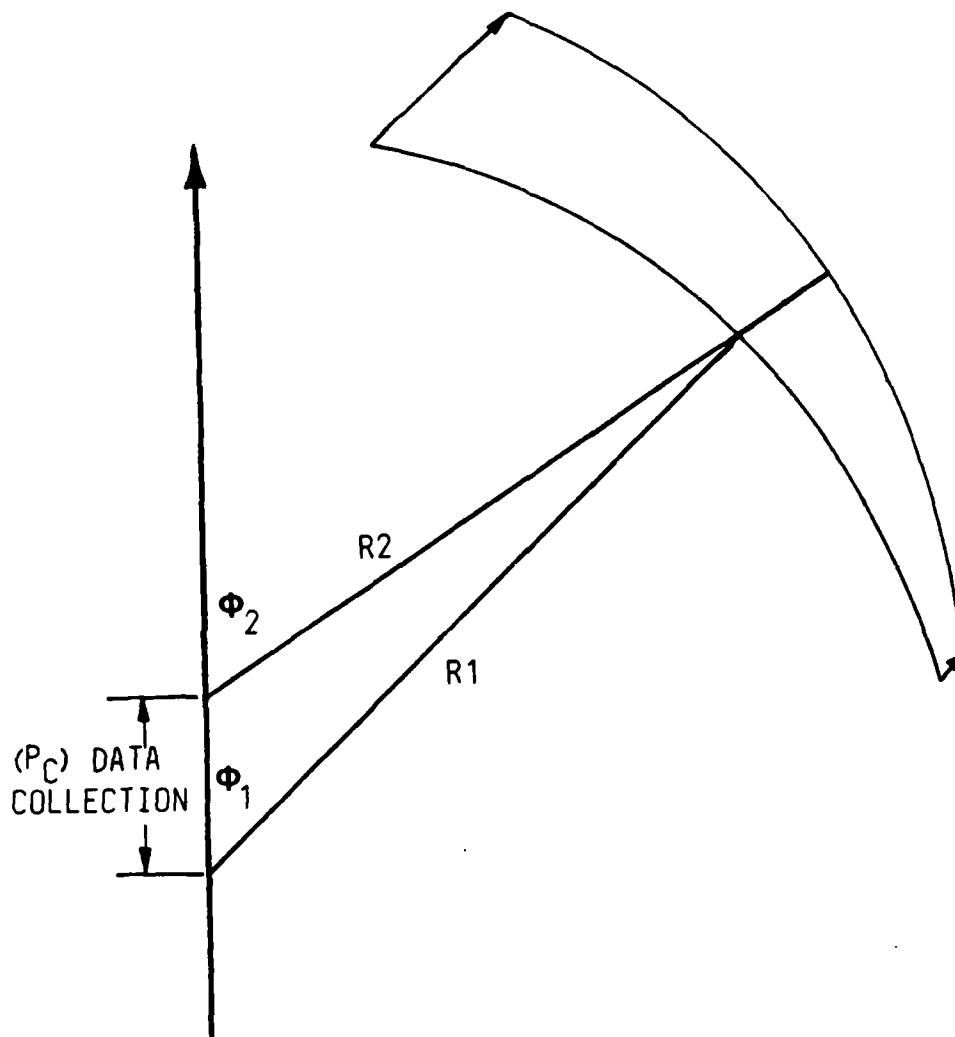
Figure 3.7-1   ROTATION AND RANGE WALK
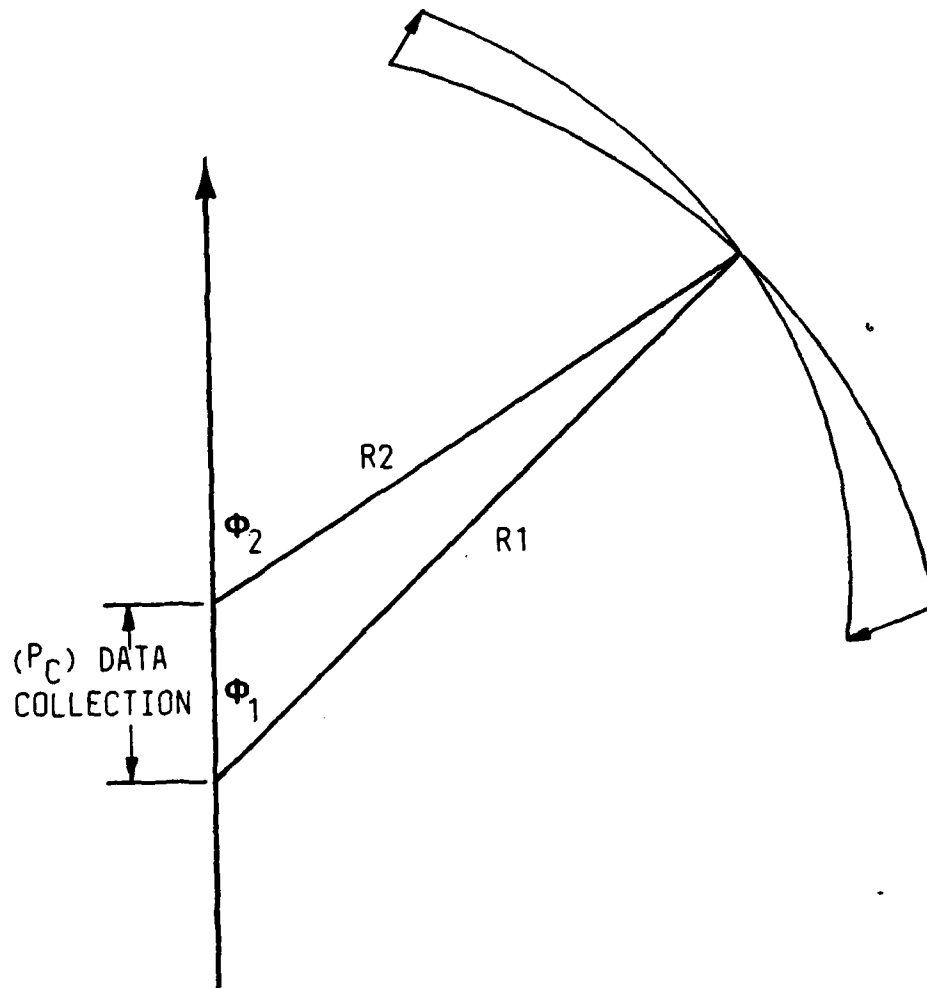
Figure 3.7-2   ROTATION WITH RANGE WALK CORRECTION

For better understanding, an example of range walk and rotation is indicated in the following parameters.

Range	10 nautical miles
Wave length	3 centimeters
Squint angle	45 degrees
Resolution	1 cycle in 20 feet (10-foot pixel)
Number of pixels	512

Path length can be solved by using Equation 3.2.23 (Section 3.2). If the path length is 0.052180 nautical miles, the range walk is 111.41 feet, and this distance is 11 pixels. It is apparent that range walk makes SAR processing much more difficult. Designers of airborne SAR systems have solved range walk in a very elegant manner. The pulse repetition rate (PRF) is programmed to remove range walk.

Rotation problems still exist, however, and an example of rotation is a continuation of the range walk problem. The solution for squint angle/two is 45.2107 degrees. At a range of 10 nautical miles, 512 ten-foot pixels cover an arc of 4.825 degrees. When these numbers are put into equations, it is found that, at their ends, the arcs are displaced from each other by 1.2 pixels. The designer of the aircraft SAR can handle this problem in one of two ways. The loss of resolution at the edge of the picture can be accepted or the problem can be resolved. In a spotlight SAR system, this migration is corrected so that very high resolution can be obtained.

In the design of a SAR simulator, there must be a clear determination of what is happening in the actual aircraft SAR system. If the problem has been eliminated in the aircraft SAR, there is no longer a problem in the simulator SAR. When the rotation problem does exist in the aircraft, there is a simple solution available for simulator design: a small amount of weighted averaging at the edges of the picture will give the right amount of defocusing.

There is an additional problem caused by rotation. In some SAR modes, the display is made up of two or more sector scans. Figure 3.7-3 shows how two sector scans are brought together to form a single picture. Since the two scans are generated from two locations, the two sectors will not have a perfect fit. In the aircraft SAR, the problem can either be ignored or there can be a small amount of overscan and scan merger. Merging is accomplished using a weighted average of the pixels that overlap. The simulator design should replicate the aircraft SAR as a solution to this problem.

3.8 PULSE COMPRESSION

As stated previously, radar has two differing resolutions for range direction and azimuth direction. The range resolution of conventional pulse radar is given by the following equation:

$$\Delta R \approx c \cdot t / 2 \qquad\qquad (3.8.1)$$

Where

C = velocity of light

R = range resolution in meters

Figure 3.8-1 presents a graphic analysis of the derivation of the above equation.

Radar return signal power varies as the inverse fourth power of range. Radar power is a function of the pulse area and radar range resolution varies inversely with pulse width. A problem occurs if a high powered radar with high range resolution is desired. In this circumstance, the best solution would be to build a radar with zero pulse width and infinite peak power. With conventional pulse radar, some type of compromise must be made between range and resolution.
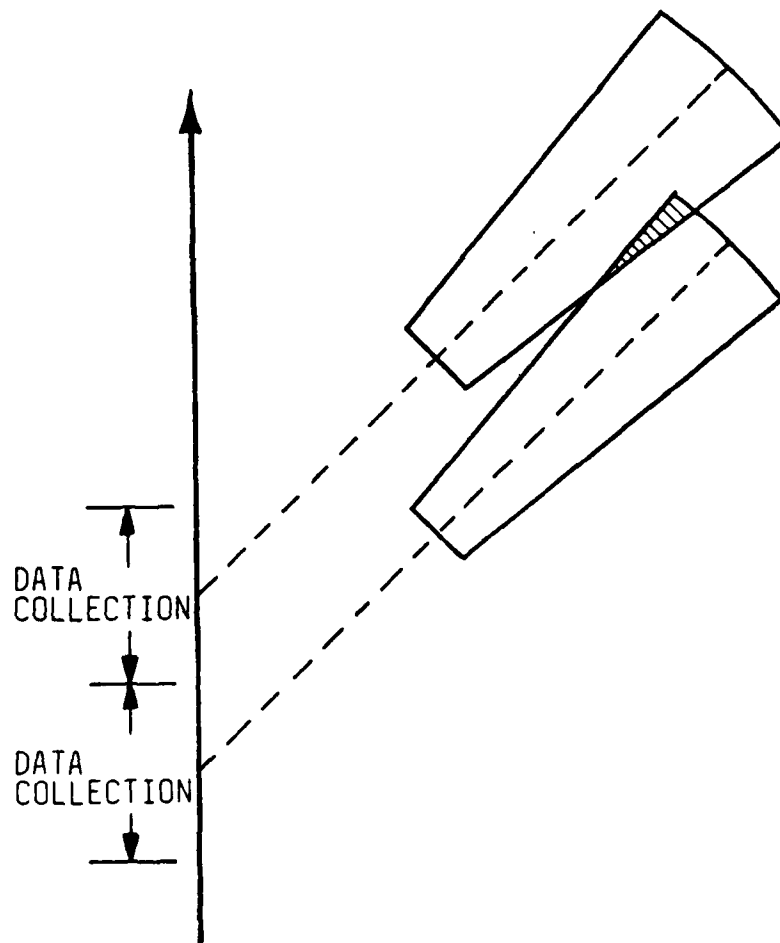
Figure 3.7-3   TWO MERGED UNCORRECTED SECTOR SCANS
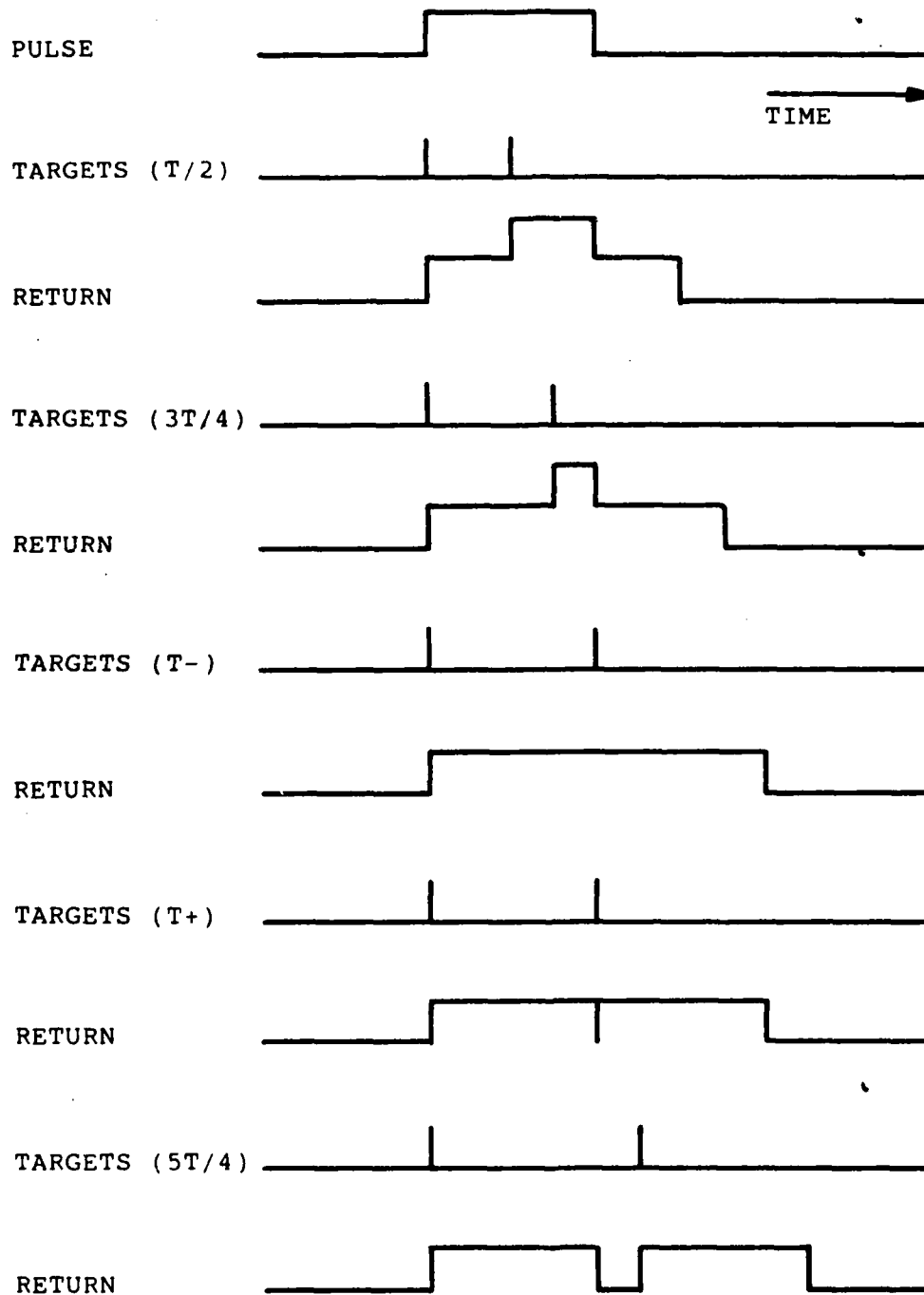
Figure 3.8-1 RADAR RESOLUTION DUE TO PULSE WIDTH

Pulse compression allows pulse length to be independently varied from range resolution. Using this technique, range resolution becomes a function of the bandwidth of the radar transmitter and receiver.

$$\Delta R \approx \frac{C}{B_W} \qquad (3.8.2)$$

Where

B_W = bandwidth

This equation implies that peak pulse amplitude can be kept to an optimum level and range resolution can be increased, if a way can be found to increase the bandwidth without increasing the peak power. Fortunately there are many ways to accomplish this. First attempts showed a modest gain in range resolution. With advances in hardware capabilities, significant increase in range resolution followed. In order to understand what is to be done to simulate radars of higher resolution, two examples of techniques for increased range resolution are included.

The first example will be linear frequency modulation radar, commonly referred to as chirp radar. The chirp radar principle consists of linearly modulating the carrier frequency over the length of the transmitted pulse and putting a matched filter in the receiver that will separate returns in time, as a function of carrier frequency. Figure 3.8-2 illustrates the concept of chirp radar. The frequency at the beginning of the pulse is delayed until the end of the pulse; all other frequencies are proportionally delayed. This delay causes the return pulse to increase in height and decrease in width. The cost for achieving this increase in range resolution is a more complex radar and a larger bandwidth. There are additional types of carrier modulation; however, for each type, a filter must be designed to match the modulation. Chirp modulation has an advantage over other methods because any mismatch between the modulator and filter causes only a constant range error. One disadvantage of basic chirp radar is the generation of side lobes in the range direction. These side lobes have the same function as a lens (sinx/x) and can be controlled in the same way. Uncontrolled side lobes are down only 13.2 dB.

PULSE

MODULATION
FREQUENCY

CARRIER
FREQUENCY

FILTER
RESPONSE

DELAY

F_S F_F

RECEIVED
PULSE   (AFTER CHIRP)
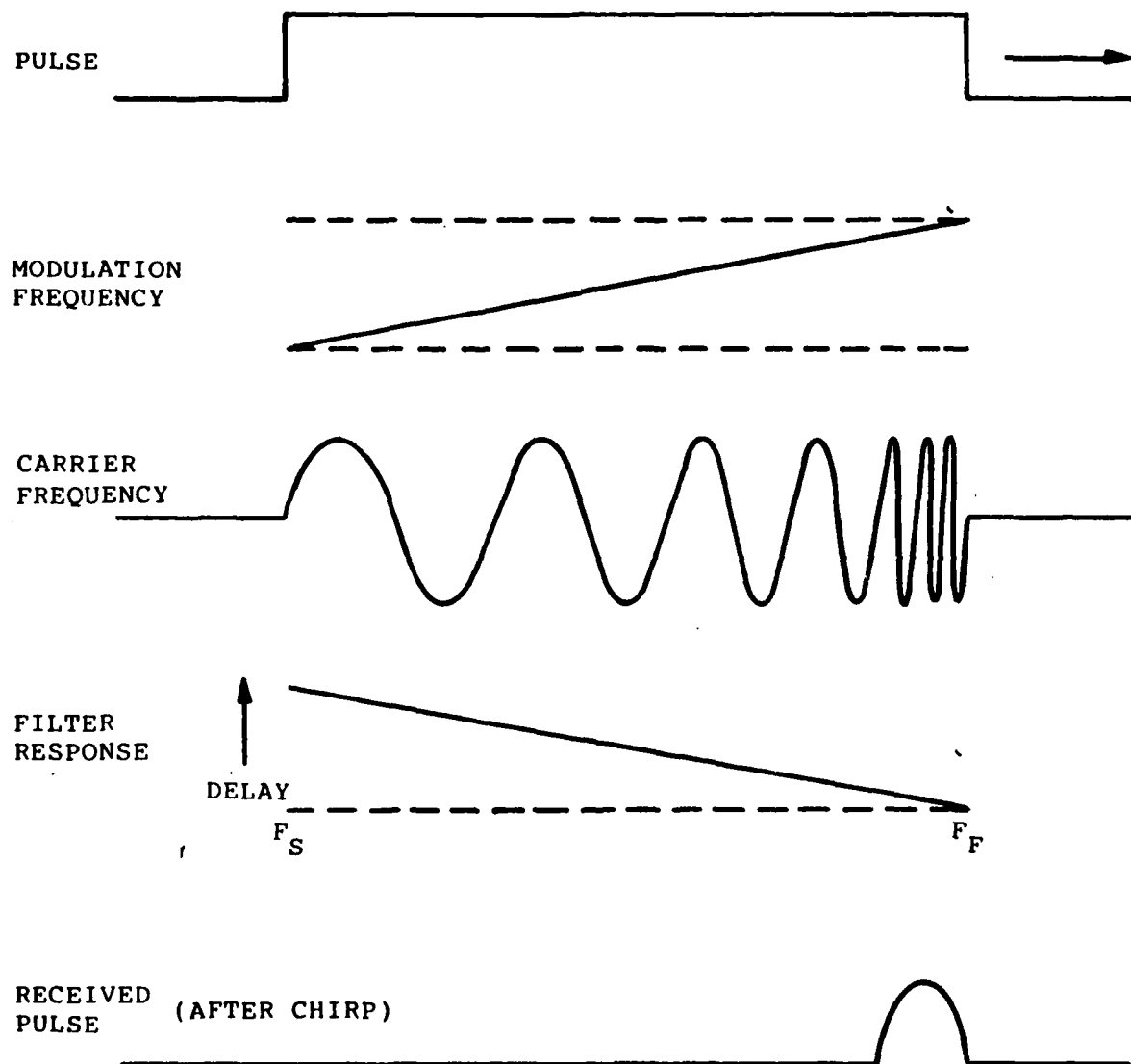
Figure 3.8-2   CHIRP RADAR DIAGRAM

3-57

If a chirp radar system is to be simulated, the aperture response of the chirp waveform must be determined and a beamspread algorithm can then be used to simulate the aperture response.

A second method divides the pulse into a number of bins and the phase or frequency is shifted from bin to bin. Although many ways of achieving this have been proposed and tested, this report only introduces the phase shifted Barker coded technique. This method seems to be most favored by modern radar designers. Barker codes were developed for the communication industry; Barker codes for 2, 3, 4, 5, 7, 11, and 13 elements have been discovered and searches for larger codes continue. Barker codes can be combined, or combined with other codes, to get higher resolution and lower side lobes. The Hughes F-15 demonstration radar has a programmable pulse compression that has a limit of 169 (13 times 13). The code in the F-15 demonstration radar could be a nested Barker code. Pulse compression codes for radar on the F/A-18 aircraft are not known at this time. Two references for Barker codes for radar use are "Principles of High-Resolution Radar" by August W. Rihaczek, and "Radar Handbook" by Merrill I. Skolnik.

Figure 3.8-3 is a diagram of autocorrelation of a single pulse and a 13-element Barker coded pulse. By phase coding 13 pulses, resolution is increased by 13 and 12 side lobes with amplitude of 1/13 are generated. To simulate a Barker code of 13 requires a beamspread algorithm that operates in the range direction. The designer of high resolution radar systems generally matches range resolution with azimuth resolution. If the radar being simulated does not have equal range resolution and azimuth resolution, the simulator designer must take this into account. Additionally, if range and azimuth side lobes can be seen in the actual SAR system, the side lobes must be simulated.

There is one area of pulse compression simulation that requires particular attention. Solution is needed for pulse compression simulation when the radar overloads or is jammed. Figure 3.8-4 is a SAR photograph that is only overloaded by 6dB. The two photographs indicate that when SAR overloads, the results are quite dramatic. A cross is formed around the target; the azimuth
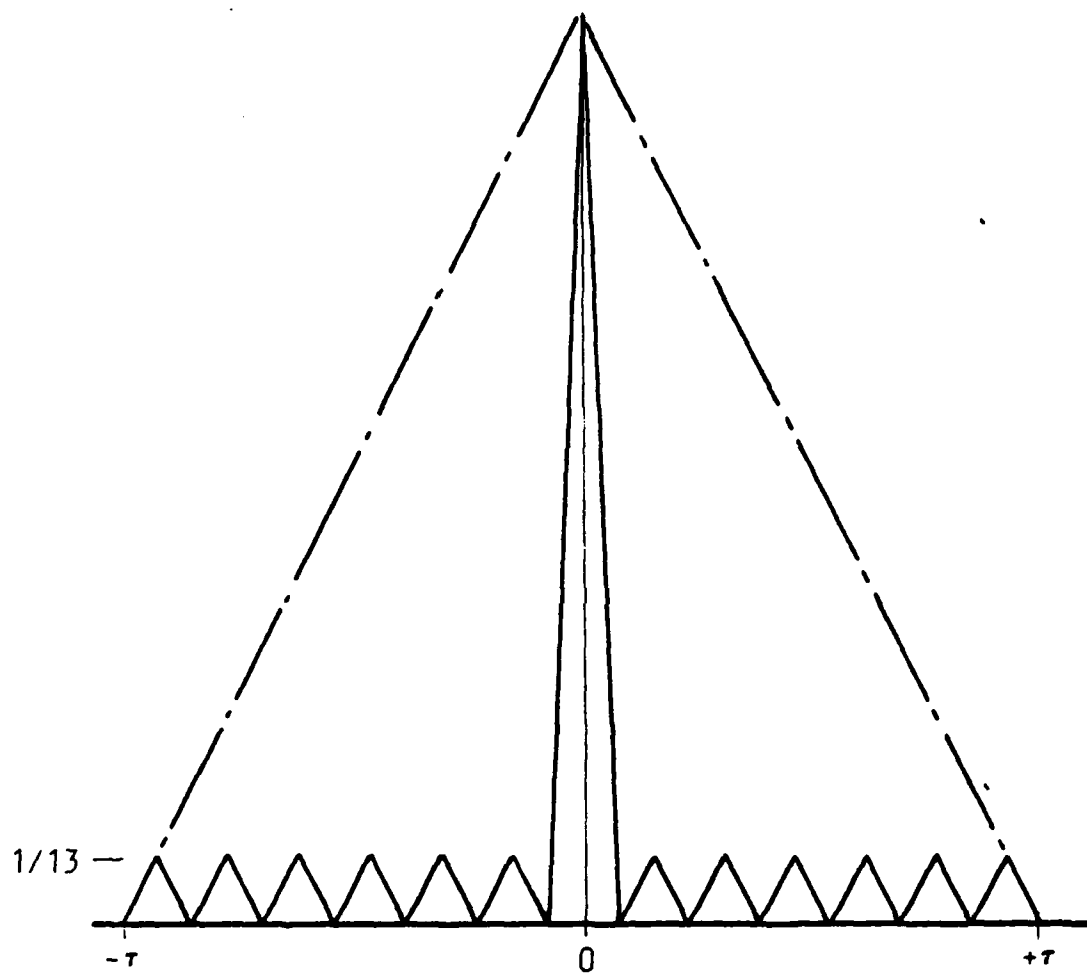
Figure 3.8-3 AUTOCORRELATION OF A SINGLE PULSE AND
13-ELEMENT BARKER CODE

HARD/SOFT TARGET SWITCH

These SAR maps of Santa Rosa Island show how scenes with very large dynamic range can be operator controlled using a repositioned dynamic range window. This feature gives the operator control of the radar return to allow him to optimize hard targets which reflect large amounts of radar energy such as bridges, tanks, ships or other objects with large amounts of metal, or to optimize the radar for soft targets with small reflectivities such as wooden buildings or grassy areas.

The map on the left, below, shows large azimuth and range sidelobes from an unusually large reflector. The dark water return has been properly used by the radar to control the front end gain up to the point where the isolated bright target is saturated. This is the normal "soft" target gain setting designed to optimize targets at the low end of the system dynamic range.

The map on the right shows how the range and azimuth smearing are eliminated by the operator choosing the "hard" target gain setting. An additional 6 dB of attenuation at the front of the radar IF amplifier is inserted to bring this hard target out of saturation. This allows the target of interest to be better resolved at the expense of details in the low end of the dynamic range.

Hard target gain setting

1.3 nmi patch map (1.7 ft resolution)

Soft target gain setting
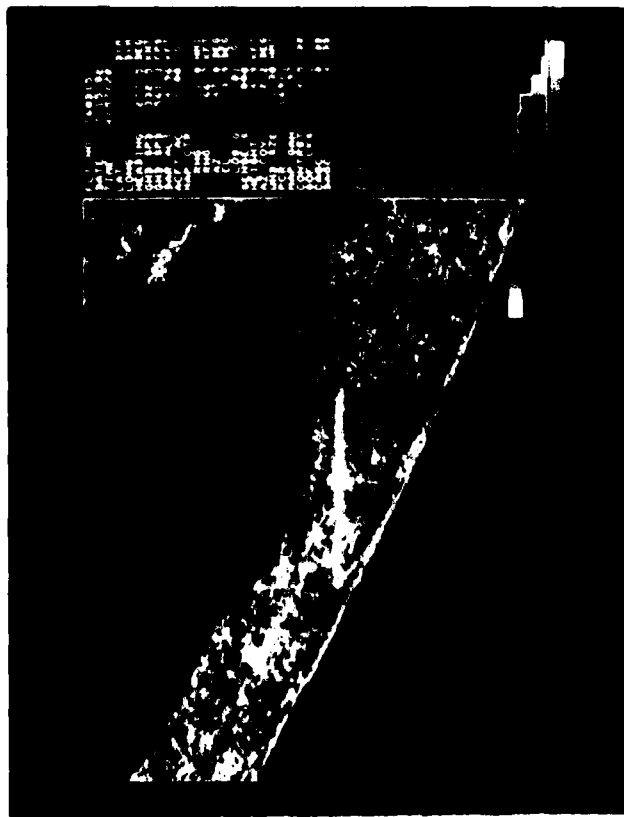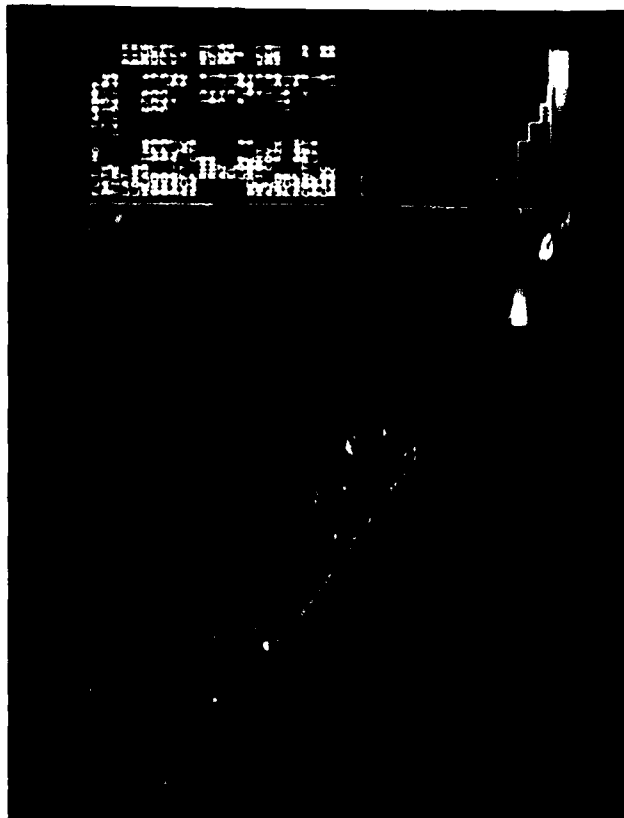
1.3 nmi patch map (1.7 ft resolution)

portion consists of a smear that is one-third of the picture. The range portion consists of a smear of one-fourth of the picture, plus dots that cover the full picture. The photograph was made from subpictures and only the center subpicture was overloaded in the azimuth direction. Since the range saturation effect extended across the picture, the radar pulse covered more than one-half the picture.

The saturation effect in the range direction will cover twice the pulse width distance. Figure 3.8-4 illustrates why overloads and jamming must be simulated. Simulation algorithms for overloads and jamming must be custom fitted to each combat radar.

4.0 RADAR SIMULATION

4.1 RADAR EQUATION MECHANIZATION

The basic radar equation was formulated in the early history of radar. Many modifications and refinements to the basic equation have been made, but the basic equation remains the best starting point for examining radar simulation. A good representative radar equation is the one developed by D.E. Kerr and "The Radar Handbook" by Merrill Skolnik also has an excellent discussion of radar equations. The radar equation given by Kerr is included here:

$$\frac{P_R}{P_T} = \frac{G_{TA} \cdot G_{RA} \cdot T_{CS} \cdot \lambda^2 \cdot P_{FT}^2 \cdot P_{FR}^2}{(4 \cdot \pi)^3 \cdot R^4} \qquad (4.1.1)$$

Adding the effects of atmospheric/weather attenuation and radar receiver gain functions to (G_C) Equation 4.1.1 generates Equation 4.1.2. The terms in Equation 4.1.2 are also regrouped.

$$\frac{P_R}{P_T} = \left[\frac{G_{TA} \cdot G_{RA} \cdot \lambda^2 \cdot G_C}{(4 \cdot \pi)^3 \cdot R^4} \right] \cdot \left[P_{FT}^2 \cdot P_{FR}^2 \right] \cdot \left[T_{CS} \right] \qquad (4.1.2)$$

Where

P_T = transmitted power

P_R = received power

G_{TA} = transmitter antenna gain

G_{RA} = receiver antenna gain

P_{FT} = pattern factor along the transmitting path

P_{FR} = pattern factor along the receiving path

T_{CS} = target cross section

G_C = gain function due to gain control, atmospheric/weather attenuation

λ = wavelength

R = range

Equation 4.1.2 now consists of three basic parts. Part one: the gain factor due to range attenuation, receiver gain, atmospheric/weather attenuation, and receiver gain control. Part two: the attenuation due to the pattern of the radar antenna (this factor varies from one to zero). Part three: the reflectivity of the target.

In part one of Equation 4.1.2, if the gain control of the radar receiver were perfect, this part of the equation will be unity until the receiver gain limit is reached (at this time we will not cover the signal-to-noise problem). It is obvious that the gain function (G_c) varies with radar systems. Since this study is not directed to a single radar system, the gain function of part one will be considered to be unity multiplied by an unknown radar system function.

Part two of Equation 4.1.2 modifies the returns for target radars and synthetic aperture radars and is also responsible for the beamspread in ground mapping real aperture radar. This function modifies the return relative to its position in the beam. Since ground mapping real aperture radar returns are the sum of all targets within the beam, the function spreads out the returns. In fire control radar, the position of the target in the antenna pattern determines the return level. SAR has two apertures that determine performance. The first aperture is the real antenna aperture which determines the footprint (the pattern factor) of the return. The second aperture (the SAR aperture) determines the resolution. The upper left section of Figure 4.1-1 is an example of a SAR picture and the effects of an antenna pattern. Note the radar antenna was positioned 11 times to obtain the SAR picture. The scalloped window blind effect is due to antenna pattern.

Part three of Equation 4.1.2 (the radar target cross section) is a very pertinent function for radar simulation. The radar target cross section consists of six variables. Hence the radar target cross section can be expressed as:

LOW SQUINT ANGLE

The two 42 ft resolution maps on the left clearly show the launch pads, runways, and an AAA site simulated at the Southeast Tactical Range, located in the Superior Valley of California. The upper map was constructed with a left squint angle of 13 to map center and cover azimuth angles from 8 to 22.5. The lower map was constructed with a left squint angle of 36. These maps show that the radar is designed to provide uniform map quality at azimuth angles from the lower limit of 8 to a maximum angle of 50.

A row of 19 ex-TWA Convair 880's and one Convair 990 parked on a ramp at Mojave Airport is contained in the 8.5 ft resolution map (lower right). This map was constructed with a right squint angle to map center of 16.2. Good map quality is maintained from 12.5 to 20 azimuth angle.

Figure 4.1-1 LOW SQUINT ANGLE

Mojave Airport — Parked Aircraft
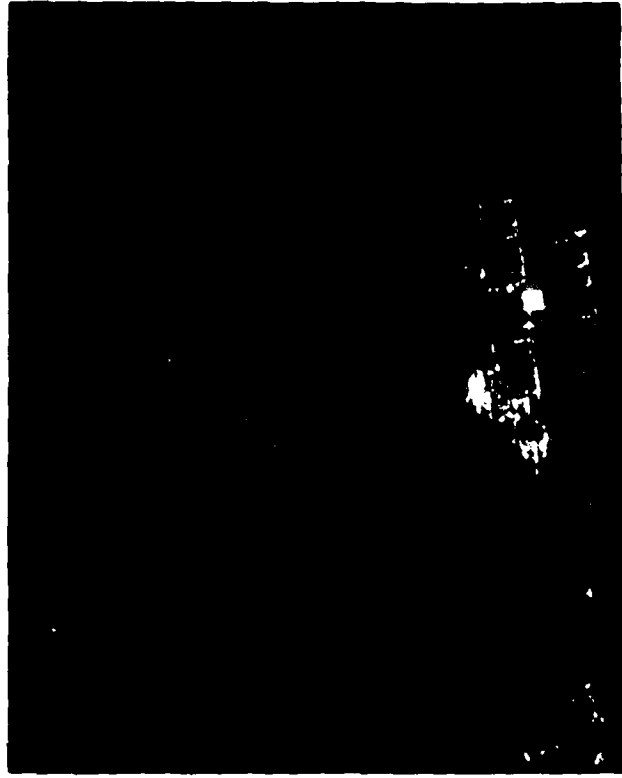
Launch Site — Southeast Tactical Range
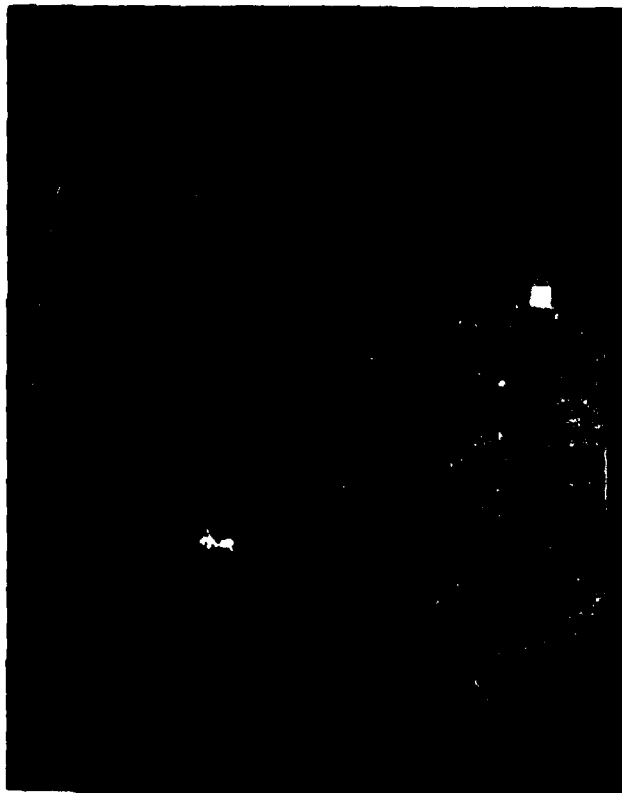
$$T_{CS} = H \cdot W \cdot A_{SP} \cdot O \cdot T_{REF} \cdot S_E \qquad\qquad (4.1.3)$$

Where

H   = height

W   = width

A_{SP} = aspect

O   = orientation

S_E = shadow effect

T_{REF} = target reflectivity

The functions that make up the radar target cross section are analyzed in later text. First, an evaluation is made of how the components of the equation determine the range target cross section. Height is modified by the shadow effect. For example, if one building blocks 90 percent of another building, the shadow effect would be 0.1. Thus the effective height would only be ten percent. If a target were wider than a pixel, then the width would be the width of a pixel. If the target is less than the width of a pixel, the width is then less than a pixel.

Aspect is the angle at which the radar beam intercepts the target or the grazing angle. The aspect angle is a function of the depression angle and the face angle of the target, with respect to the horizon.

Orientation is a function of the azimuth angle that the radar beam intercepts in the target. An example of this function could be mapping that includes an outdoor movie screen. Because the front of the screen slants downward, the reflected light is directed toward the earth and little energy is reflected. At a 90 degree angle, the cross section is small and little energy is reflected. The back side of the screen is tilted toward the aircraft and is a textured surface; thus, the radar return is strong. T_{REF} is the actual reflectance of the target. Every surface material has a different reflectance level; for instance, metal is highly reflective and grass is almost non-reflective. In simulated radar, the reflectance value is derived from the data base and is not calculated.

4.2 ATTENUATION RESULTING FROM ORIENTATION

DMA Level I, Level II, Level V, and Level X data bases have provisions for coding radar returns as a function of azimuth. Point features have the maximum return specified on 11.25 degree increments from true north, or specified as omnidirectional. Linear feature coding of returns can be unidirectional, bidirectional, and omnidirectional. Unidirectional is defined as a reflective surface on the right side of a line from Point 1 to Point 2. Bidirectional is defined as a reflective surface on both sides of the line from Point 1 to Point 2. Omnidirectional is defined as a surface with equal reflectivity on all sides.

Simulation of orientation is calculated to the nearest 11.25 degree increment. The feature identification code number (FICN) and orientation are then used to obtain a reflectance multiplier from a look-up table. A large number of features will have identical orientation functions.

4.3 ASPECT

One of the six functions that determine the cross section of the radar is the aspect or grazing angle. A simulation algorithm can be derived that is accurate and easily implemented. The grazing angle return function is determined by the grazing angle (or the angle of incidence), radar wavelength, radar beam polarization, amount of moisture on the target surface, and by surface vegetation and cultural features. A simplified algorithm for aspect is a determination of grazing angle and target type and a look-up table entry of the proper value of the multiplier in order to obtain the reflectance value of the target.

An infinite number of look-up tables could be generated for each set of aspect conditions, but only a few tables are actually needed. Simulated seasonal effects are generated from aspect tables. For instance, a field of summer grass reflects some return at all grazing angles. In winter, if heavy snow had covered the same area, forward scatter of the return would be increased and back scatter return would be decreased. In some circumstances the area could disappear from the radar screen.

Figure 4.3-1 is a generalized curve versus grazing angle. The generalized curve changes very little in the center medium grazing angle. At a high grazing angle the curve has a high return, referred to as cliff effect or vertical incidence. As the grazing angle approaches zero, return approaches zero. This grazing angle effect is responsible for hilltop and distance fading and for loss of resolution at long ranges. In simulating radar, all grazing angles are of concern, but high and low grazing angles should receive greater emphasis and attention.

Terrain aspect effects are generated from the elevation data base. Any data base limitations restrict aspect effects. For example; consider simulation of a flat plane, a 300-foot vertical cliff and continuing flat plain, viewed at a low angle. The Defense Mapping Agency Aerospace Center (DMAAC) elevation data base is on 300-foot posts. A 300-foot cliff will give a 45 degree aspect angle with this post spacing. If the cultural data base has a cliff feature, the cliff is treated properly; otherwise, the return is treated as a 45 degree aspect angle. Most man-made structures have horizontal or vertical flat surfaces and have the greatest returns when viewed at a low grazing angle (perpendicular or upright). Figure 4.3-2 is a diagram of a grazing angle curve for a feature with a flat roof, and Figure 4.3-3 is a diagram of grazing angle curve for a feature with a peaked roof. Conversely, a rounded and highly reflective roof is almost invisible to radar.

An aspect algorithm consists of the sum of the depression angle and the slope of the terrain. If the target is a cultural object, terrain slope is set to zero. Figure 4.3-4 is a vertical aspect diagram.

The equation for the slope in Figure 4.3-4:

$$\sigma = \tan^{-1}\left[\frac{E2 - E1}{R_{DG}}\right] \qquad (4.3.1)$$

Where

σ = terrain slope of a line connecting E1 & E2

R_{DG} = delta ground range

E2 & E1 = two adjacent elevation posts
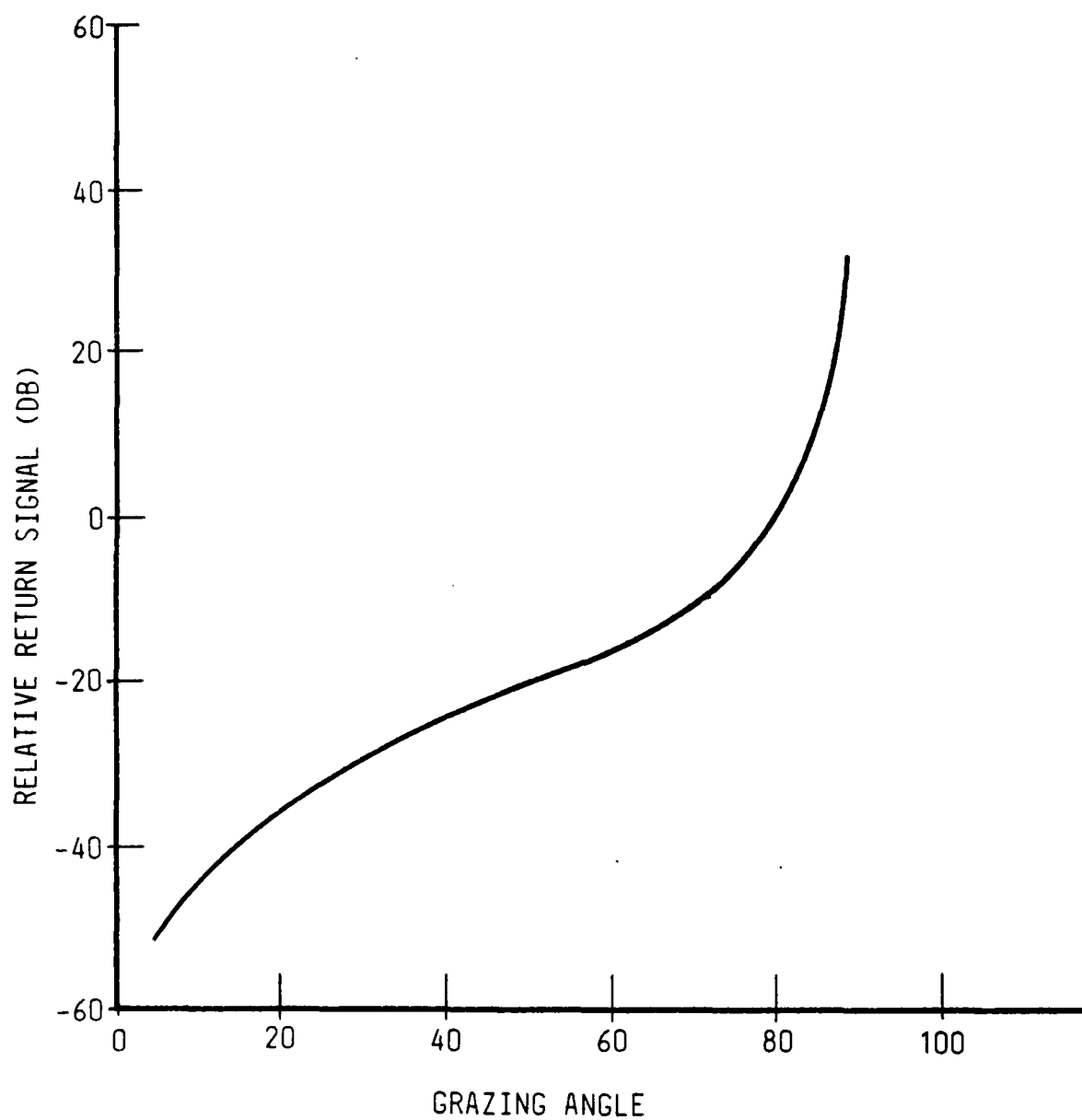
Figure 4.3-1   GRAZING ANGLE FUNCTION FOR TERRAIN
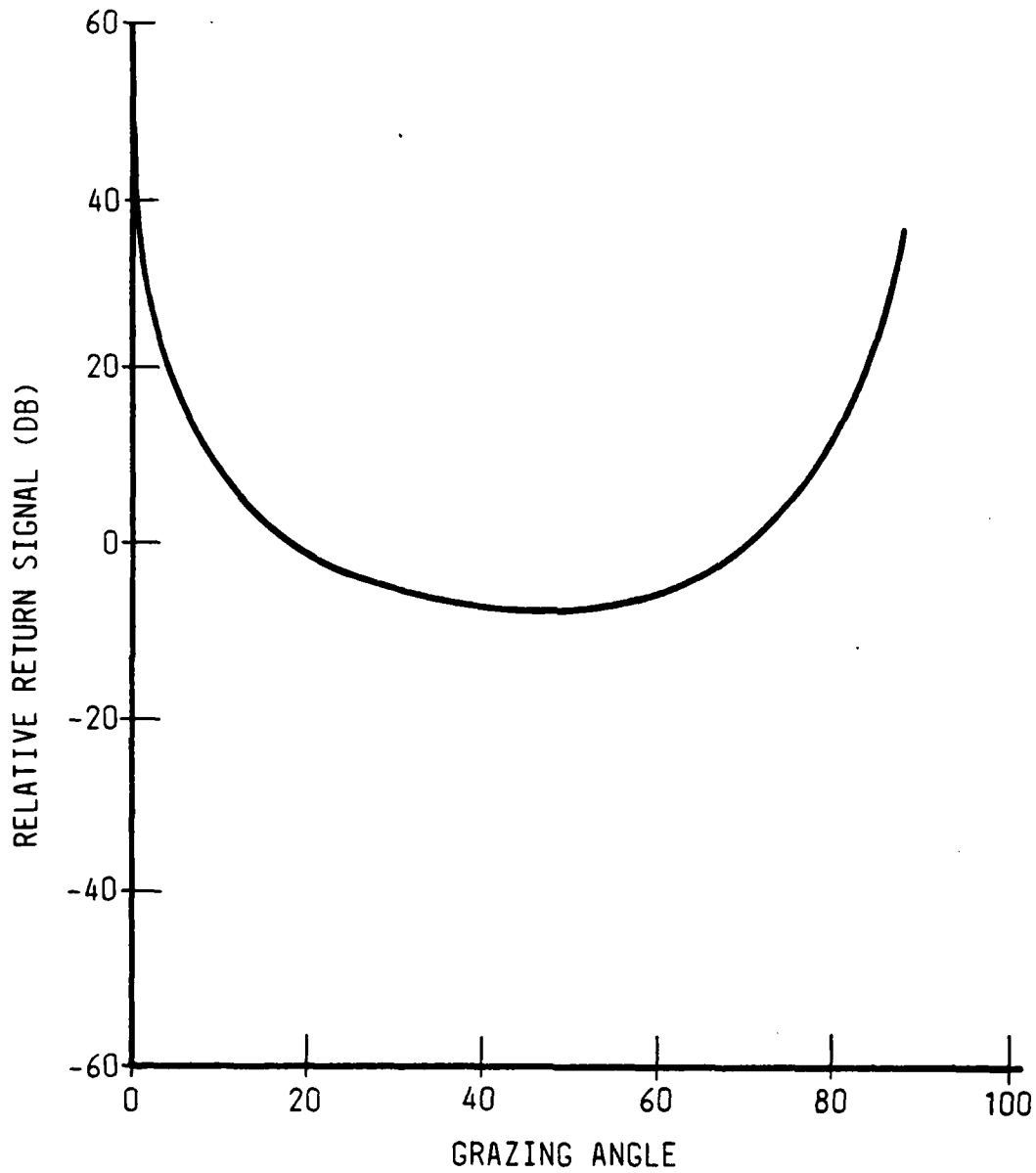
Figure 4.3-2 GRAZING ANGLE FUNCTIONS FOR A FLAT ROOF
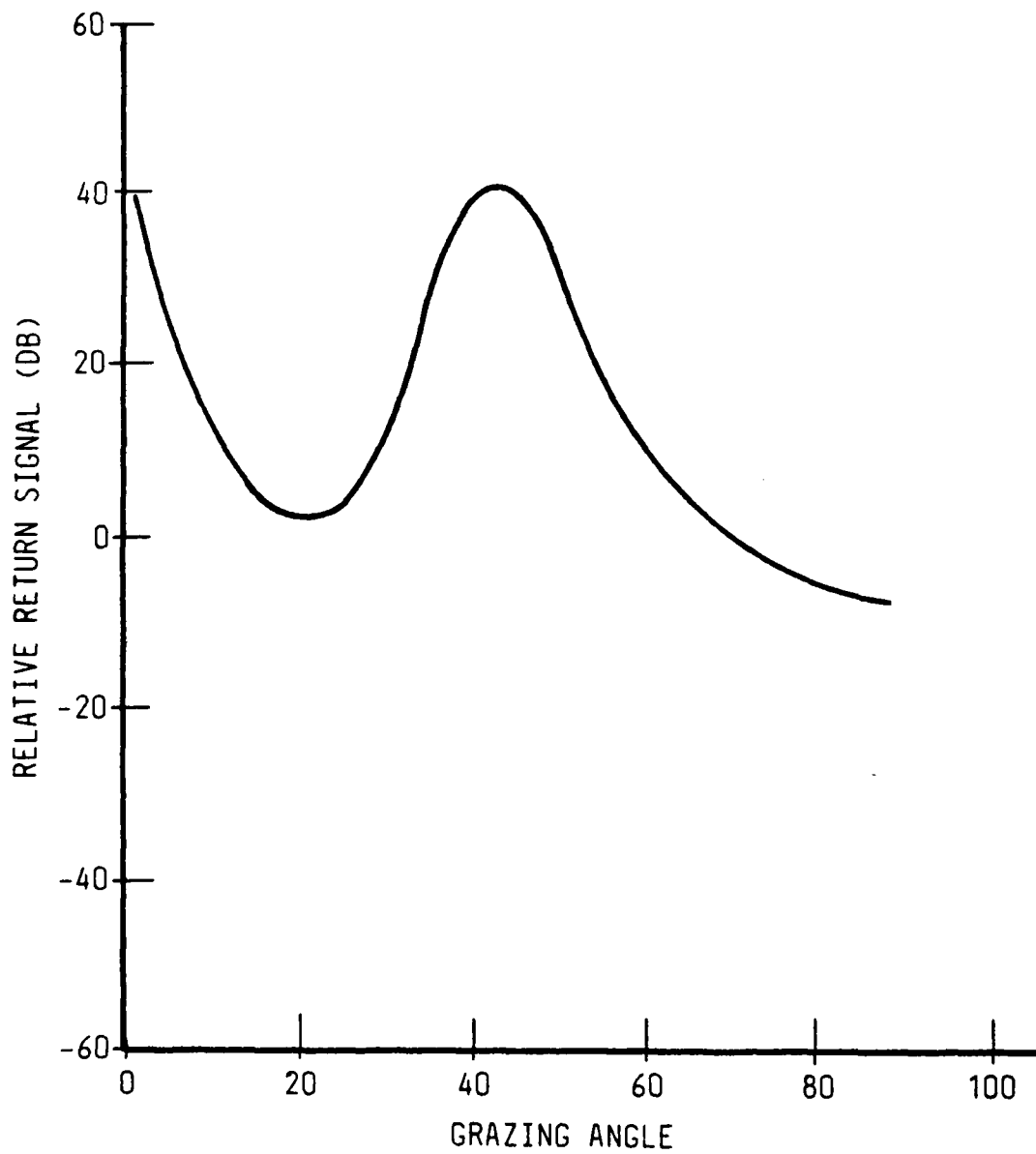
Figure 4.3-3 GRAZING ANGLE FUNCTION FOR A PEAKED ROOF
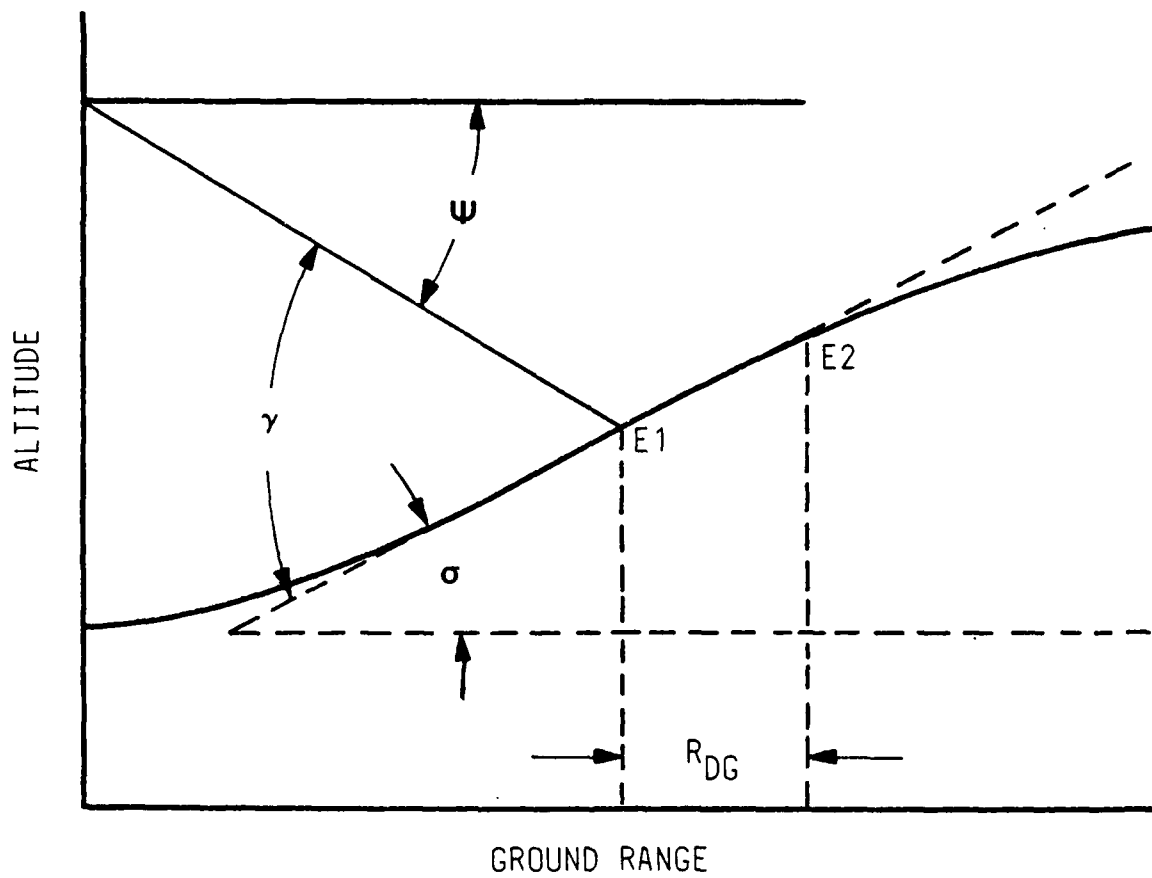
Figure 4.3-4   VERTICAL ASPECT DIAGRAM

Depression angle calculation becomes more complex if earth curvature is considered. Figure 4.3-5 is a diagram of geometry used to calculate the depression angle. Value of the earth's radius can be adjusted to accommodate the earth's atmospheric refraction; a commonly used value is four-thirds. By using simple geometry, the equation for depression angle (Equation 4.3.2) can be obtained.

$$\psi = \tan^{-1}\left[\frac{H + R_{EC} - \cos(\xi) \cdot R_{EC}}{\sin(\xi) \cdot R_{EC}}\right] \qquad (4.3.2)$$

simplifying equation 4.3.2 gives

$$\psi = \tan^{-1}\left[\frac{H}{R_{EC} \cdot \sin(\xi)} + \tan\left(\frac{\xi}{2}\right)\right] \qquad (4.3.3)$$

Where

R_{EC} = modified earth radius for atmospheric refraction

ξ = ground range angle

The grazing angle for terrain is:

$$\gamma = \sigma + \psi \qquad (4.3.4)$$

The grazing angle for culture objects is:

$$\gamma = \psi \qquad (4.3.5)$$

Where

γ = grazing angle

The SARS used in combat aircraft have the capability of generating images at large depression angles. Most SAR systems are limited to 65 degrees or less. This means that a look-up table from 0 to 65 degrees for culture targets would suffice. A terrain look-up table from 0 to 65 degrees would match the culture look-up table. Computer-generated images have shown that one-quarter degree increments are sufficient for the look-up table.
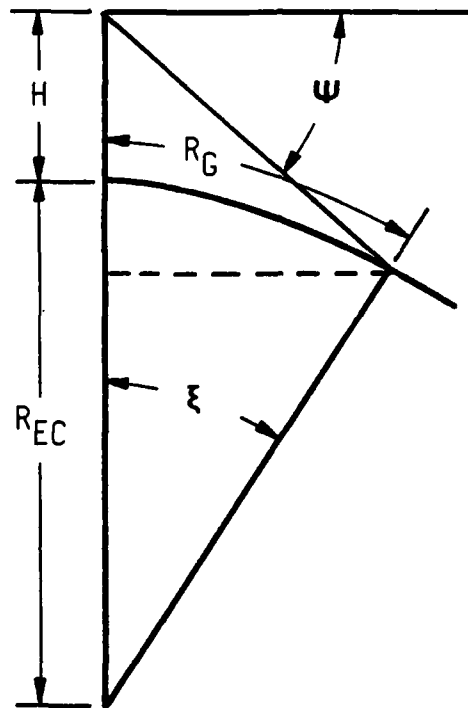
Figure 4.3-5 DIAGRAM FOR DEPRESSION ANGLE

Equation 4.3.3 can be simplified at short ground ranges by ignoring the curvature of the earth. Equation 4.3.6 is this simplification.

$$\psi = \tan^{-1}\left[\frac{H}{R_G}\right]$$
(4.3.6)

It has been brought out that reflectance is a function of the grazing angle and the orientation of the target. The grazing angle can be calculated for all targets but orientation can only be calculated when the orientation is in the data base. Level I and Level II data bases code the orientation for point and linear features. Level V data bases include orientation for point, linear, and aerial features. These features can be randomly selected to have either north/south orientation or east/west orientation. This function is called the Homestead Law Effect.

Farms in the mid-West and also the central valley of California were laid out on north/south, east/west grids. Farmers plow parallel to these grid lines and radar returns are stronger at the cardinal points of the compass. To determine the number of aspect and orientation look-up tables that are required, each feature specified in the DMAAC data base must be analyzed.

4.4 SLANT RANGE AND DEPRESSION EFFECTS

Two important parameters in radar simulation are slant range and depression angle. Slant range is used to map pixels from the ground range scan into the display scan. The depression angle is used to calculate both the aspect effect and the shadow effect. Figure 4.4-1 is a diagram used to derive equations for slant range and depression angle.

The earth's atmosphere causes a certain amount of refraction of the radar signals and a simple method of simulating this refraction is to increase the earth radius during simulation calculations. A value most often used is
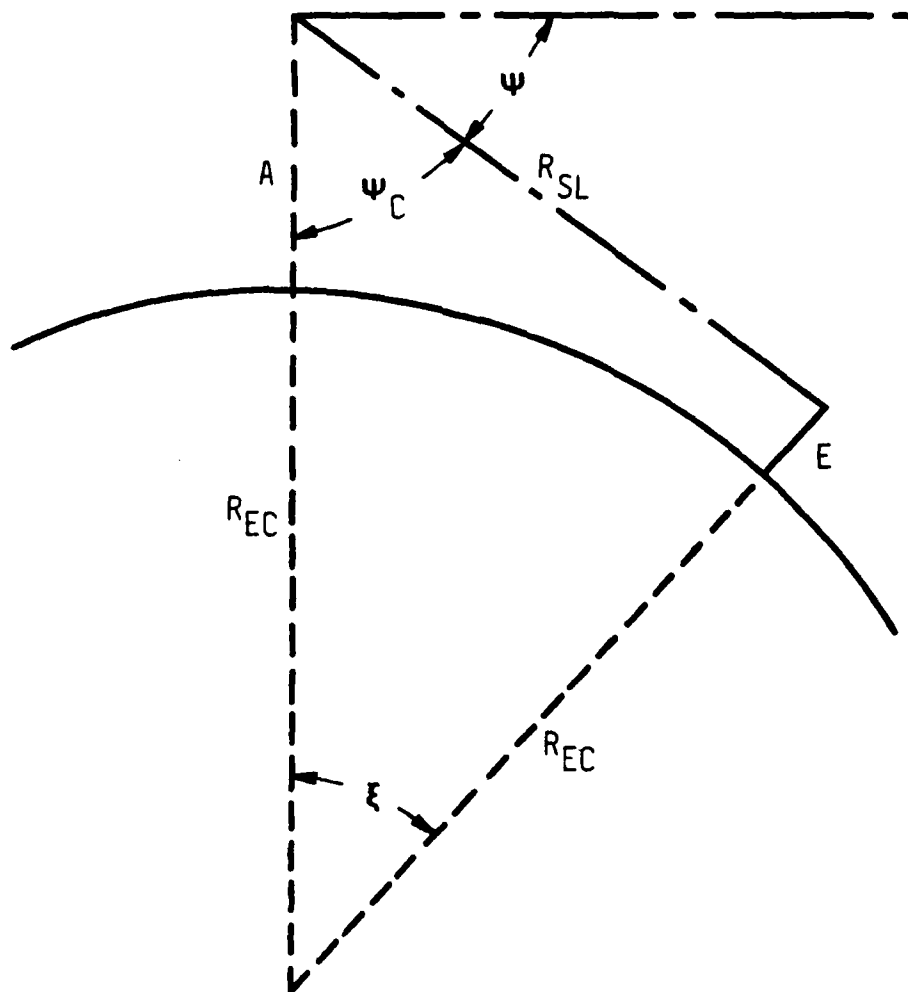
Figure 4.4-1   SLANT RANGE AND DEPRESSION ANGLE DIAGRAM

four-thirds. In the equations, the modification of the earth's radius will be referred to as R_{EC}. The range angle is related to range by Equation 4.4.1. Figure 4.4-2 is a diagram for deriving equations in slant range/top of structure mapping.

$$\xi = \frac{R_G}{60} \cdot K_E \tag{4.4.1}$$

Where

K_E = earth radius modification factor

The law of cosines can be used to solve for slant range in Figure 4.4-1.

$$R_{SL} = \left[\left(R_{EC} + A\right)^2 + \left(R_{EC} + E\right)^2 - \left(R_{EC} + A\right) \cdot \left(R_{EC} + E\right)\cos(\xi) \right]^{1/2} \tag{4.4.2}$$

By using the law of sines and the slant range, the depression angle can be derived.

$$\psi_C = \sin^{-1}\left[\sin(\xi) \cdot \frac{(R_{EC} + E)}{R_{SL}} \right] \tag{4.4.3}$$

Therefore

$$\psi = \cos^{-1}\left[\sin(\xi) \cdot \frac{(R_{EC} + E)}{R_{SL}} \right] \tag{4.4.4}$$

Noting that $\psi_C + \psi = 90^{\circ}$

Where

ψ_C = depression angle complement

By letting the line E remain parallel to line A, more simple equations can be derived, although with a slight error. The depression angle is given by Equation 4.4.5 and the slant range is given by Equation 4.4.6.

$$\psi = \tan^{-1}\left[A - E + \frac{R_{EC}[1 - \cos(\xi)]}{R_{EC}} \cdot \sin(\xi) \right] \tag{4.4.5}$$

WHERE

R_{SLT} = SLANT RANGE AT THE TOP OF THE STRUCTURE

R_{SL} = SLANT RANGE AT THE BOTTOM OF THE STRUCTURE

Ψ = DEPRESSION ANGLE
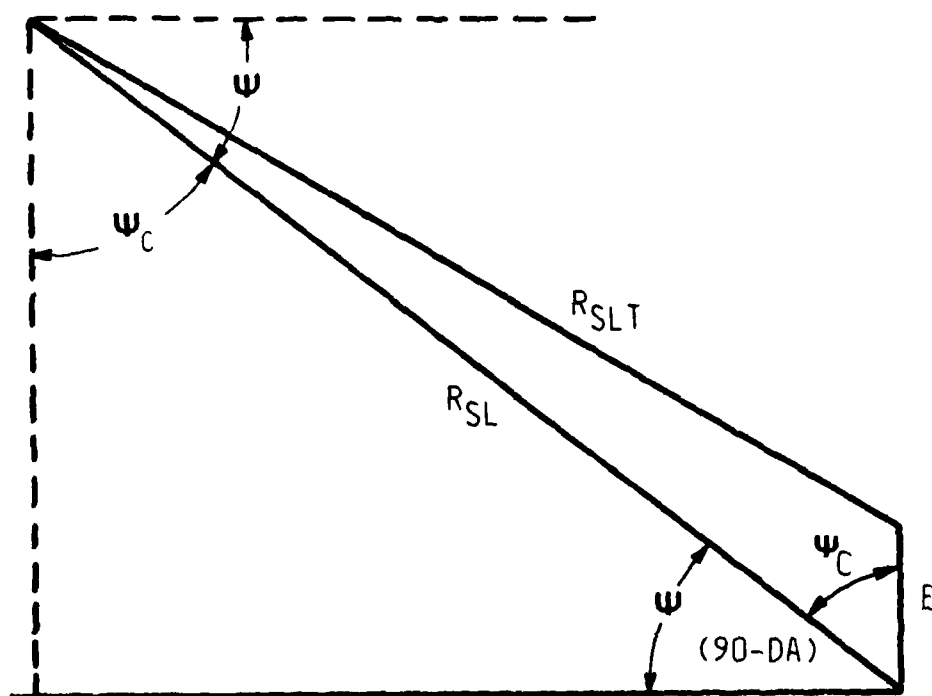
Figure 4.4-2 SLANT RANGE MAPPING DIAGRAM: TOP OF STRUCTURE

Where

E = elevation

$$R_{SL} = R_{EC} \cdot \frac{\sin(\xi)}{\sin(\psi)} \qquad (4.4.6)$$

The top of a building will map toward the aircraft. An equation will be derived to show what happens when mapping high structures. The equation will express the error from the bottom to the top of the building. Figure 4.4-2 is the diagram that will be used.

One task is to find the difference in lengths between lines R_{SL} and R_{SLT}. By the law of cosines, Equation 4.4.7 can be derived:

$$R_{SLT} = \sqrt{E^2 + R_{SL}^2 - 2 \cdot E \cdot R_{SL} \cdot \cos(\psi_c)} \qquad (4.4.7)$$

Expanding Equation 4.4.7 by using the binomial series gives:

$$R_{SLT} = R_{SLT}\left[1 + \frac{E^2}{2R_{SL}^2} - \frac{2 \cdot E \cdot R_{SL}\cos(\psi_c)}{2R_{SL}^2}\right] \qquad (4.4.8)$$

Since E^2/R_{SL}^2 is much less than one and $\cos(\Psi_c)$ is equal to $\sin(\Psi)$ Equation 4.4.8 can be written:

$$\qquad (4.4.9)$$

$$R_{SL} \approx R_{SL} - E \cdot \sin(\psi)$$

Taking the difference between the slant range at the bottom of a structure and the top of a structure will give the slant range mapping error at the top of a structure.

$$R_{FM} \approx - E \cdot \sin(\psi) \qquad\qquad (4.4.10)$$

Where

R_{FM} = range forward mapping due to elevation

Equation 4.4.10 shows that the error in slant range mapping at the top of a structure is directly related to the height of the structure and the depression angle.

To get an idea of this mapping of tall structures, two examples will be given.

Example One

Depression Angle	15 Degrees
Range	10 Nautical Miles
Structure Height	1200 Feet
Pixel Size	10 Feet
Resolution	20 Feet
Slant Range Error	310 Feet
Pixels Mapped Into	31 Pixels

Example Two

Depression Angle	15 Degrees
Range	10 Nautical Miles
Structure Height	150 Feet
Pixel Size	50 Feet
Resolution	100 Feet
Slant Range Error	38.8 Feet
Pixels Mapped Into	2 Pixels

4.5 SHADOWS

The radar shadow algorithm is one of the most important algorithms for SAR simulation. The depression angle of SAR is quite low; thus, in any SAR radar display there will be large shadows. For proper simulation, the shadow algorithm must realistically duplicate the actual radar. Three shadow algorithms will be presented and defined. Choice of algorithm is based on complexity versus realism.

The first algorithm that will be presented is the on/off shadow algorithm. This was the first and most frequently used algorithm in radar simulation. Figure 4.5-1 is a diagram of this algorithm. The term on/off algorithm is used because the target either has a full reflectivity or has none. The algorithm is simple. The algorithm saves the smallest depression angle and compares the following return depression angle with the saved smallest depression angle. When the return depression angle is greater than the reference angle, the return reflectance is set to zero. When the return depression angle is less than the reference angle, the return reflectance is unchanged; the return depression angle replaces the reference angle. At low depression angles this algorithm is not very realistic.

The second shadow algorithm can be called the partial shadow algorithm. This algorithm modifies the radar return as a function of the degree of shadowing of the target. Figure 4.5-2 is a diagram of this algorithm. This algorithm differs from the first shadow algorithm by the addition of a shadow function that lies between the on/off function. This function modifies the target return by the amount of shadowing. When the target is half-shadowed the target return is reduced by half. An example of how this algorithm increases realism is to look at a village that is observed at a low grazing angle. Only the first row of houses will be fully reflective. All other houses will be partially shadowed by the first row of houses. The partial shadow algorithm greatly increases the realism of radar simulation.
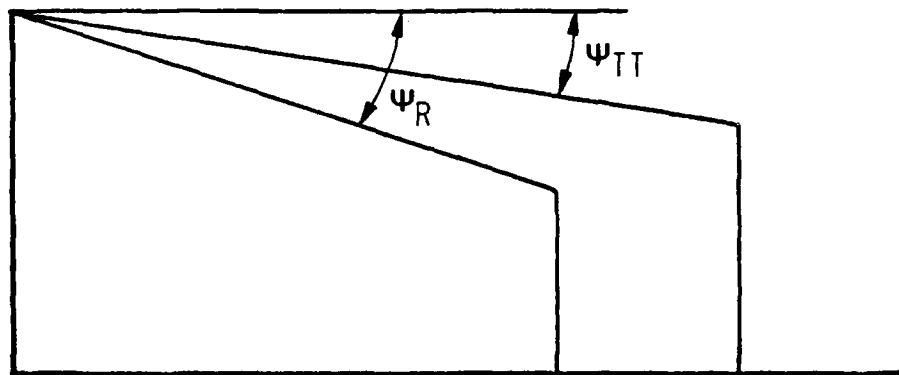
$$T_S = T_{REF} \text{ WHEN } \Psi_{TT} \leq \Psi_R$$

$$T_S = 0 \qquad \text{ WHEN } \Psi_{TT} > \Psi_R$$

Figure 4.5-1 ON/OFF SHADOW DIAGRAM

END
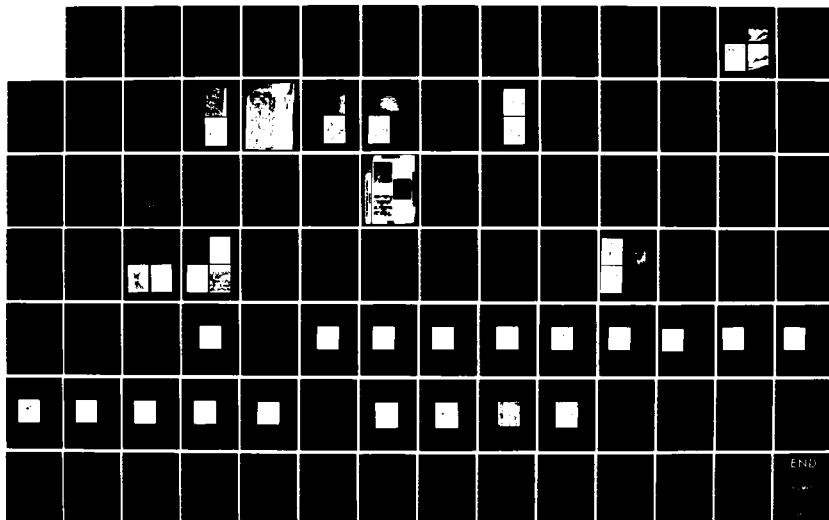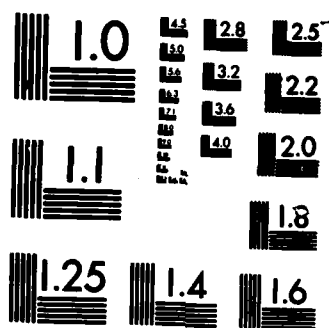
MICROCOPY RESOLUTION TEST CHART

NATIONAL BUREAU OF STANDARDS-1963-A
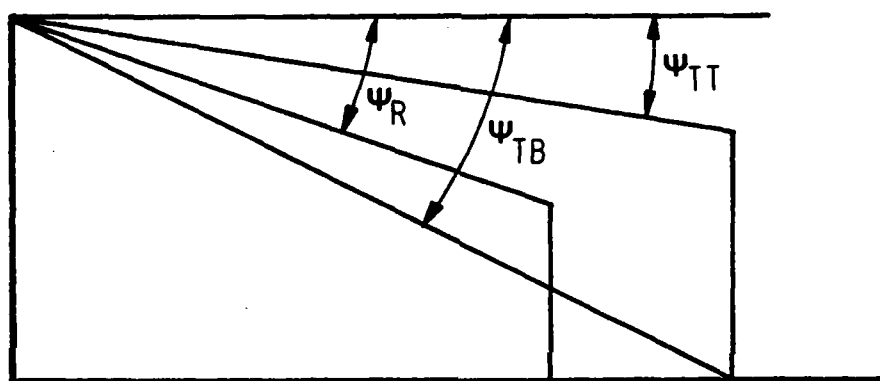
$$T_S = T_{REF} \qquad\qquad \text{WHEN} \quad \Psi_{TB} \leq \Psi_R$$

$$T_S = 0 \qquad\qquad\qquad \text{WHEN} \quad \Psi_{TT} > \Psi_R$$

$$T_S = \left(\frac{\Psi_R - \Psi_{TT}}{\Psi_{TB} - \Psi_{TT}}\right) REF \qquad \text{WHEN} \quad \Psi_{TT} < \Psi_R < \Psi_{TB}$$

Figure 4.5-2   PARTIAL SHADOW ALGORITHM

The third algorithm is used when SAR simulation is used for tactical training that requires a high degree of navigational accuracy. Literature that is available on the use of SAR in a tactical situation suggests that bridges, towers, and piers are some of the most important radar features to update the inertial platform. Since bridges are above terrain, a bridge does not shadow from the terrain level to the top of the bridge, but rather from the bottom of the bridge to its top. This means that for proper shadowing a more complex shadowing algorithm must be used. Figure 4.5-3 is a diagram of this algorithm. The data base must supply the top and bottom bridge elevations. This algorithm provides the proper signatures of bridges and any target that has an overhang.

Three algorithms for the radar shadow have been presented. The choice of algorithm for implementation is a matter of cost versus realistic SAR simulation. There are more complex shadow algorithms that could have been presented, but the more complex algorithms deal with radars (i.e., naval warship signatures) that are not as close to being operational as SAR systems.

One important fact that should be emphasized is that in all shadow algorithms for SAR simulation, shadow calculations must be performed from the nadir point to the end of the scan. An example of this is a one square mile patch scan at a 40 mile range. All of the SAR simulation algorithms operate only on the one mile patch except the shadow algorithm. The shadow algorithm operates on 40 times as much elevation data. Since tactical aircraft are going to fly as low as possible, low level SAR simulation is essential.
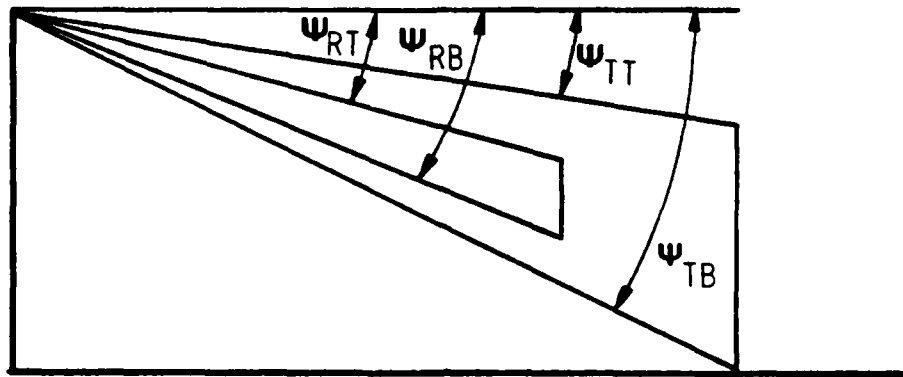
$$T_S = T_{REF} \qquad\qquad \text{WHEN} \quad \Psi_{TB} < \Psi_{RT}$$

$$T_S = \left[\frac{\Psi_{RT} - \Psi_{TT}}{\Psi_{TB} - \Psi_{TT}}\right] T_{REF} \qquad \text{WHEN} \quad \Psi_{RT} > \Psi_{TT}$$

$$T_S = \left[\frac{\Psi_{TB} - \Psi_{TT} - \Psi_{RB} + \Psi_{RT}}{\Psi_{TB} - \Psi_{TT}}\right] T_{REF} \qquad \begin{array}{l} \text{WHEN} \quad \Psi_{TT} < \Psi_{RT} \\ \text{WHEN} \quad \Psi_{RB} < \Psi_{TB} \end{array}$$

$$T_S = \left[\frac{\Psi_{RT} - \Psi_{TT}}{\Psi_{TB} - \Psi_{TT}}\right] T_{REF} \qquad \begin{array}{l} \text{WHEN} \quad \Psi_{TT} < \Psi_{RT} \\ \text{WHEN} \quad \Psi_{RB} > \Psi_{TB} \end{array}$$

$$T_S = 0 \qquad\qquad \text{WHEN} \quad \Psi_{TT} \geq \Psi_{RB}$$

Figure 4.5-3   BRIDGE SHADOW ALGORITHM

5.0 SAR ANOMALIES AND SPECIAL EFFECTS

5.1 MOVING TARGETS

A surprising phenomenon of synthetic aperture radar that does not occur in real aperture radar is the mapping characteristics of moving objects. In SAR moving objects are mapped at a different location than in RAR but the moving objects leave their shadows. In the simulation of SAR, mapping of moving objects is required. Moving targets of interest could be trucks, tanks, etc. This relocation of moving objects in SAR is a function of the object's relative heading and velocity. The development of an algorithm for simulation is straightforward.

The Doppler frequency is represented by Equation 5.1.1.

$$F_{DS} = 2 \cdot V_{AC} \cdot F / C \tag{5.1.1}$$

Let

V_P be the velocity along the vector $\overline{NP}$ the aircraft nadir point to a point on the ground.

The problem is approached by calculating the Doppler frequency shift for a moving object and finding a stationary location on the ground that will generate the same frequency. Figure 5.1-1 is a diagram of the velocity vectors for the moving object problem. To start, the point of reference will be the nadir point. The velocity V_P along the direction of the nadir point to the ground point P is:

$$V_P = V_{AC} \cdot \cos(\Theta_{VV}) \tag{5.1.2}$$

Equation 5.1.3 relates the moving object velocity to the nadir:
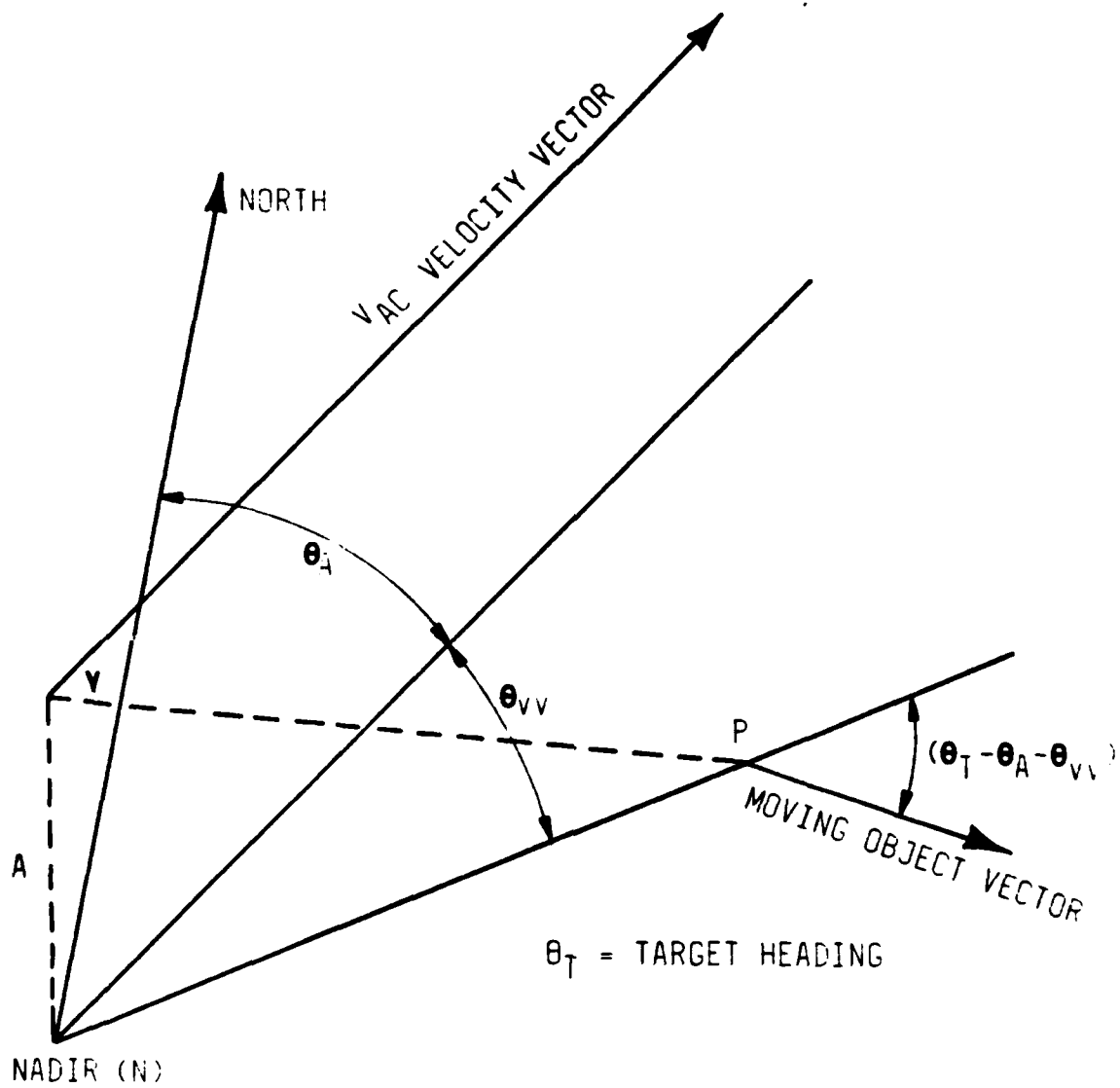
Figure 5.1-1 MOVING OBJECT DIAGRAM

$$V_{MP} = V_{GT} \cdot \cos\left(\Theta_T - \Theta_A + \Theta_{VV}\right) \tag{5.1.3}$$

Where

V_{GT} = Moving target velocity relative to the ground

V_{MP} = Velocity between the aircraft nadir point and a point on the ground extcluding the aircraft velocity

Θ_T = Target heading

Θ_A = Aircraft heading

Θ_{VV} = Angle between aircraft ground track and vector from nadir to the target

Equations 5.1.2 and 5.1.3 can be combined to give the total velocity with respect to the nadir:

$$V_{MP} = V_{AC} \cdot \cos\left(\Theta_{AA}\right) - V_{GT} \cdot \cos\left(\Theta_T - \Theta_A + \Theta_{VV}\right) \tag{5.1.4}$$

Equation 5.1.4 can now be referenced to the aircraft by multiplying the cosine of the depression angle:

$$V_{TAC} = \cos(\psi)\left[V_{AC} \cdot \cos\left(\Theta_{VV}\right) - V_{GT} \cdot \cos\left(\Theta_T - \Theta_A + \Theta_{VV}\right)\right] \tag{5.1.5}$$

Where

V_{TAC} = aircraft velocity relative to a target on the ground

The relative velocity between a point on the ground and the aircraft is:

$$V_{GAC} = V_{AC} \cdot \cos(\psi) \cdot \cos(\Theta_{VV})$$

(5.1.6)

Where

V_{GAC} = aircraft velocity relative to to the ground

Equation 5.1.7 is the result of equating Equations 5.1.5 and 5.1.6 into Equation 5.1.1.

$$V_{AC} \cdot \cos(\psi) \cdot \cos(\Theta_M) = \cos\psi \left[V_{AC} \cdot \cos(\Theta_{VV}) - V_{GT} \cdot \cos(\Theta_T - \Theta_A + \Theta_{VV}) \right]$$

(5.1.7)

$$\Theta_M = \cos^{-1} \left[\cos(\Theta_{VV}) - V_{GT}/V_{AC} \cdot \cos(\Theta_T - \Theta_A + \Theta_{VV}) \right]$$

(5.1.8)

Where

θ_M = azimuth mapping angle

Equation 5.1.8 is a complete description of azimuth for a moving object. The shadow of a moving object is calculated using the original azimuth. The slant range is not influenced by the motion of the moving object. Although there is some interaction between object motion and some pulse compression algorithms, it is not documented in this report. An object moving from the aircraft maps away from the velocity vector and an object moving toward the aircraft maps toward the velocity vector. Moving objects in the radar beam with their ground location out of the radar display can map into the radar display. Also, moving objects in the radar display can map out of the radar display and leave a remaining shadow. An example of a moving object is given below.

Example: Moving Object

Range   = 10 nautical miles
Aircraft Heading   = 45°
Target Heading   = 90°
Azimuth Angle   = 20°
Aircraft Velocity   = 300 knots
Target Velocity   = 10 knots
θ_M = 24.75°

At a range of 10 nautical miles, a moving object would map 4852 feet to the right of its shadow.

Equation 5.1.8 is not a complete answer when considering the real world. Collecting data for a SAR display requires a finite amount of time. A moving object could be traveling in a curved path. When this occurs the signature is many velocities and the moving object is spread over a number of pixel locations rather than one. A difficult case for simulation would be that of a long train traveling on a curve, in which the curvature is at the midpoint of the train.

Figures 5.1-2 and 5.1-3 are photographs of a train moving along a curved track. For moving objects, the reflectance pixel should be spread over several pixels.

5.2 NOISE

The return signal of radar is attenuated by range to the fourth power. In order to simulate noise in a SAR picture, some type of noise model must be developed. Assume that a target occupying the full area of a pixel is 100 percent reflective and generates a signal that gives 50 percent output on the SAR indicator. Now there is a difficulty: the range of combat radars is a closely guarded secret and to simulate noise properly, the range that gives an average noise output of 50 percent must be known. This range can be derived from radar manuals or can be calculated. The simulator should also have provisions to modify this range, as the radar can be operating at reduced power or weather can attenuate the radar signal. Because the calculated range can have a slight error, adjustments can be easily made.

Figure 5.2.1 is a block diagram of a proposed noise generator. The look-up table contains a normal distribution table that is offset to give only positive numbers. The hardware noise generator for the counter is used to avoid generating any patterns that would occur if the look-up table were sequenced. There are two multipliers that modify the noise signal. The first multiplier modulates the noise signal as a function of range. The second multiplier modifies the noise signal for weather, transmitter power, or to change range noise reference. The last function in the noise generator is an adder, where the noise signal is added to the simulated radar signal.

MOVING GROUND TARGET

Mudd's Landing

A moving train attracts notice on the 3.3 nm patch map from flight number 59. Due to the Doppler frequency shift, the moving train is displaced to the left of the track. The train is moving along the S-curve away from the river at a calculated speed of 15 mph. The drawing to the right and the photograph below showing the train in the S-curve are displayed to assist in locating the railroad track and the apparent position of the moving train in the patch map.

The photograph (taken on a previous flight) below the patch map shows two parked trains in the area of the high reflectance return shown in the patch map.

Figure 5.1-2 MOVING GROUND TARGET

PARKED TRAIN

RADAR IMAGE OF MOVING TRAIN

APPARENT POSITION OF MOVING TRAIN

GRAY SCALE

MISSISSIPPI RIVER

TRAIN
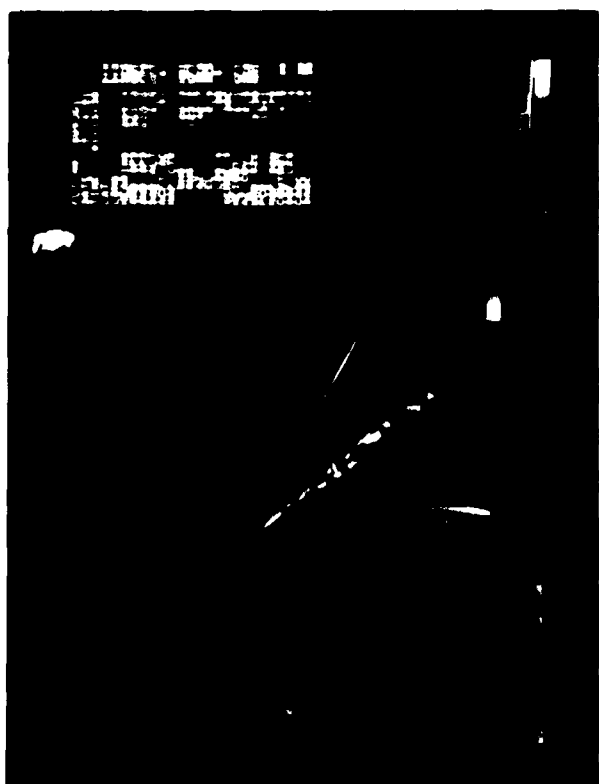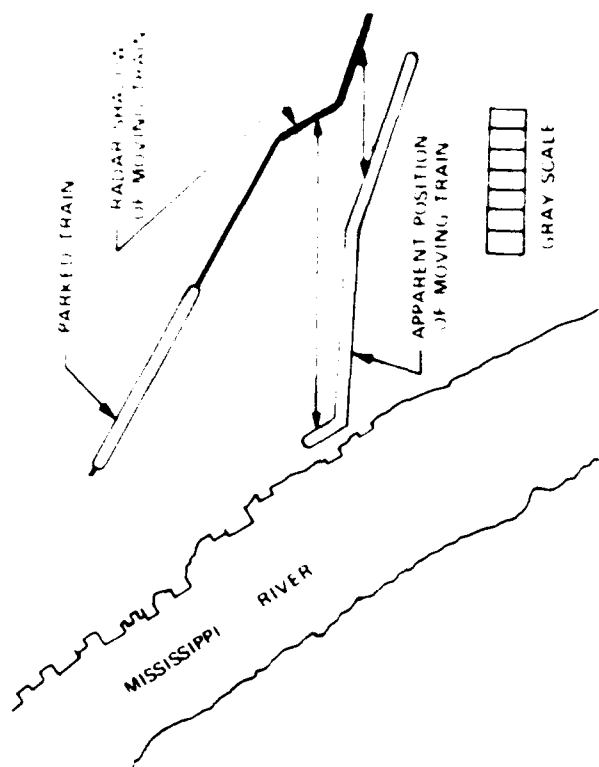
Figure 5.1-3 MOVING GROUND TARGET

```
┌──────────┐        ┌──────────┐  ADDRESS  ┌──────────┐
│ NOISE    │───────▶│ COUNTER  │──────────▶│ LOOKUP   │
│ GENERATOR│        │          │           │ TABLE    │
└──────────┘        └──────────┘           └──────────┘
```

```
        ┌──────────┐        ┌──────────┐        ┌──────────┐
     ──▶│MULTIPLIER│───────▶│MULTIPLIER│───────▶│  ADDER   │────▶
$R^4$──▶│          │        │          │        │          │
        └──────────┘        └──────────┘        └──────────┘
         REFERENCE           REFLECTANCE
```
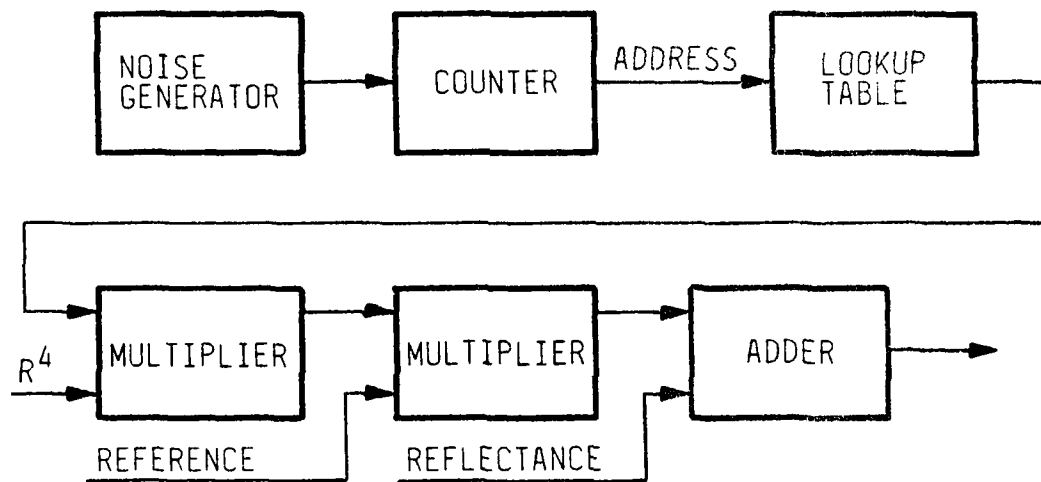
Figure 5.2-1 NOISE GENERATOR DIAGRAM

An example of noise generator operation is the best way to understand this concept. The parameters are a sector scan 20 by 40 nautical miles with noise equal to half of full scale on the display at 70 nautical miles. Additionally, heavy rain effects will be calculated and will reduce the noise range by 20 nautical miles from 70 nautical miles (from 50 to 70 nm) as shown in two examples:

Example One

Noise range	70 nautical miles
Signal to noise at 20 nm	150.06
Signal to noise at 40 nm	9.38

Example Two

Noise range	50 nautical miles
Signal to noise at 20 nm	39.06
Signal to noise at 40 nm	2.44

The noise model can be adjusted to any radar or mode by changing the software-controlled constant of the second multiplier.

5.3 GLITTER

Synthetic aperture radar and real beam radar exhibit a strong return phenomenon that appears on one or several scans and then disappears. This phenomenon is called glitter and is caused when an object on the ground becomes a radar corner reflector for a brief period. Figure 5.3.1 is a diagram of an ideal three-dimensional corner reflector and a two-dimensional corner reflector and shows the path of the reflected waves. The three surfaces of a three-dimensional corner reflector need not meet. As an example; two buildings and the ground would form a three-dimensional corner reflector. Buildings separated by small distances only reduce reflectance by a small amount. Three-dimensional corner reflectors are quite common when mapping cities as most buildings are laid out on grids. The return from the corner reflector in SAR is orders of magnitude greater than in those of RAR because of SAR's greater resolution.
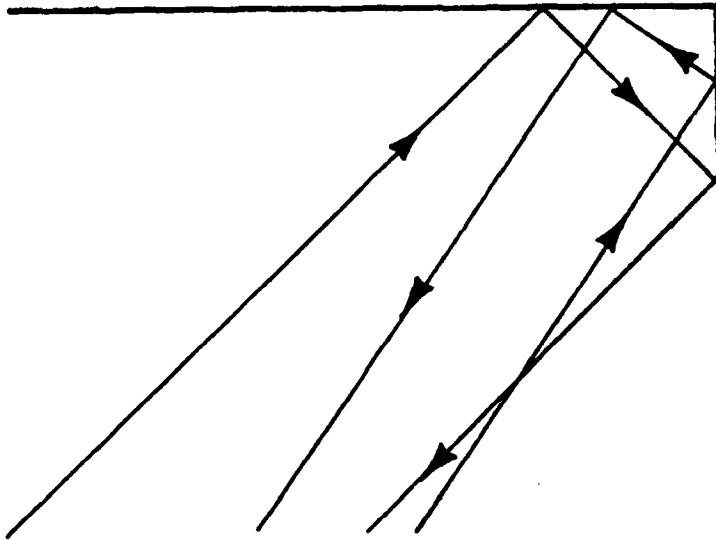
TWO-DIMENSIONAL
CORNER REFLECTOR
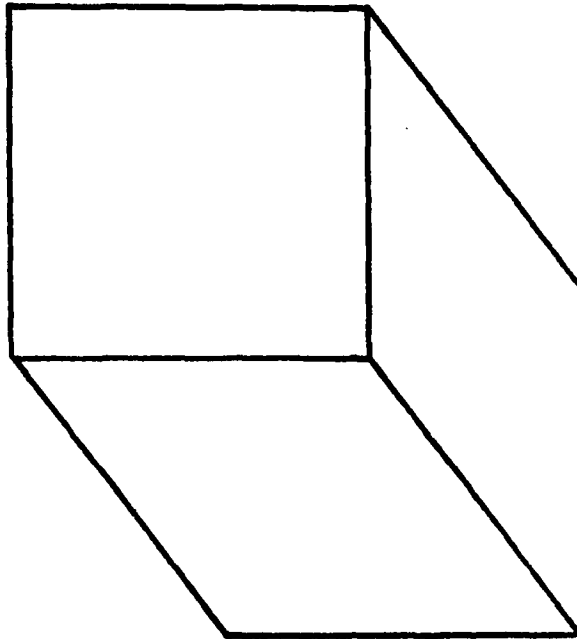
THREE-DIMENSIONAL
CORNER REFLECTOR

Figure 5.3-1   2-D & 3-D CORNER RELECTORS

There are two methods for simulating glitter. First, all objects that cause glitter can be added to the data base. However, because present data bases are lacking in detail and individual buildings are not coded, this method of glitter generation must await the generation of high resolution data bases. A second method to generate glitter is to randomly and/or selectively put out a high level return, particularly in commercial and industrial areas where most glitter is generated. In SAR, the glitter return will last for more than one display. Since SAR is a high resolution device, squint angle changes will be minor in comparison to the angle of return for the corner reflector.

There is another important aspect to glitter and high resolution SAR. Study Figures 5.3-2, 5.3-3, 5.3-4 and 5.3-5. Note that Figures 5.3-2 and 5.3-3 are photographs of Busch Stadium in St. Louis, Missouri. The product specification for the Digital Landmass System (DLMS) data base has a code (321) for an enclosed stadium. At the present time, most radar simulators generate a point for DLMS code 321. For SAR, code 321 should be decoded as a ring with a vertical outside wall, a sloping interior, and glitter returns at the locations of light towers. Figure 5.3-4 is a SAR display of the Daggett Marine Corps depot. The DLMS code for warehouses is 861. For Daggett Marine Corps warehouses, SAR simulation requires insertion of glitter warehouse roofs where vents and air conditioning units are located. The DLMS code that generates glitter should be identified for proper SAR simulation. One rule of thumb for surface codes in the DLMS codes is that surfaces which are highly reflective generate weak returns or generate glitter. The codes can also be omnireflective. DLMS code 155 is a heavy fabrication industrial building with a sawtooth roof. In low grazing angles, this roof will reflect from steep sides of the sawtooth.

5.4 SCINTILLATION AND MULTILOOK

SAR has another effect that differs from conventional pulse radar known as scintillation or speckle. SAR, as a coherent system, is very sensitive to any change in the transmission path length and target movement and multipath returns also downgrade SAR performance. The quality of the atmosphere is not homogeneous, but variable and subject to constant changes. The twinkling of

0.67 NMI PATCH MAP OF BUSCH STADIUM

Busch Stadium is shown with 8.5 ft resolution elements in the radar map on the opposite page below, and in the enlargement of the stadium below made from that radar map. This 0.67 nmi patch map, made at a range of 7.7 nmi and an altitude of 11.000 ft. is part of the sequence of radar maps from the previous page.

Individual reflective elements of the stadium stand out clearly. Large metal objects, possibly lighting stands, show up as a series of bright returns evenly spaced across the bottom, and the radar "shadow" of a large downtown hotel (Stouffers) is seen to blank out a small square at the bottom of the stadium.

Aerial photograph

4X enlargement of 0.67 nmi patch map
showing 8.5 ft resolution elements

Figure 5.3-2   PATCH MAP OF BUSCH STADIUM
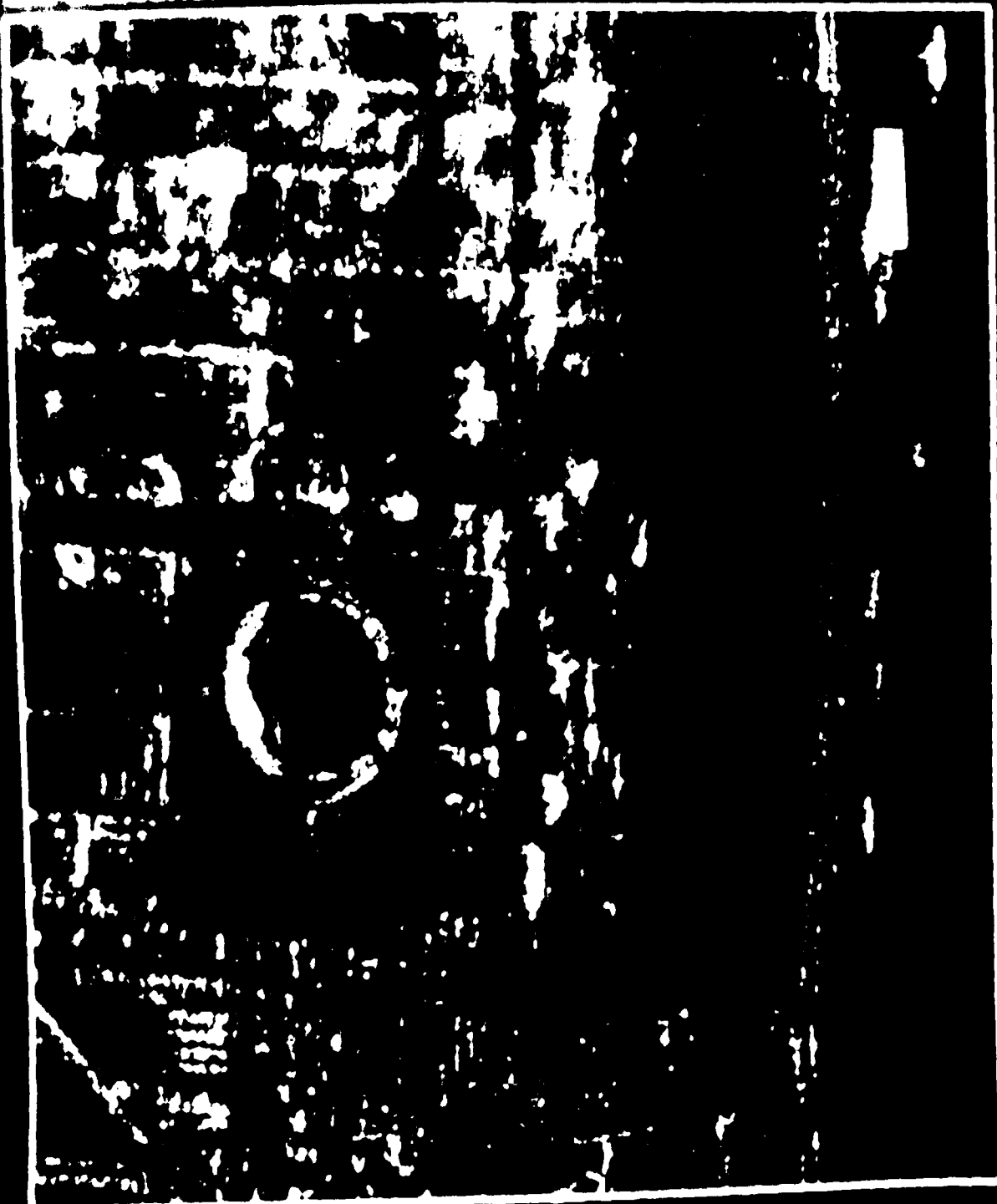
DAGGETT MARINE CORP SUPPLY CENTER – SOLAR ONE POWER PLANT

Daggett is located east of Barstow along Interstate 40. Highlights of the Daggett area are the Solar One solar powered electricity plant and the U.S. Marine Corp Supply Center, located adjacent to Solar One. Both facilities can clearly be recognized in the 42 foot resolution map below. The solar power plant's rings of mirrors provide a very large radar return as seen in the map. Power lines are evident, leading into the large industrial complex adjacent to the power plant's water storage area. The large building groups of the Marine Corp depot are also evident, as well as the major roads throughout the Daggett area. An aerial photograph is provided for comparison.

Aerial Photograph of the Daggett Area Including Solar One

3.3 nmi Patch Map (42 ft Resolution)

DAGGETT MARINE CORPS SUPPLY CENTER

1

The 17 foot resolution map of the Daggett Marine Corp depot provides coverage of the entire base with the ability to distinguish separate buildings and groups of parked military vehicles. Two large columns of six storage buildings span nearly half the length of the 1.3 nmi patch map. The length of each building can be determined to be approximately 1000 feet.
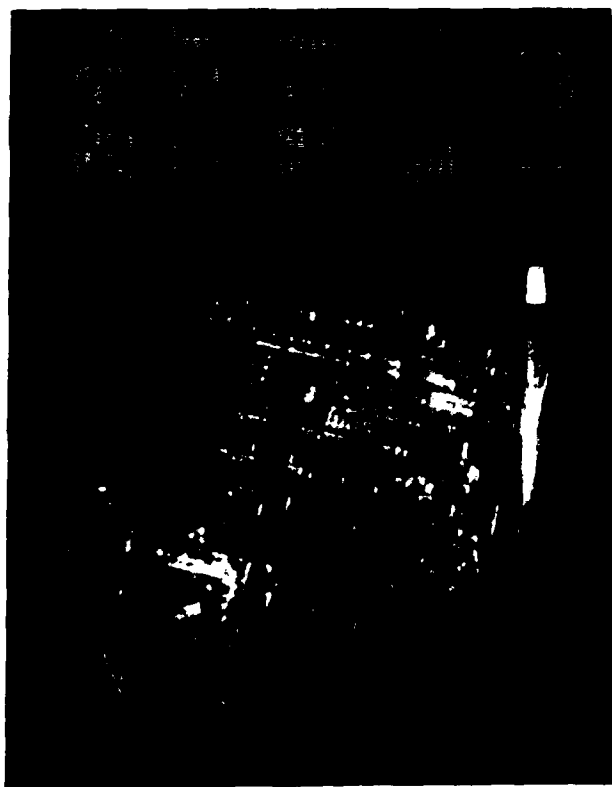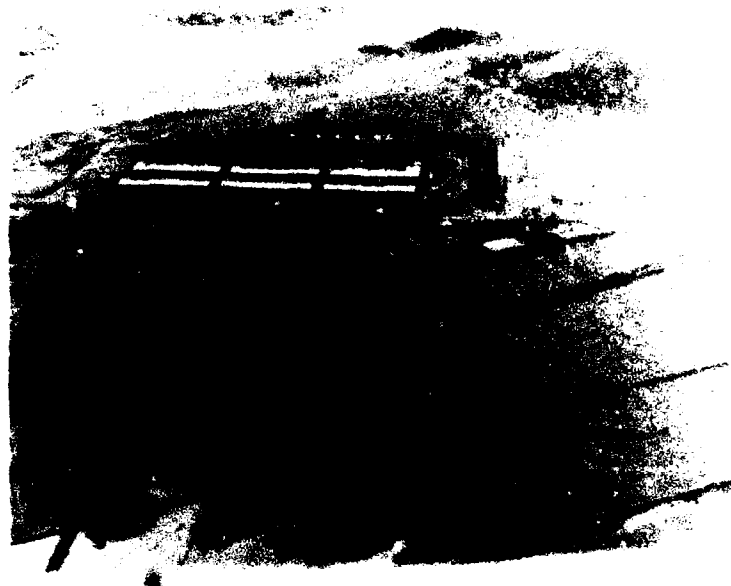
Aerial Photograph of the Daggett Marine Corp Depot

**1.3 nmi Patch Map (17 ft Resolution)
Daggett Marine Corp Depot**

DAGGETT MARINE CORPS SUPPLY CENTER

stars is an example of scintillation. Some SAR systems reduce scintillation by a tradeoff with resolution. This tradeoff is accomplished by averaging a number of returns of the same area. For combat SAR's the number used for averaging is generally two or four.

Nonmobile target motion is caused by wind. Strongly built structures do not give any notable scintillation but vegetation driven by wind can cause scintillation, as well as smearing the return. As would be expected, grass generates more scintillation than trees; water varies from nonreflective to a highly reflective return.

The simulation of wind, rough water scintillation, and multilook are implemented in the same manner. Simulation begins with an unmodified display. The overall picture can then be modified by using a Gaussian multiplier look-up table to generate atmospheric scintillation; there should be three look-up tables (i.e., for one, two, or four looks). If rough water is identifiable in the data base, a random look-up table can be used to vary the returns and the returns should also be smeared. A coastline return can be modified by rough water in an area such as the Columbia River Bar. Vegetation driven by wind is simulated by modifying returns with a look-up table and smearing. For high or gusty winds all the look-up tables could be used. Low velocity winds can be simulated by not modifying data on some scans.

Figure 5.4-1 is a photograph of two SAR displays. The first display is made up of six subscans and has a multilook of one. Note that fading is due to the antenna footprint and the amount of glitter. The second display is of the same area except that the display has a multilook of two. Fading and glitter have been reduced. Simulating multilook for the antenna footprint is not complicated. For Multilook 1 use the antenna footprint multiplication table calculated from the actual radar to modify picture returns; for Multilook 2 use a modified antenna footprint table to modify picture returns; and for Multilook 4 do not modify the picture.

RADAR MAP QUALITY

To qualitatively evaluate the effect of azimuth (squint angle), air speed, altitude (graze angle), aircraft altitude, number of looks, and aircraft maneuvering on radar map quality was a major objective for the evaluation flight test. The aircrews reported that, with the exception of grazing angle, these parameters had a negligible effect on map quality. As grazing angle decreased below 1.5°, the elongation of radar shadows was readily apparent as some missions were flown at terrain altitudes of less than 300 feet.

Typical maps illustrative of these parameters are shown below.

Multilook 1
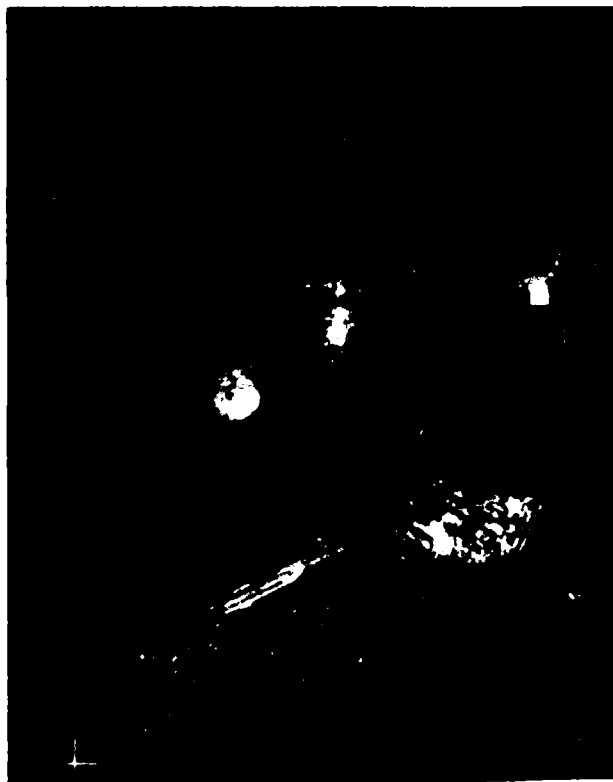
Multilook 2

MARINE CORPS SUPPLY CENTER, DAGGETT, CALIFORNIA

Figure 5.4-1 RADAR MAP QUALITY

5.5 FOOTPRINT

The area size that can be processed by SAR is limited to the area size illuminated by the antenna. For SAR processing, this is generally considered to be the area within the two-way path, 3 dB points.

There are generally two types of antenna used in aircraft SAR. For patch mode, a pencil beam is considered best as it concentrates the most RF energy in the area of interest. The sector scan mode requires a long and narrow area to be illuminated. A fan-shaped beam is used for this purpose. Figure 5.5-1 is a diagram of an aircraft antenna footprint.

Simulation of the antenna footprint is relatively simple. The antenna footprint algorithm consists of multiplying the reflectance values by a coefficient that is a function of the azimuth angle. A simple approach is to assume that the coefficients are constant with slant range. This is not entirely true, but for simulation purposes it is a valid assumption. Figure 5.5-2 is a diagram of a typical antenna pattern. Using Figure 5.5-2, a velocity error example can be demonstrated. Figure 5.5-3 shows the amplitude response with velocity errors. If significantly great velocity error occurs, the display could become blank.

The velocity error algorithm consists of a multiplier and a look-up table. The pointer to the look-up table is advanced from scanline to scanline and is offset by velocity errors. Coefficients that are in the look-up table will be determined by the aircraft's antenna and the mode of the SAR.

5.6 DOPPLER ELEVATION MAPPING

In previous sections, it has been stated that SAR mapping is performed on isodoppler lines and that the theory of SAR developed by considering that the earth's plane is flat. We now look at the problem that occurs when points of interest are not in the reference plane, such as tall buildings, mountains and depressions. The information that is needed when considering SAR elevation mapping is a determination of how the aircraft SAR determines elevation of the
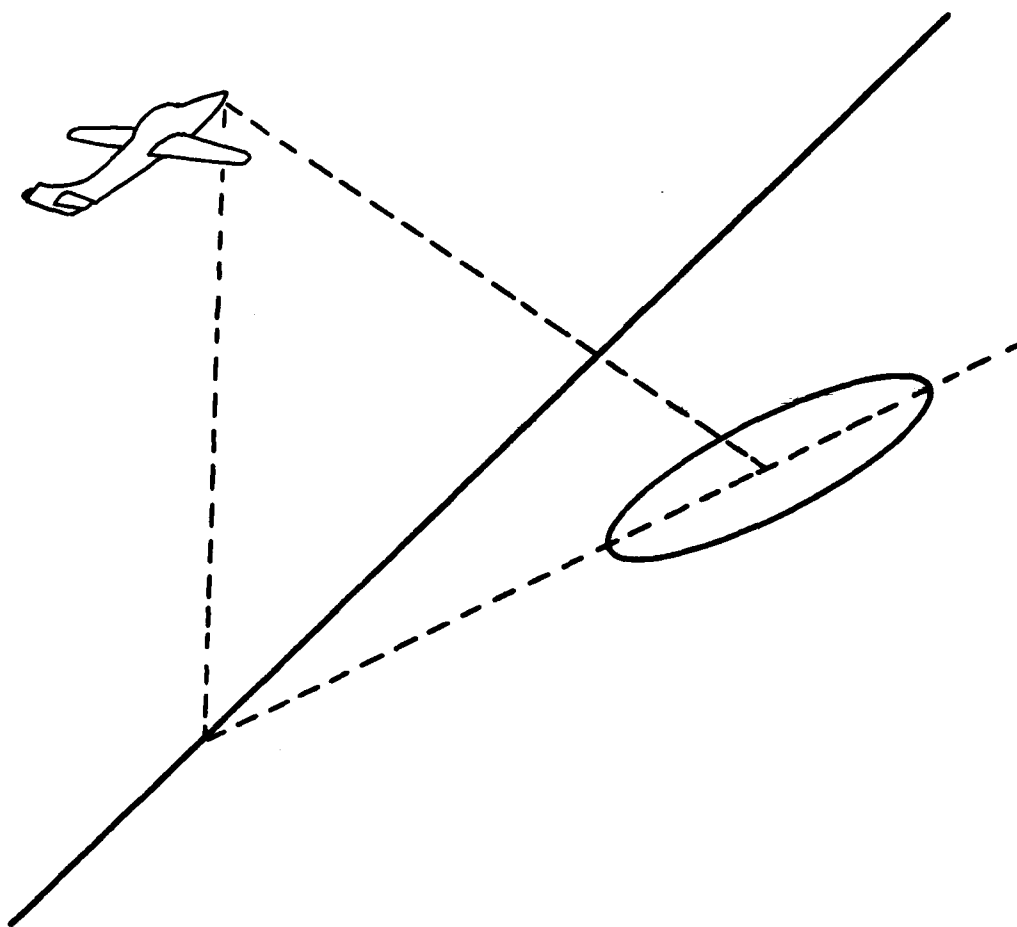
Figure 5.5-1 ANTENNA FOOTPRINT

DEGREES

RELATIVE RESPONSE
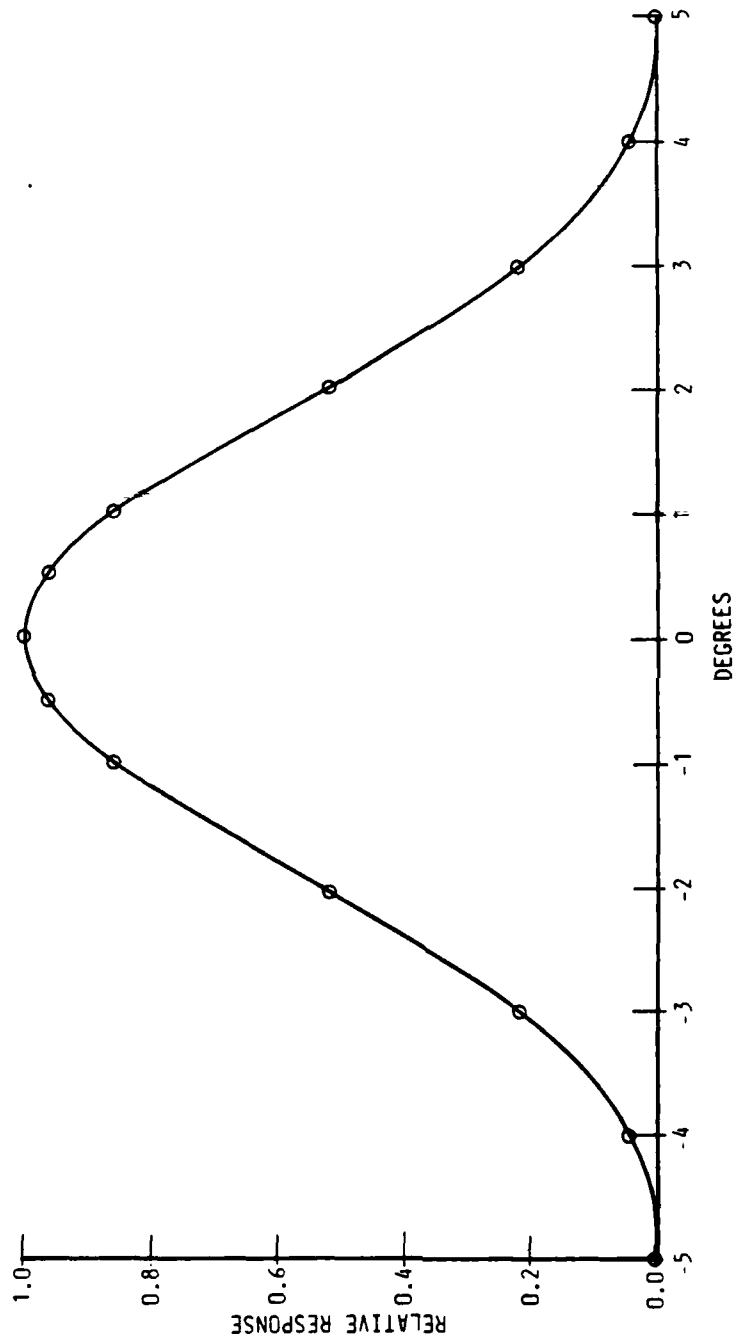
Figure 5.5-2 ANTENNA PATTERN
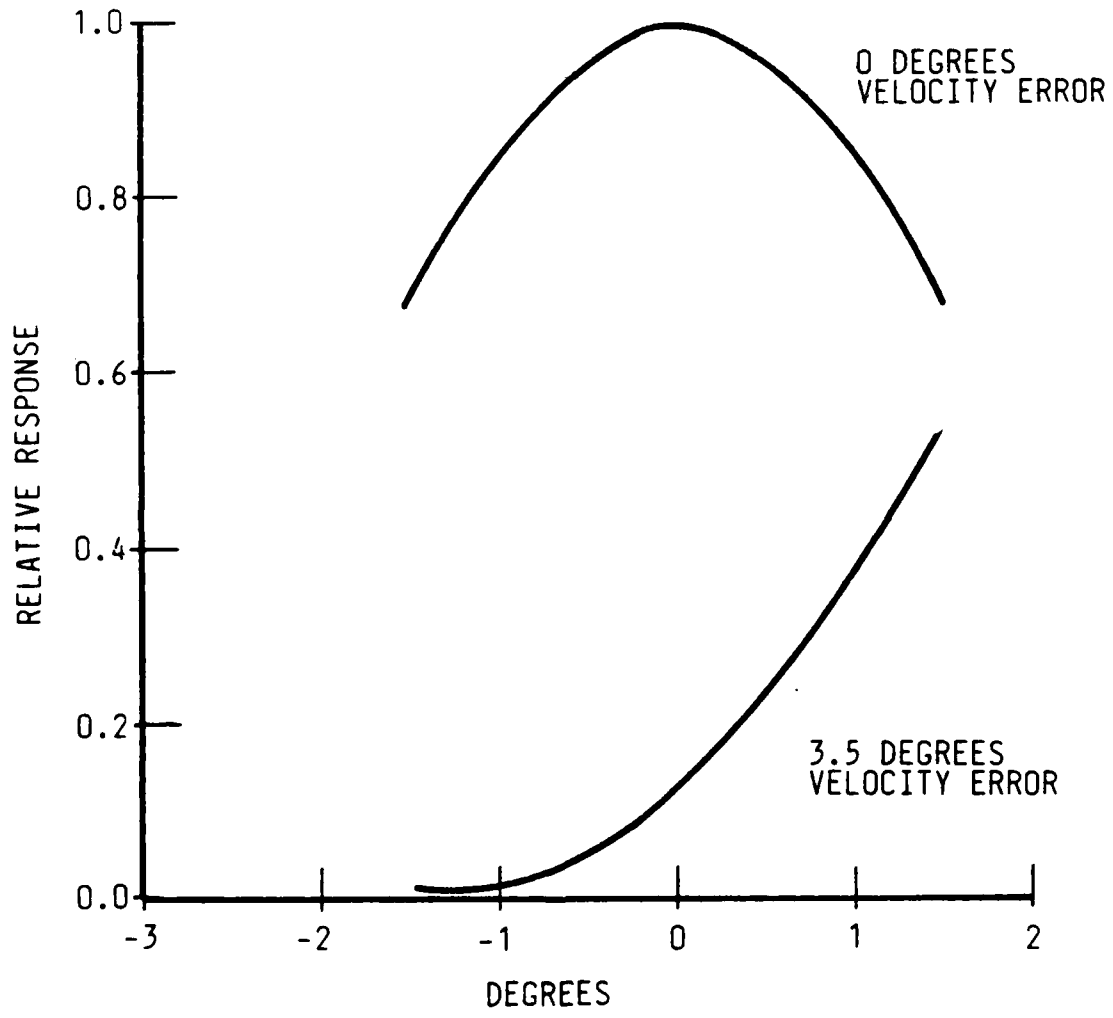
Figure 5.5-3 DISPLAY AMPLITUDE WITH VELOCITY ERROR

SAR reference plane. The relative velocity of the center point of the scan on the ground and the aircraft is used as a reference in aircraft SAR processing. The algorithm that determines this velocity should be a guide when determining what algorithm will determine the elevation reference plane. One type of algorithm is to average a number of points. For SAR elevation mapping, we will make an assumption that the elevation reference plane is known.

A comparison has been made of SAR to a large lens or antenna. For all calculations, the center of this lens/antenna is considered to be halfway along the data collection path; the nadir point is the origin of the isodoppler map. Now each point in the isodoppler map has its own signature in azimuth depression angle and slant range. The isodoppler lines are represented by Equation 5.6.1.

$$L_{ID} = \cos(\psi) \cdot \cos(\Theta_{VV}) \qquad\qquad (5.6.1)$$

Where

L_{ID} = an isodoppler line

The depression angle is represented by Equation 5.6.2:

$$\psi = \tan^{-1}\left[\frac{A_{RP} - E_{RP}}{R_G}\right] \qquad\qquad (5.6.2)$$

Where

A_{RP} = altitude above the reference plane

E_{RP} = elevation above the reference plan

R_G = ground range

Let the depression angle of the ground range be the reference when the value of elevation above the reference plane is zero. Since SAR processing is performed along isodoppler lines, the equation for a point that is not in the reference plane is:

$$L_{ID} = \cos(\Theta_{AM}) \cdot \cos(\psi) = \cos(\Theta_{VV}) \cdot \cos(\psi_R) \qquad (5.6.3)$$

Where

Θ_{AM} = mapping azimuth from the velocity vector

Solving for the azimuth angle Θ_{AM} gives the azimuth location of a point that is not at the elevation of the reference plane.

$$\Theta_{AM} = \cos^{-1}\left[\cos(\Theta_{VV}) \cdot \frac{\cos(\psi)}{\cos(\psi_R)}\right] \qquad (5.6.4)$$

$$\Theta_{AMD} = \Theta_{VV} - \cos^{-1}\left[\cos(\Theta_{VV}) \cdot \frac{\cos(\psi)}{\cos(\psi_R)}\right] \qquad (5.6.5)$$

To indicate how Equation 5.6.5 varies with azimuth and depression angle, Equation 5.6.5 can be differentiated.

$$\frac{d\Theta_{AMP}}{d\psi_R \, d\Theta_{VV}} \approx \frac{\tan(\psi_R)}{\tan(\Theta_{VV})} \qquad (5.6.6)$$

This type of equation has been shown before; it has the same form as the rate of change of the isodoppler lines, as one would expect. An object that is above the reference plane will plot in azimuth toward the velocity vector and an object that is below the reference plane will plot away from the velocity vector. Figure 5.6-1 is a plot of the amount of shift in azimuth for a 1000-foot object, at 10 nautical miles.

This layover is peculiar to SAR and has several implications in SAR simulation. One characteristic is that the shadow of an object with layover stays where it is. Another characteristic is that an object with layover maps into other objects or shadows. Figure 5.6-2 is a diagram of a 1000-foot object and an indicator of the layover phenomenon. The difference in slant

LINEAR DISPLACEMENT

GROUND RANGE = 10 NAUTICAL MILES
HEIGHT OF OBJECT = 1000'

ANGULAR DISPLACEMENT
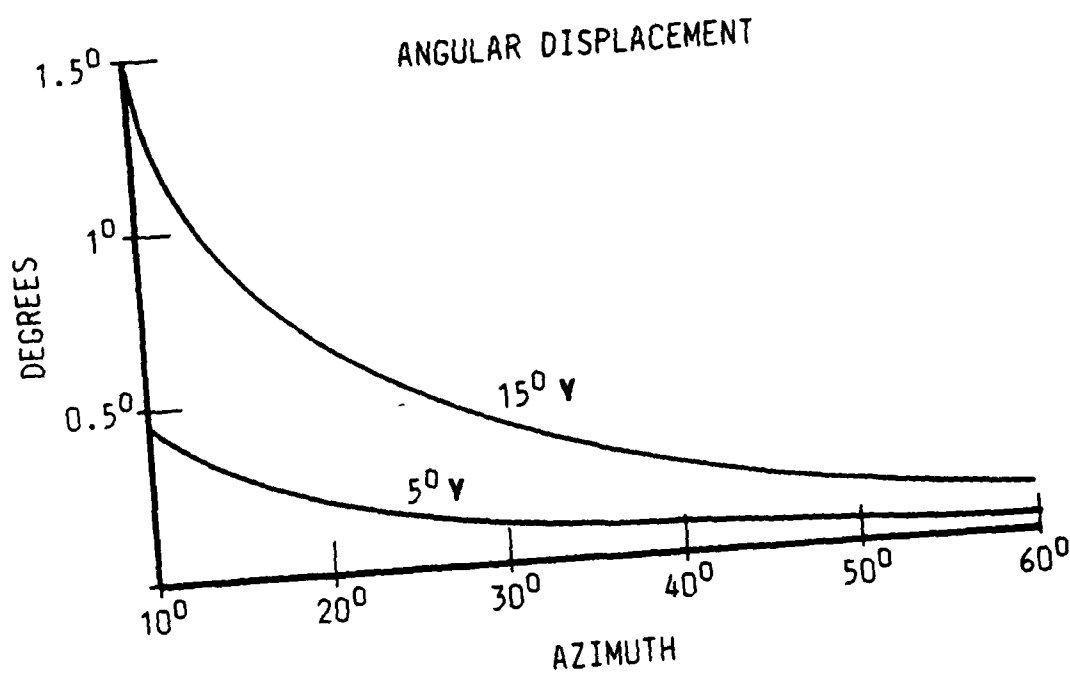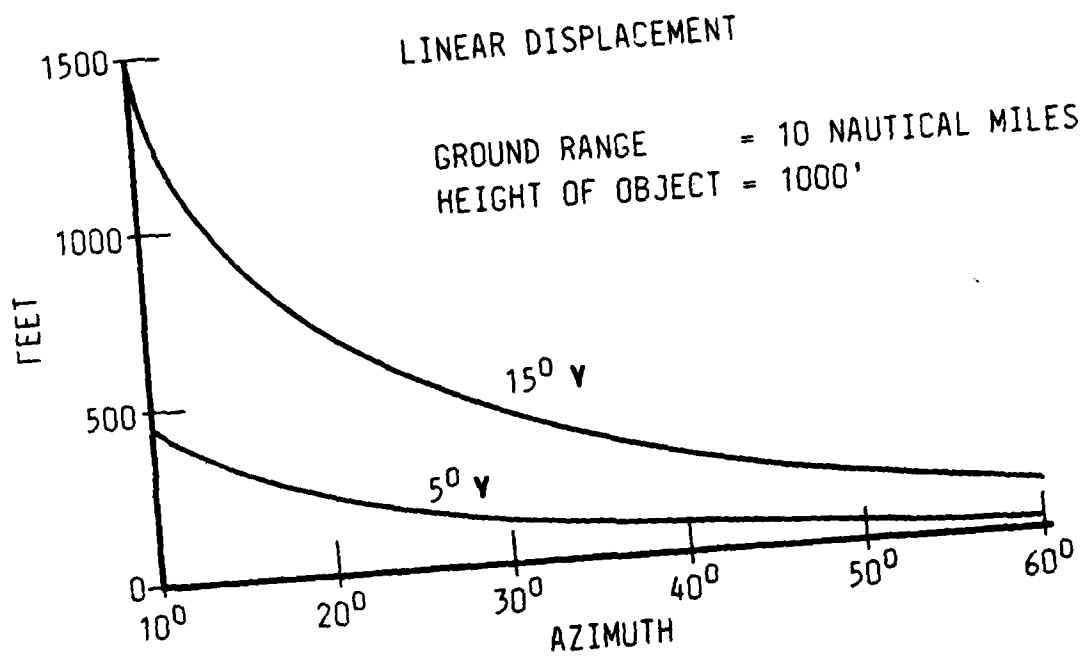
Figure 5.6-1   LAYOVER VS AZIMUTH FOR 5 AND 15 DEGREE DEPRESSION ANGLE

SHADOW

VELOCITY
VECTOR

RANGE   = 10 NM
DEPRESSION ANGLE = 15°
AZIMUTH   = 10°

FEET

3000

2000

1000

0

1500   1000   500   0
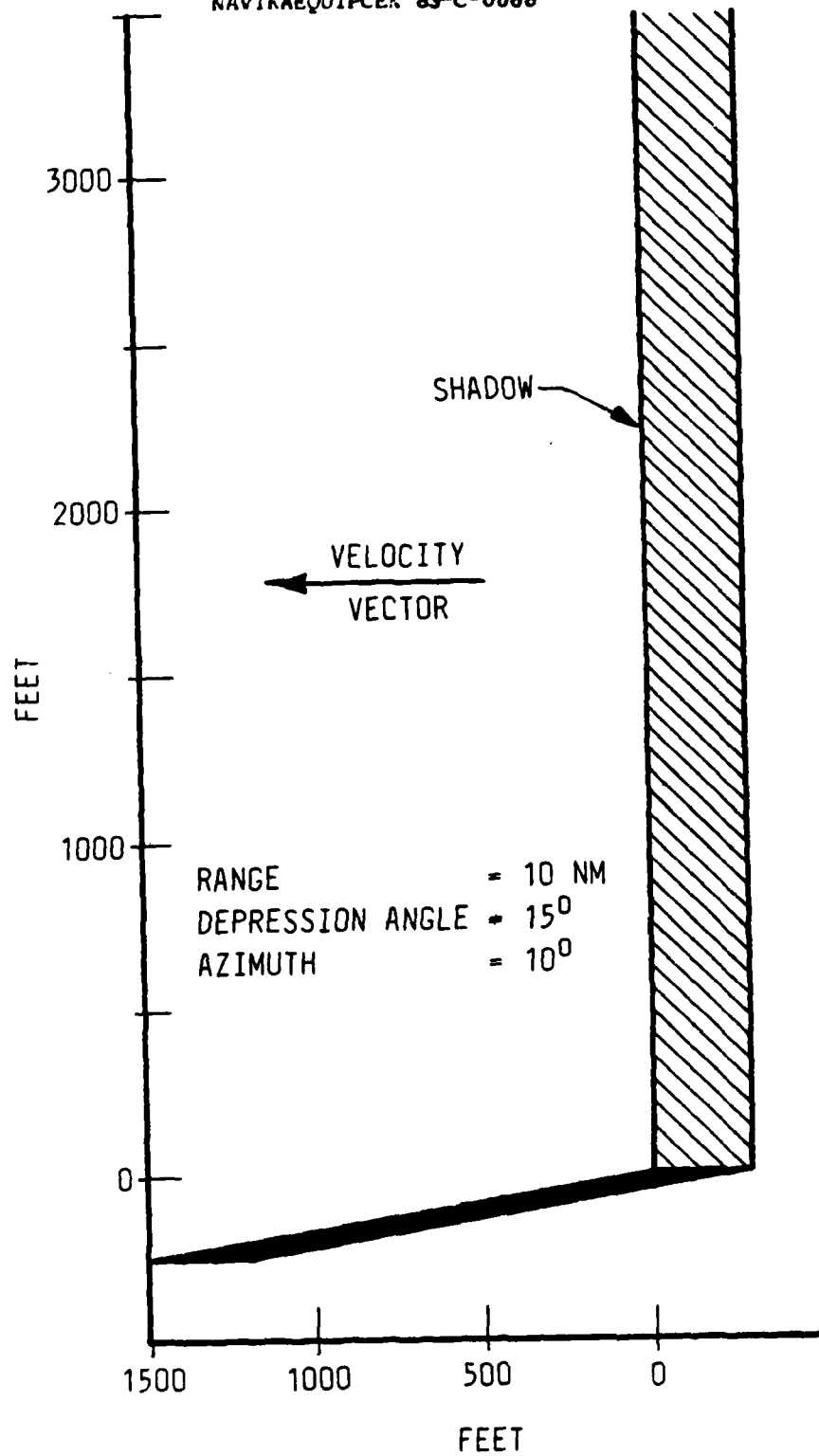
FEET

Figure 5.6-2   LAYOVER FOR A 1000 FOOT BUILDING

5-26

range between the top and bottom of the building is 251 feet. The top of the object maps toward the aircraft and also toward the velocity vector. The layover mapping of terrain (mountains) requires only one pixel to be mapped. A tall object must be represented by a number of pixels and each pixel must be remapped. Layover can be simulated but this requires a considerable amount of calculation.

The specification of the layover function in a SAR simulator will depend upon three factors: 1) the degree of realism that is required, 2) structural heights of the area to be simulated, and 3) SAR resolution. Two examples are included as a basis for the decision-making process:

Example One

Range	10 nautical miles
Pixel size	10 feet
Resolution	20 feet
Height of structure	1200 feet
Azimuth	15 degrees
Depression angle	15 degrees
Layover	1.06 degrees
	112 pixels

Example Two

Range	10 nautical miles
Pixel size	50 feet
Resolution	100 feet
Height of structure	150 feet
Azimuth	15 degrees
Depression angle	15 degrees
Layover	0.13 degrees
	3 pixels

In the first example; without layover the simulator display would be a poor match to the real world display. In the second example, the simulator could produce a good match without layover simulation. A word of caution should be inserted here: all modern radars are designed to be upgraded and even if layover is not specified, a capability for inserting overlay at a later date should be designated.

5.7 MALFUNCTION EFFECTS

For proper simulation velocity errors must be included. In the principles of SAR it was emphasized that velocity was a linear phase shift across the aperture. This linear phase shift causes the aperture to be steered. Figure 5.7-1 and 5.7-2 are examples of steering the aperture out of the area being illuminated by the radar antenna. Figure 5.7-3 is a diagram indicating velocity error. A solution for velocity error simulation is given in Equation 5.7.1.

$$F_{DS} = \frac{2V_{AC} \cdot F}{C} \qquad (5.7.1)$$

The solution for azimuth shift is to equate two Doppler frequencies that have different aircraft velocities:

$$\cos(\Theta_{VVE})\cos(\psi) \cdot V_{AC} = \cos(\Theta_{VV})\cos(\psi) \cdot (V_{AC} + V_{ERR}) \qquad (5.7.2)$$

Where

Θ_{VVE} = azimuth from the velocity vector when a velocity error exists

V_{ERR} = velocity error

Solving for the azimuth angle for a velocity error gives Equation 5.7.3.

$$\Theta_{VVE} = \cos^{-1}\left[\cos(\Theta_{VV}) \cdot \frac{(V_{AC} + V_{ERR})}{V_{AC}}\right] \qquad (5.7.3)$$

PVU CORRECTION OF ANTENNA SHADING

Shading across individual map arrays occurs when the doppler filter processor looks at a patch on the ground that is not concurrently illuminated by the antenna pencil beam, as illustrated by the map on the left. The doppler filters are biased by a small error in ownship velocity provided by the Inertial Navigation System (INS).

The degraded map is restored to normal by using the Precision Velocity Update (PVU) mode to correct the erroneous INS velocity.

In the flight number 62 sequence shown below, the PVU mode was engaged 17 seconds after completing the degraded map. Approximately 12 seconds later, the PVU calculated a 4.8 knot vector velocity error as shown to the operator in the center picture.

The equivalent 158.4 Hz frequency error was resolved into the antenna LOS and used to position the doppler filters. The next map constructed is corrected for the INS velocity error and is shown on the right. This correction to the INS will give better mark and designation accuracies in the AZ filters for blind bombing.

Figure 5.7-1 PVU CORRECTION OF ANTENNA SHADING

PVU CORRECTION OF ANTENNA SHADING

———— = DESIRED AREA

————— = VELOCITY ERROR AREA
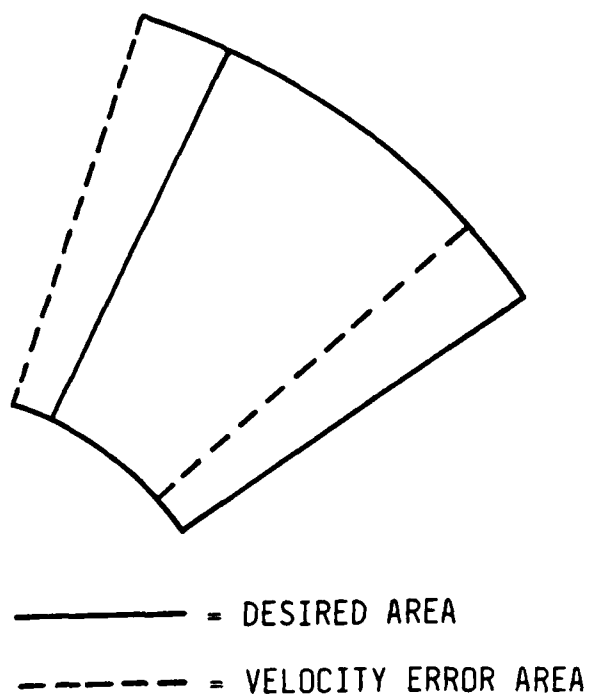
Figure 5.7-3 RADAR PICTURE SHIFT DUE TO VELOCITY ERROR

A velocity used for SAR calculations that is higher than the actual velocity will shift the aperture toward the velocity vector. A velocity error on the low side will shift the aperture away from the velocity vector. An example of velocity error is provided:

    Example: Velocity Error

    Azimuth angle   = 20 degrees
    Range   = 10 nautical miles
    Velocity   = 300 knots
    Velocity Error   = 10 knots

This 10 knot velocity error shifts the aperture 6.17 degrees toward the velocity vector. At a range of 10 nautical miles this is a shift of 6570 feet, emphasizing that a small velocity error makes a large SAR processing error.

To find out how azimuth error varies as a function of the azimuth angle and velocity, Equation 5.7.4 is differentiated with respect to the velocity error:

$$\frac{d\Theta_{VVE}}{dV_{ERR}} \approx \frac{1}{V_{AC}\cdot\tan(\Theta_{VV})} \qquad\qquad (5.7.4)$$

Equation 5.7.4 shows that velocity errors give a large azimuth error near the velocity vector.

The simulation of velocity errors is straightforward. First, consider the center of the radar picture as a reference. The azimuth shift in this reference pixel due to velocity error is now calculated. This azimuth shift is now used to calculate a set of new data retrieval coordinates. This new data is then used to generate a radar display. Figure 5.7-1 is an illustration of data shift due to a velocity error.

Velocity error causes a fading or shading of the radar picture. During normal operation of SAR, the area of interest occupied is within the 3 dB points of

the antenna footprint. A velocity error shifts the designed display area out of the display and brings in an area that is outside the 3 dB points of the antenna footprint. In the simulator the solution for fading due to velocity error is to shift the antenna footprint multiplying table to match the velocity error.

Acceleration is defined as the derivative of velocity relative to time. Acceleration errors can be caused by three related factors. The first factor could be a faulty inertial system; the second factor could be a maneuver of the aircraft that exceeds the inertial system's correction capability. The third factor is flexing of the aircraft that causes motion between the inertial system and the radar antenna.

Acceleration errors cause loss of resolution in the azimuth direction. Acceleration simulation is straightforward. This simulation consists of spreading the reflectance data of one pixel over a number of pixel locations. A small acceleration error would involve only a few pixel locations and a large acceleration error would involve many pixels. Most acceleration errors in an actual aircraft are very complex and would be impossible to simulate. To understand acceleration errors, a linear acceleration can be used.

The starting point will be Equation 5.7.1 (a velocity error equation). This equation is rewritten to include acceleration errors:

$$F_D = \frac{2 \cdot F}{C} \left[V_{AC} + \int_{t_1}^{t_2} f(A_{CC}) \, dt \right] \qquad (5.7.5)$$

For example, the acceleration function is set to a constant. This is a linear acceleration error. Equation 5.7.6 is the equation for a linear acceleration error:

$$F_D = 2 \cdot \frac{F}{C} [V_{AC} + A_{CC}(t_2 - t_1)] \qquad (5.7.6)$$

At the time t_1 the Doppler frequency is $2 \cdot F \cdot V_{AC}/C$ and at t_2 the Doppler frequency is $2 \cdot F/C[V_{AC} + A_{CC}(t_2 - t_1)]$.

By replacing the velocity error in Equation 5.7.1 with the acceleration error, the equation for the azimuth angle of the end of the data collection can be obtained.

$$\Theta_{VVE} = \cos^{-1}\left[\frac{\cos(\Theta_{VV}) \cdot [V_{AC} + A_{CC}(t_2 - t_1)]}{V_{AC}}\right] \tag{5.7.7}$$

The azimuth angle at the start of the data collection is Θ_{VV}. The data for one pixel is spread over the azimuth from Θ_{VV} to Θ_{VVE}.

An example of the effects of acceleration errors is given:

Example: Acceleration Error

Azimuth angle	=	20 degrees
Range	=	10 nautical miles
Velocity	=	300 knots
Acceleration	=	1.2 knots per second
Start of data collection	=	0 seconds
End of data collection	=	10 seconds
Azimuth angle at the end of data collection	=	12.23 degrees
Pixel spread	=	7.76 degrees

Although this example is quite drastic, it does illustrate what acceleration errors can do to a SAR image. In this case, a real beam radar would give a better picture.

6.0 DATA BASE REQUIREMENTS FOR SAR SIMULATION

6.1 ELEVATION DATA BASE

Requirements for SAR elevation data are more exacting than those for real aperture radar because SAR resolution is from 16 to more than 100 times greater. For this reason, short cuts that work for RAR fall short in SAR. The Digital Landmass System (DLMS) data base for elevation specifies elevation data on 3-second by 3-second posts from 0 to 50 degree latitude. At the equator this would be 303.6 feet by 303.6 feet. A high resolution SAR operating at 10-foot resolution with a display of 230,400 pixels uses only 256 posts to generate all of the elevation data. The above figures were calculated for a location of zero latitude. Fortunately there are a number of things that can be done to make the DLMS useful for SAR.

The most simple way to refine the DLMS elevation data base is to use a two-dimensional linear interpolation algorithm to obtain elevation data for points between posts. Figure 6.1-1 depicts the two-dimensional linear interpolation algorithm. However, this algorithm has two shortcomings: 1) the elevation slope is essentially made up of linear lines, and 2) the elevation slope has discontinuities. These discrepancies can be tolerated in some RAR systems but are not acceptable in high resolution SAR systems. To remove the straight lines and discontinuities, the derivative of the slope is required to be a continuous function. The use of 16 posts and the two-dimensional weighted parabolic interpolation algorithm does this. There are other algorithms that would do the same function, but the two-dimensional weighted parabolic interpolation algorithm is one of the most simple. Figure 6.1-2 is the diagram and equations of the two-dimensional weighted parabolic interpolation algorithm. This algorithm and any other algorithms will give an overshoot for a step function. Figure 6.1-3 is an example of the overshoot. The maximum overshoot for a two-dimensional weighted parabolic interpolation algorithm is 0.0741 of the step. The DLMS data base contains very few step functions, hence the step function response should not be a problem.

$$EA = (E3 - E2)Y + E2$$
$$EB = (E4 - E1)Y + E1$$
$$A = (EB - EA)X + EA$$

$$0 \leq X \geq 1$$

$$0 \leq Y \geq 1$$
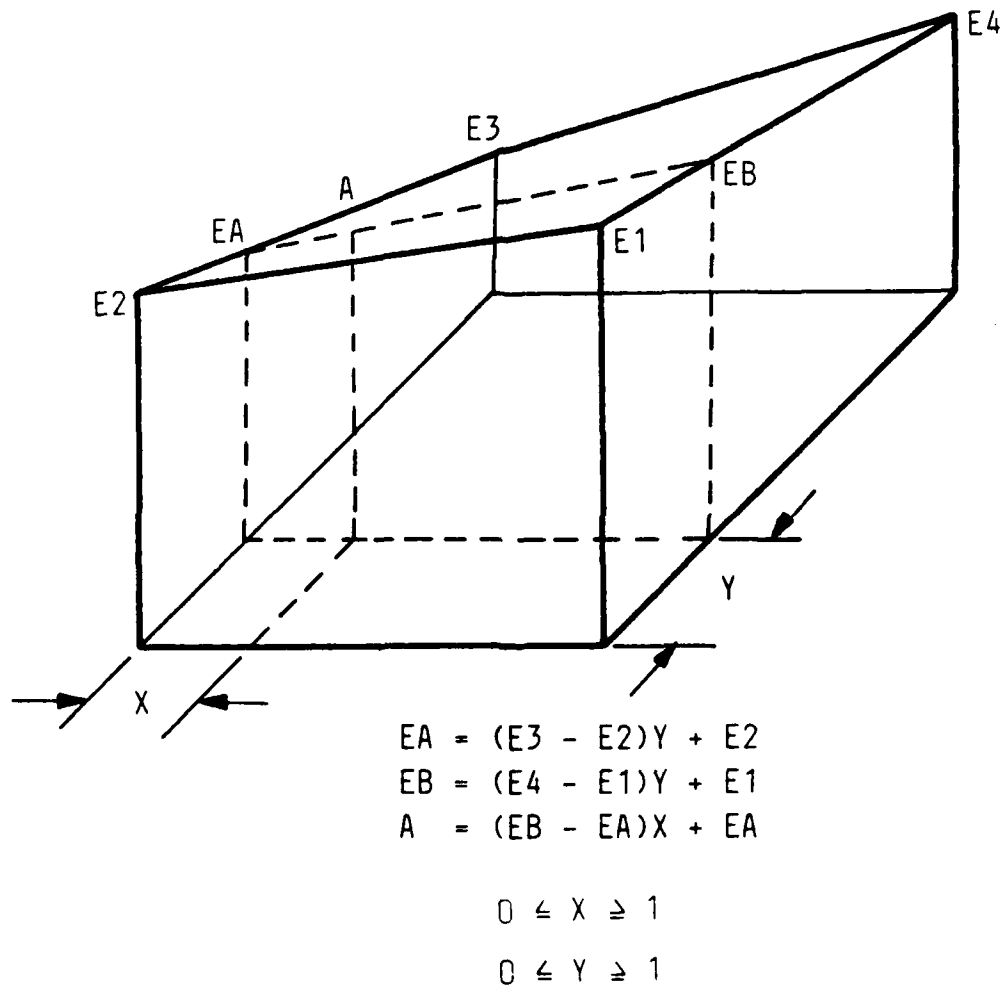
Figure 6.1-1   2-D LINEAR INTERPOLATION
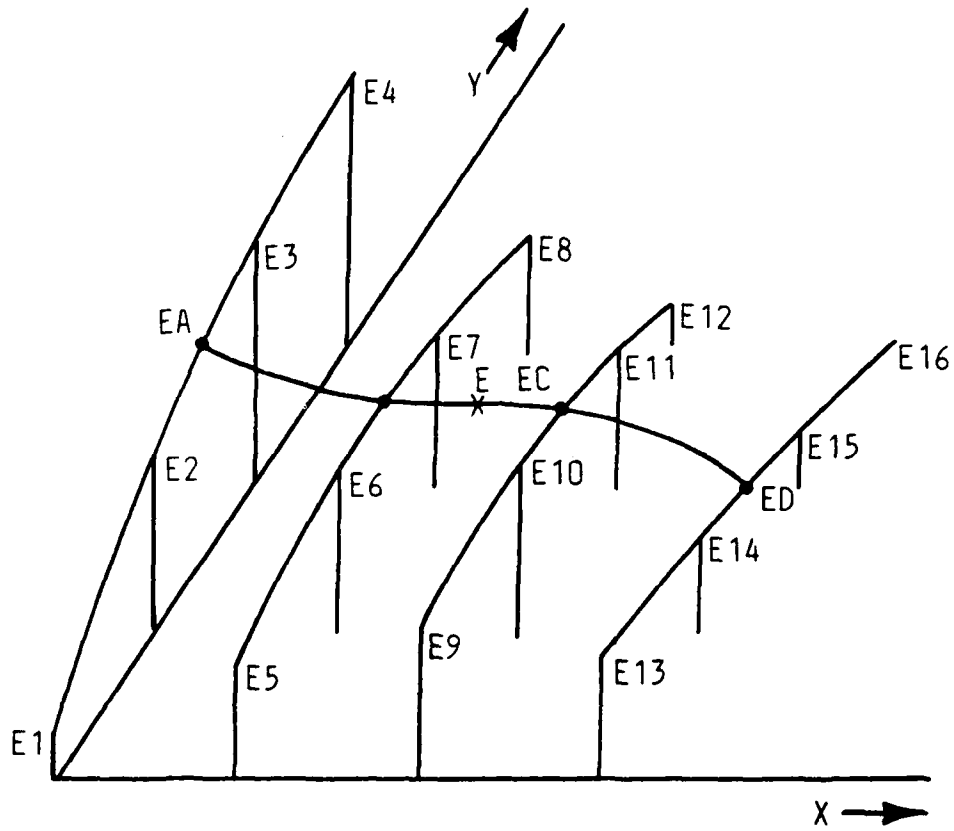
$$EA = 0.5 \ [(-E1+3E2-3E3+E4)y3]$$
$$+0.5 \ [(2E1-5E2+4E3-E4)y^2]$$
$$+0.5 \ [(E3-E1) \ y \ ]+E2$$
$$EB = f[E5,E6,E7,E8]y$$
$$EC = f[E9,E10,E11,E12]y$$
$$ED = f[E13,E14,E15,E16]y$$
$$E = f[EA,EB;EC,ED]X$$

Figure 6.1-2   PARABOLIC INTERPOLATION ALGORITHM

0.0742
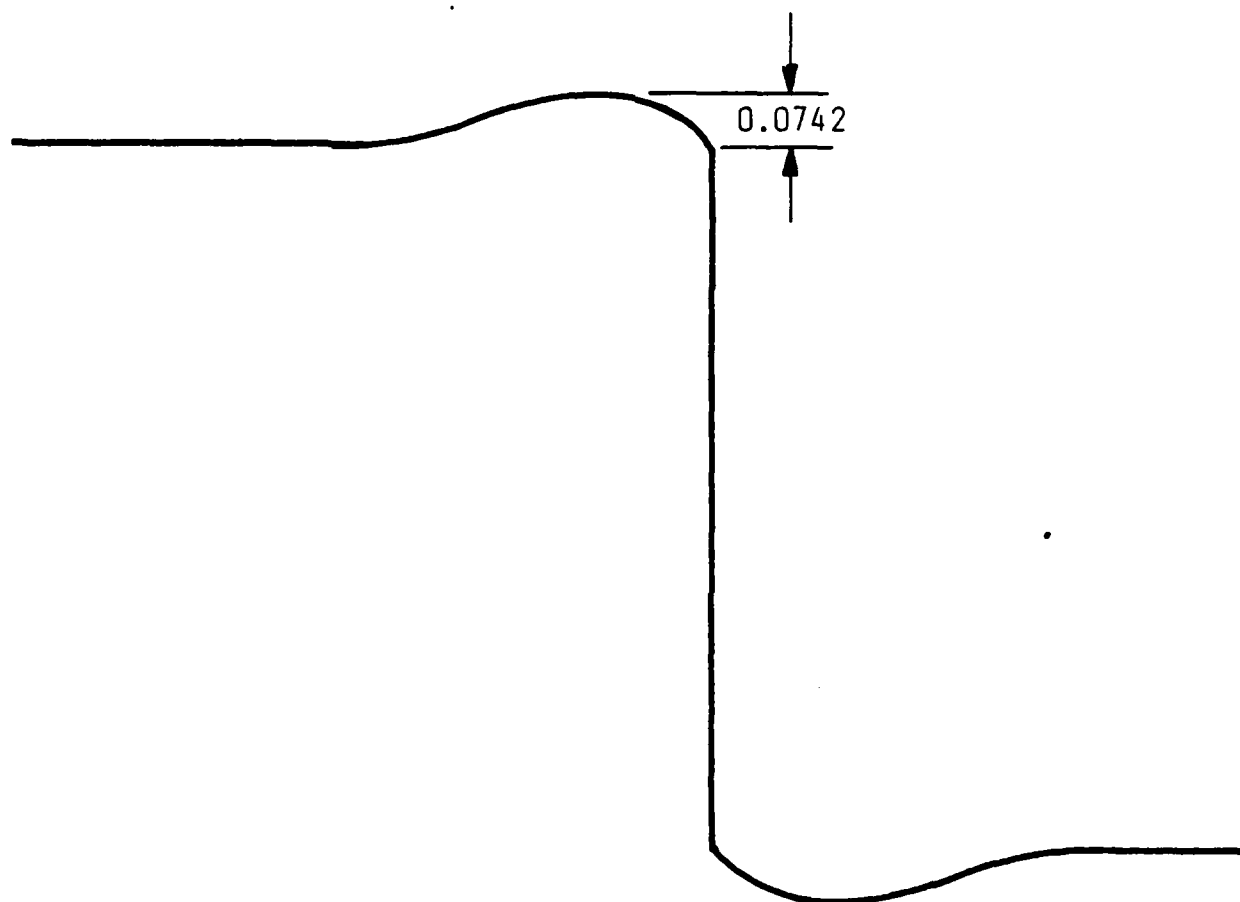
Figure 6.1-3 STEP RESPONSE FOR 1-0 WEIGHTED PARABOLIC INTERPOLATION

High resolution SAR has finer shadow details than can be obtained by just
interpolating the DLMS data base. Figures 6.1-4 and 6.1-5 show how much
shadow detail there is in low grazing angle high resolution SAR. There is a
simple solution to make the elevation data base more detailed with little loss
of accuracy at the data posts. Only at the data posts is the elevation known
and this data has a tolerance assigned to it. By putting in a roughness
algorithm that modifies the elevation from the two-dimensional weighted
parabolic interpolation algorithm, the fine variations in the elevation data
can be obtained with little loss in accuracy. Figure 6.1-6 is a block diagram
of how a roughness algorithm can be implemented. A random delta X generator
and a random delta Y generator are the starting points for this algorithm;
magnitude and time of change are both random. Each delta is put into an
integrator and the outputs are summed. The sum is subject to an out-of-limits
check. If the sum is out of limits, the sum is truncated to the limit. The
output of the limiter is now summed with the elevation. This algorithm can be
made coherent with the terrain location.

At this time the DLMS elevation data base does not provide for a roughness
coefficient in terrain. A clue to roughness can be obtained from the
elevation data base. The amount of elevation modification is a function of
the terrain. For example, take three locations and assign a roughness index.
The first location considered is wheat fields of Kansas. In this case the
roughness index will be zero, hence the elevation will not be modified. The
second location considered is foothills of the Coast Range Mountains of
California. This location should be assigned a medium roughness index. The
last example is Bad Lands of South Dakota. The roughness index for this
location should be a high index. Although the elevation that is generated by
the roughness algorithm is not an exact reproduction of the actual terrain,
the added realism gained by using the roughness algorithm more than makes up
for any loss of accuracy in elevation at the posts. Figure 6.1-7 is an
example of the roughness algorithm.

BRIDGE DETECTION AND CLASSIFICATION

The high resolution radar map in the upper left is a 60 foot resolution map of the San Luis Reservoir, located southwest of the San Francisco area on Highway 152. At this resolution, detection of the Highway 152 bridge is possible as it is seen in the center of the radar map. To the left is an 8.5 foot resolution map of the same bridge. At this resolution, two parallel bridges, approximately 500 feet in length, are easily recognized, in addition to the support structures appearing as evenly spaced bright returns on the bridges. At this resolution, the bridge can be classified as a multi-lane highway bridge. In addition, a hydro-electric power plant, hidden by radar shadows in the 60 foot resolution map, is clearly visible in the lower left corner of the 8.5 foot resolution map.

4.7 nmi Patch Map (60 ft Resolution)

0.67 nmi Patch Map (8.5 ft Resolution)

HAIWEE RESERVOIR

The Haiwee Reservoir, located south of Owens Lake is part of the Los Angeles Aqueduct. A series of high resolution maps of varying resolutions is shown. In the 3.3 nmi map on the left the entire reservoir can be seen, in addition to an industrial complex to the north and a row of power line towers to the west. In the 17 foot and 8.5 foot resolution maps below, Interstate 395 and other roads, which were not apparent in the 42 foot resolution map, become recognizable.

0.67 nmi Patch Map (8.5 ft Resolution)
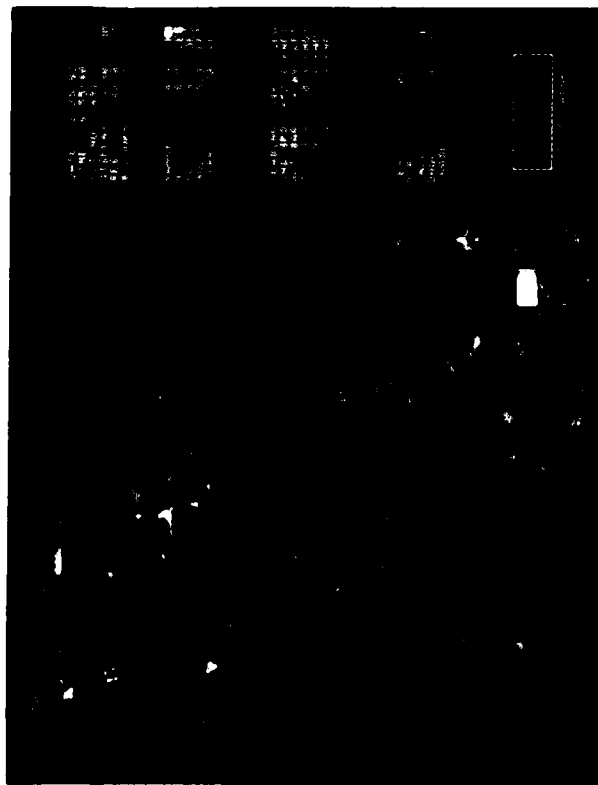
3.3 nmi Patch Map (42 ft Resolution)
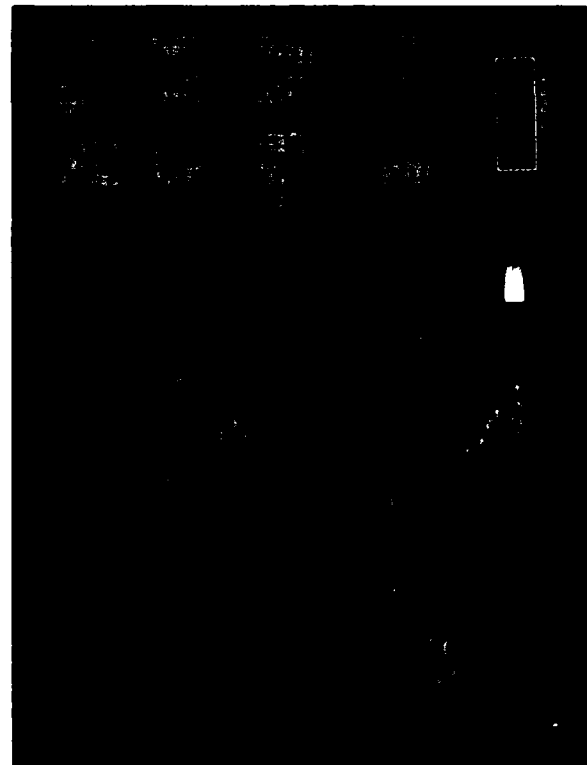
1.3 nmi Patch Map (17 ft Resolution)

Figure 6.1-6   ROUGHNESS ALGORITHM DIAGRAM

```
△X    1   1   1   1   1   0   0   0  -2  -2  -1  -1
 X    1   2   3   4   5   5   5   5   3   1   0  -1
△Y    2   2   0   0  -1  -1  -1  -2  -2   0   0   1
 Y    2   4   4   4   3   2   1  -1  -3  -3  -3  -2
SUM   3   6   7   8   8   7   6   4   0  -2  -3  -3
```

Figure 6.1-7   EXAMPLE OF ROUGHNESS ALGORITHM

6.2 PLANIMETRIC DATA BASE

The best algorithms for radar simulation will not give a good simulated radar display unless these algorithms have a realistic planimetric data base for computation. For this reason, the planimetric data base is the heart of radar simulation.

In 1972 the Defense Mapping Agency (DMA) was directed to produce a digital data base for radar simulation. In this same time frame, Link built a digital radar simulator for the U.S. Air Force. This simulator (the 1183) used the DMA data base directly. In 1974 DMA published the production specification (DLMS) for digital data base generation of radar data. The 1183 simulator and the data base generated by DMA were tested and evaluated by the Air Force, DMA, and Link. The DLMS specification was revised in July of 1977 and again in June of 1983. In 1978 the Air Force requested DMA to generate a data base to support visual, infrared (IR), and radar. This request resulted in publication of a product specification for a prototype data base to support high resolution sensor simulation in December of 1979. The B-1B SAR requirements have been responsible for generation of a product specification to support high resolution Level X data bases for synthetic aperture radar, effective in June of 1983. DMA has developed two areas of Level X data bases for evaluation and is currently working on a third. At this time, DMA has generated a modified Level I test data base for evaluation of SAR simulation. The specification title is: DMA Product Specification Supporting Prototype Level X for STRC, January 1984, Stock No. Spec X HRD/B1B. The DMA high resolution effort is being conducted for the Air Force in support of the B-1B radar simulator.

A comparison of Level I, Level II, and Level X data bases is given to indicate the degree of data base support for SAR simulation. Minimum limits for coding are listed:

CATEGORY: ROADS

	Length	Width	Height
Level I	300m	Any	Any
Level II	300m	Any	Any
Level X	10m	Any	Any

CATEGORY: BRIDGES

	Length	Width	Height
Level I	30m	Any	Any
Level II	30m	Any	Any
Level X	10m	Any	Any

CATEGORY: ISOLATED STRUCTURES

	Length	Width	Height
Level I	30m	Any	3m
Level II	10m	Any	3m
Level X	10m	Any	-

There is not a great difference between Level I and Level II. Level X, however, is of much greater resolution than Level I or Level II. At this time, the Defense Mapping Agency and the Air Force are trying to resolve the requirements for SAR. The amount of Level X data will be limited because of the high cost of generation. Where there is a lack of Level X data, Level I or Level II data will have to suffice. Only with Level X data will a SAR simulated image be ground truth. DMA will be the source for all production data, but a short turnaround for a test or quick update and small areas of data bases can be generated on-site. The problem of enhancing Level I data to give a realistic SAR image is a large one. These realistic images will not be ground truth.

A short explanation of some terms used in radar simulation is included prior to discussion of ways to enhance the data base. The first two radar simulation terms to be discussed are reflectance and signature. In the past, only a reflectance was calculated and the signature was ignored. An example is given:

EXAMPLE: LEVEL I CODE

Feature analysis	N/A
Feature type (aerial)	2
Predominant height (24 feet)	4
Feature identification code (houses)	420
Surface material category code (composition)	4
Number of structures per square kilometer (680-825)	5
Percent tree cover (20%)	2
Percent root cover (20%)	2
An outline of the area	-

Present simulators generate a reflectance code based on the surface material category. DMA has provided all the information necessary to generate a realistic signature of a residential neighborhood with trees and streets. The signature would be realistic but it would not be ground truth. This realistic signature could be generated by at least four methods. The first method expands the DMA data base off line. The second method expands the data base on line. The third method uses an interim buffer and interlocking overlays to generate the signatures with hardware. The residential neighborhood signature has four reflectance levels. These levels are ground, trees, roottops, and roads. A RAR simulator makes use of one level of reflectance coding for medium and long ranges. But at short ranges, RAR simulators lack realism due to the lack of signatures. For SAR simulation a good signature is required. Every feature identification number has its own signature that consists of more than one reflectance level.

The predominant height and individual height have been used interchangeably in the past. To get good SAR simulation, the predominant height must be broken up in a random way as a function of the feature identification number. A residential tract would have very little modification of predominant height, but an area of commercial buildings would have large variations in predominant height. Much work needs to be done in the expansion of DMA feature codes.

6.2.1 China Lake Air Base Data Base Generation

The generation of a high resolution data base for China Lake Air Base was straightforward. The first task was to generate a computer program that would allow input of data through a console into a file that matched the Link 32-bit word, Level I format. The next task was to obtain all information that was available on the China Lake Air Base region. The following information was obtained from the U.S. Geological Survey in Menlo Park, California.

1) Ridgecrest North, California: map scale 1/24000
2) Ridgecrest North, California: orthophotograph
3) Ridgecrest aerial photograph

The area around the airport was enlarged photographically by a factor of four. The enlargement scale factor is 1/6000.

This means that one inch on the enlargement is equal to 500 feet. The program contained a scale factor adjustment that was accurate to one part in 1/100000, but it was not required as the enlargement error was less than one part in 10000. A gridded vellum was placed on the enlarged photograph. The lower left corner of the vellum was referenced to the DMA manuscript that covers the China Lake Air Base. The major task was to identify the targets on the map and code them according to the DMA Level I product specification. The output of the file that was manually coded was plotted out and the errors were identified and corrected. The DMA manuscript was searched and the features that conflicted with the manually generated data base were deleted. The last step was to merge the manually generated data base with the DMA data base. Figure 6.2.1-1 is an F-15 SAR picture of the China Lake Air Base.

China Lake – 42 ft Resolution Map

Invokern   17 ft Resolution Map

Aerial Photograph of China Lake
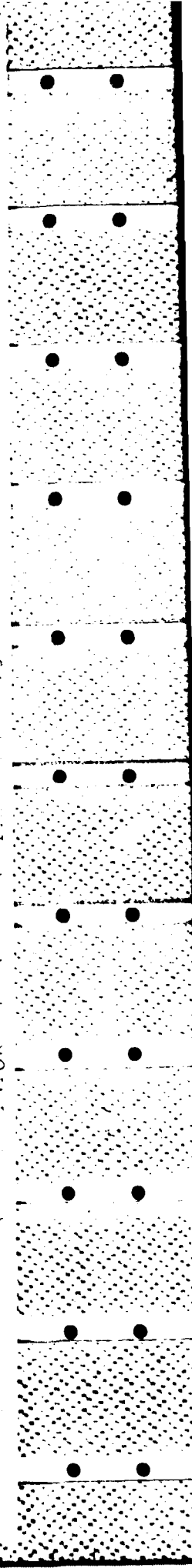
6.3 COMMENTS ON SAR PHOTOGRAPHS

6.3.1 Comments on Hard/Soft Target Switch

Reference: Figure 3.8.4

These two photographs are a good example of what happens when SAR saturates. The azimuth is smeared across one-third of the width of the picture. The smearing stops abruptly which would indicate that the total picture consists of three processed SAR pictures that were merged together. The azimuth resolution is determined by SAR processing and the range resolution is determined by pulse compression. These two processes do not show the saturation characteristics. Pulse compression saturation shows a slight amount of smear around the target and definite side lobes. A good guess would put the number of pixels in the range direction at 320. The saturation target is in the middle of the picture. In the Hughes Reports, the pulse compression ratio has been referred to as 169. Half of 320 is 160; hence it would be expected that the range saturation would extend across the picture. The saturation does extend the full range length of the picture.

6.3.2 Comments on Low Squint Angle

Reference: Figure 4.1.1

The three SAR pictures in this figure illustrate that a modern SAR can map within eight degrees of the velocity vector to 50 degrees from the velocity vector.

6.3.3 Comments On Moving Ground Target (Mudd's Landing)

Reference: Figures 5.1.2 and 5.1.3

This radar photograph is of two trains. One train is stationary and the other is moving. The stationary train has a very strong return with a radar shadow directly behind it. The second train is moving and leaves a shadow at the same place it would be if it were stationary, except that the shadow is longer

and tapered due to movement along the track. Note the return extends out of the picture while the shadow is within the picture. Uneven movement breaks up the return and the return is stretched out and dimmed where the train is going around a curve. All of the above mentioned features can be simulated, but the simulation can be complex.

6.3.4 Comments On 0.67 Nmi Patch Map Of Busch Stadium

Reference: Figures 5.3.2 and 5.3.3

These two figures are a challenge to the data base designer. The stadium light towers seem to show and the press box is a good radar reflector. There is a great deal of difference in reflectivity among the buildings. The arch, if it did reflect any energy, is not recognizable. Note the Stouffer Hotel consists of a number of bright reflectors and they map in several range buckets. There seem to be several pixel displacements in the Stouffer Hotel due to layover.

6.3.5 Comments On Daggett Marine Corps Supply Center Solar One Power Plane

Reference: Figures 5.3.4 and 5.3.5

These two SAR photographs illustrate how large buildings become complex targets at high resolution. A close look shows the roofs to be gabled roofs with a monitor. These roofs can be corner reflectors. There also seems to be a large number of roof vents that are strong reflectors. In the 17-foot resolution SAR picture, the long building that faces the aircraft is such a strong reflector that it is saturating the SAR. In fact, quite a number of targets are saturating the SAR. There seems to be a chain link fence around the base that is a strong reflector.

6.3.6 Comments On Radar Map Quality

Reference: Figure 5.4.1

These two photographs show what effect the multilook algorithm has on picture quality. The photographs are composed of six subpictures. A multilook of one gives a scalloping effect (venetian blind effect) due to the antenna footprint. When two pictures are combined and the footprints are staggered, the scalloping is eliminated. This is a multilook of two; multilooks greater than two have been generated. The simulation world differs from the real world in that you start with a good quality picture and put the scalloping in.

6.3.7 Comments On PVU Correction Of Antenna Shading

Reference: Figures 5.7.1 and 5.7.2

This radar picture is an excellent example of velocity error in SAR. The simulation of the phenomenon of SAR should be a requirement as it will train the pilot to update the altitude that is used in SAR processing, as well as checking on the inertial platform. The velocity error has been covered in SAR theory.

6.3.8 Comments On Bridge Detection and Classification

Reference: Figure 6.1.4

The San Luis Reservoir SAR photographs are very good for SAR simulation evaluation. The potential targets in these photographs include two dams, a highway bridge, a pumping station, two transmission lines, and a switching yard. The elevation in the top photograph goes from less than 180 feet to over 1100 feet. In the top photograph the O'Neill Dam is in the top of the photograph, and the San Luis Dam is about three-eighths of the way up in the photograph. The top dark area is the O'Neill Forebay. The bright spots running across the forebay are piers that contain transmission lines. The white dots running across the picture are transmission line towers. The highway bridge is just a dot at the bottom of the forebay. Note the water inlet extending out from the San Luis Dam.

The bottom photograph has seven times the resolution, half the range and twice the depression angle of the top picture. The details of the highway bridge are apparent, and the pumping station with its switching yard are now out of the shadow of the San Luis Dam. The pumping station is on the lower left and the switching yards are to the right of the pumping station. The transmission line towers are not as apparent as in the top photograph. SAR returns are also showing up from the bottom of the reservoir. The two photographs seem to be processed in a different manner by the SAR.

6.3.9 Comments On Haiwee Reservoir

Reference: Figure 6.1.5

These three SAR photographs are of the northern half of the North Haiwee Reservoir. They are good examples of SAR gain setting and moving targets. The 42-foot resolution picture has very good dynamic range. Interstate 395 and power line towers run north and south at the left of the picture, with the highway to the west of the power line towers. Interstate 395 is a very faint line, but the motor vehicles and buildings are its signatures. The shadows and water are quite dark.

The 17-foot resolution picture has a high gain setting and the shadows have quite a bit of noise. The bottom of the reservoir shows up quite well and the face of the dam gives a very strong radar return. The power line towers are almost completely eclipsed by the high gain setting. In the lower left corner Interstate 395 can be seen with the motor vehicles displaced from the highway. The faces of the hills give very strong returns.

The 8.5 foot resolution picture has a lower gain setting, but the bottom reservoir is still visible. The face of the dam can still be recognized with the reduced return and shadow. The road leading to the base of the dam is now visible. The base of the dam at the right seems to have some man-made building. There are other bright returns that can only be explained by an on-site inspection.

6.3.10 Comments On Airfield Recognition

Reference: Figure 6.2.1

Airports are of special interest to the military. These SAR pictures show two airports. The China Lake Airport is modeled in the Link-generated data base. The other airport is the Inyokern Airport. Both airports are in an isolated desert area; hence they are very prominent. Both pictures show saturation.

7.0 EMULATIONS OF SAR IMAGES

To verify that today's state of the art in electronics is adequate to build its SAR simulator, Link emulated the design in the Link Emulation Laboratory. The emulation consisted of a FORTRAN program that performed the same function in non-real time as the SAR simulator would in real time. The generation of each image required typically 20 to 40 minutes.

Two different types of data bases were used. The first one was DMA level I, for the area of China Lake NAS, California. This area was chosen because Link has actual SAR inquiry of the area.

In addition to the Level I data, three areas covered by Level X were also used to generate SAR images. These areas were: Scott AFB, Lambert Field, St. Louis Missouri, and Chester, Illinois.

As anticipated, DMA Level I data is clearly inadequate for realistic SAR simulation. To produce realistic SAR images, the DMA data base had to be enhanced by adding buildings, taxiways, and other features as explained; i.e., Section 6.2.1.

In this section the emulated SAR images will be shown with and without certain effects. They clearly demonstrate that synthetic signature generation, the addition of noise and various other effects, is necessary for realistic simulation.

The first six images are at 42 foot resolution, the same as the photograph made by the F-15 radar for the same area, as shown in Figure 6.2-1. The emulated images were made at the same estimated aircraft position, depression angle and other parameters as the real photograph. A short explanation of each image follows.

Figure 7.0-1 was produced from DMA Level 1 data by using present radar landmass simulation techniques; i.e., without synthetic signature generation, noise, overload, etc. Only the computational accuracy was increased to correspond to a five foot least significant bit. A diagonal line in the upper
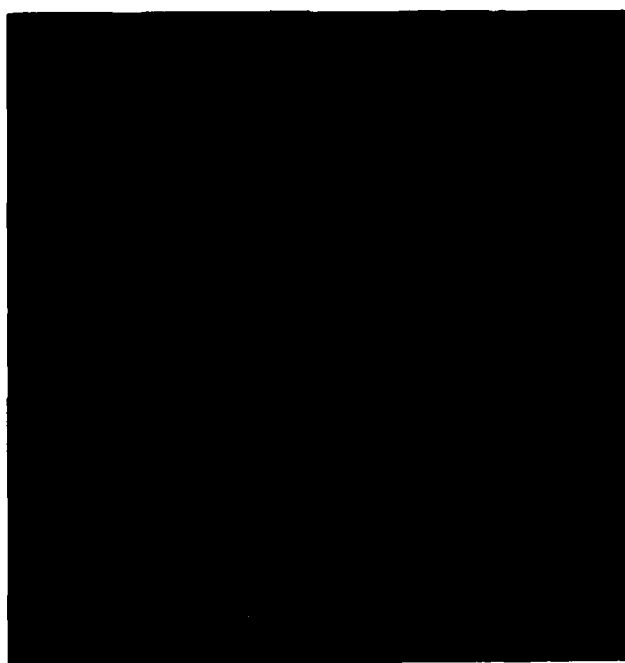
Figure 7.0-1   EMULATED SAR IMAGE AT 42-FOOT RESOLUTION

right hand corner is apparent as well as some line structure in the lower right hand corner. Both are due to problems in the DMA elevation data base. The dark line is due to an "embankment" being created by the elevation data base. Such problems are generally not noticeable with *real beam radars* because of the lower resolution. The single large feature above the runway is, in fact, a collection of buildings. At SAR resolution, the individual building would be distinguishable, but the Level I data base does not provide such detailed information.

Figure 7.0-2 is the same image but synthetic signature generation (a hardware subsystem in the simulator) has been added to break up the ground return and the return from the buildings.

Figure 7.0-3 is the same area but the data base has been manually enhanced on the basis of other data as explained in Section 6.2.1. Figure 7.0-3 has no synthetic signature generation, while Figure 7.0-4 uses synthetic signature generation.

Figure 7.0-5 again uses the unenhanced data base but with synthetic signature generation, glitter and the "ventetian blind effect," caused by a fall-off in the antenna gain towards the edges of the swath. (A venetian blind effect may also be caused by velocity error or footprint error as explained in the report.) Figure 7.0-5 is an enhanced data base version of Figure 7.0-6.

The next tour images, Figures 7.0-7 through 7.0-10 are at a resolution of 20 feet and all use the enhanced data base. Figure 7.0-7 has only synthetic signature generation. Figure 7.0-8 has receiver noise added. Figure 7.0-9 contains the effect of filter broadening due to a strong return. This effect occurs in both the azimuth and range directions. In Figure 7.0-10 noise/glitter has been added, while Figure 7.0-11 has filter broadening and analog-to-digital overload.

The remaining tour images, 7.0-12 through 7.0-15 have a 10 foot resolution. The enhanced data base has 12 F/A-18 aircraft lined up in a row, parked

Figure 7.0-2   SAME AS FIGURE 7.0-1 BUT WITH SYNTHETIC SIGNATURE GENERATION

Figure 7.0-3 SAR IMAGE OF MANUALLY ENHANCED VERSION OF FIGURE 7.0-1

Figure 7.0-4   SAME AS FIGURE 7.0-3 BUT WITH SYNTHETIC SIGNATURE
GENERATION ADDED

Figure 7.0-5 SAME AS FIGURE 7.0-1 WITH VARIOUS SAR EFFECTS
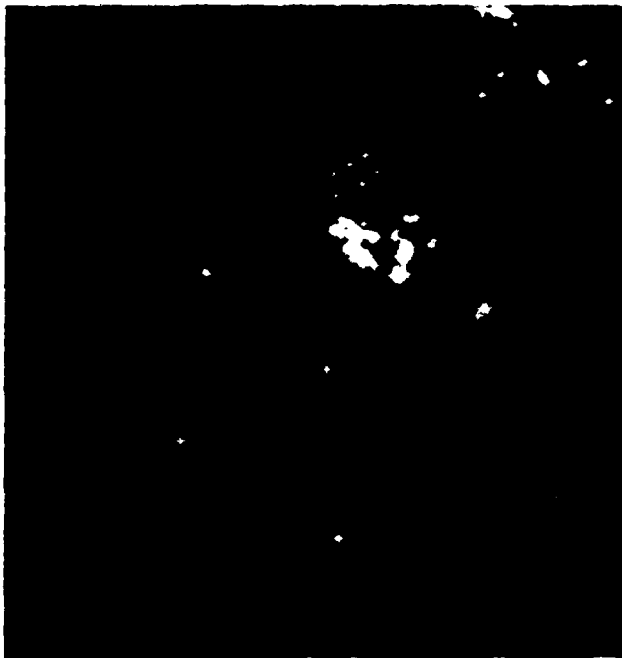
Figure 7.0-6   ENHANCED DATA BASE VERSION OF FIGURE 7.0-5

Figure 7.0-7 MANUALLY ENHANCED SAR IMAGE AT 20-FOOT RESOLUTION
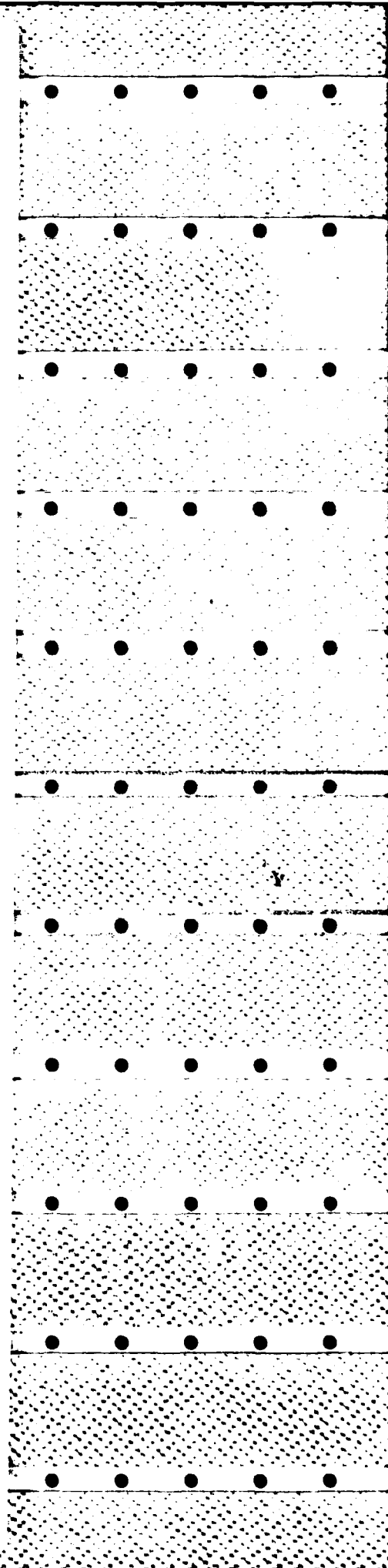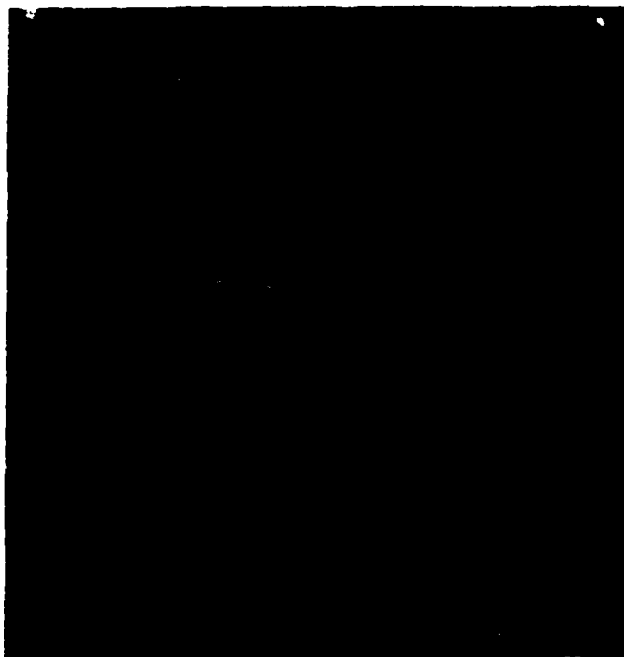
Figure 7.0-8 SAME AS FIGURE 7.0-7 WITH NOISE ADDED

Figure 7.0-9   SAR IMAGE WITH FILTER BROADENING EFFECT
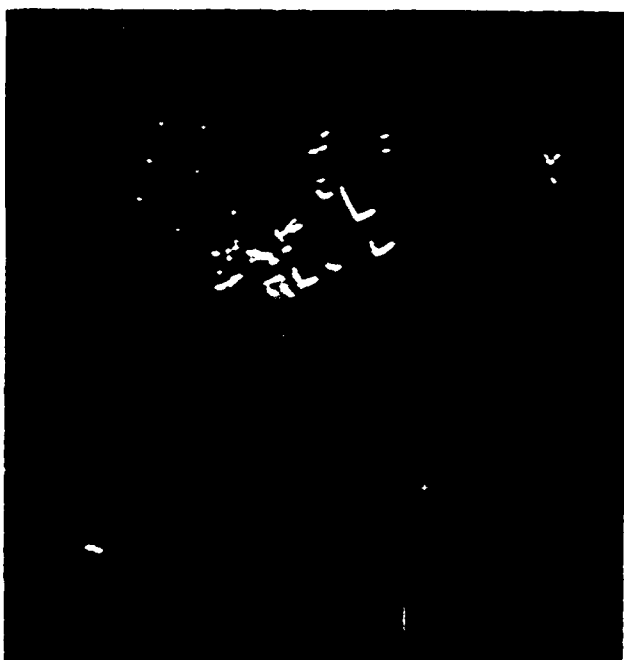
Figure 7.0-10   SAR IMAGE WITH RECEIVER NOISE AND GLITTER
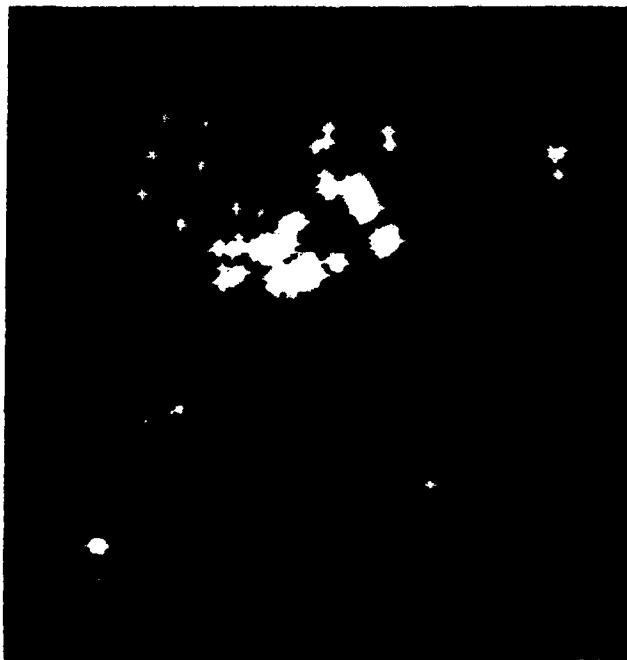
Figure 7.0-11 SAR IMAGE WITH ADDITIONAL SAR EFFECTS

Figure 7.0-12 SAR IMAGE AT 10-FOOT RESOLUTION

Figure 7.0-13 SAR IMAGE WITH NOISE
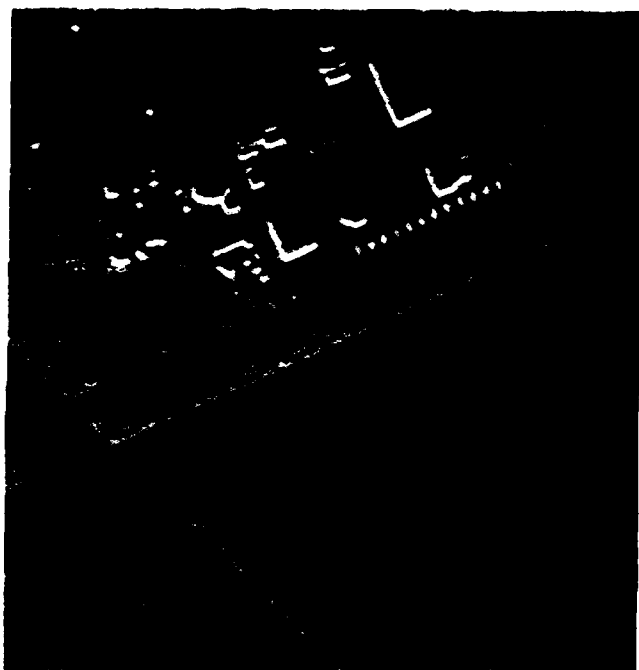
Figure 7.0-14   SAR IMAGE WITH FILTER BROADENING
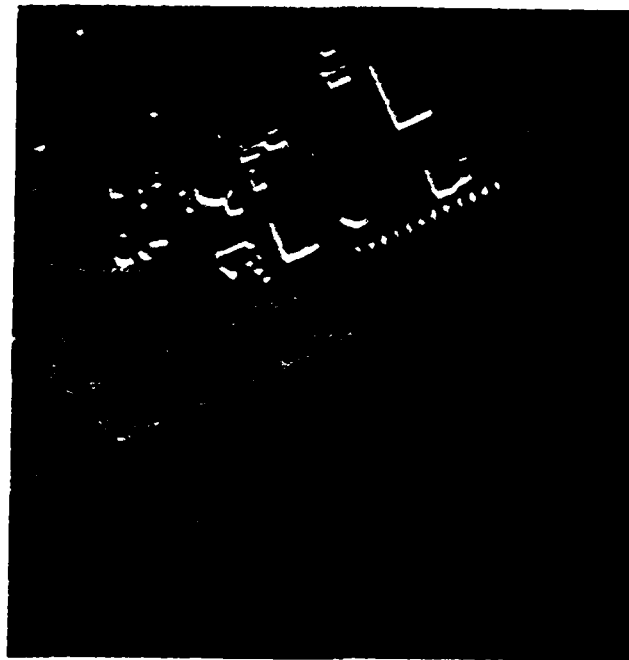
Figure 7.0-15 SAR IMAGE WITH ALL EFFECTS EXCEPT ANALOG TO DIGITAL
CONVERTER OVERLOAD

parallel to a runway (Figure 7.0-12). All images have synthetic signature generation. Figure 7.0-13 has noise added, Figure 7.0-14 has tiller broadening, while Figure 7.0-15 incorporates the effects of synthetic signature generation, filter broadening, and noise/glitter.

The next four images (7.0-16 through 7.0-19), were generated from DMA Level X data. The first of these, Figure 7.0-16 is a false color map of Scott AFB. The different colors correspond to different surface material . The shades are not representive of the reflectance values magnitude. Figure 7.0-17 shows a radar image of a portion of Scott AFB at a resolution of 10 ft.

Figure 7.0-18 is the SAR image of Lambert Field at a resolution of 20 ft., while Figure 7.0-19 shows a bridge near Chester, Illinois.
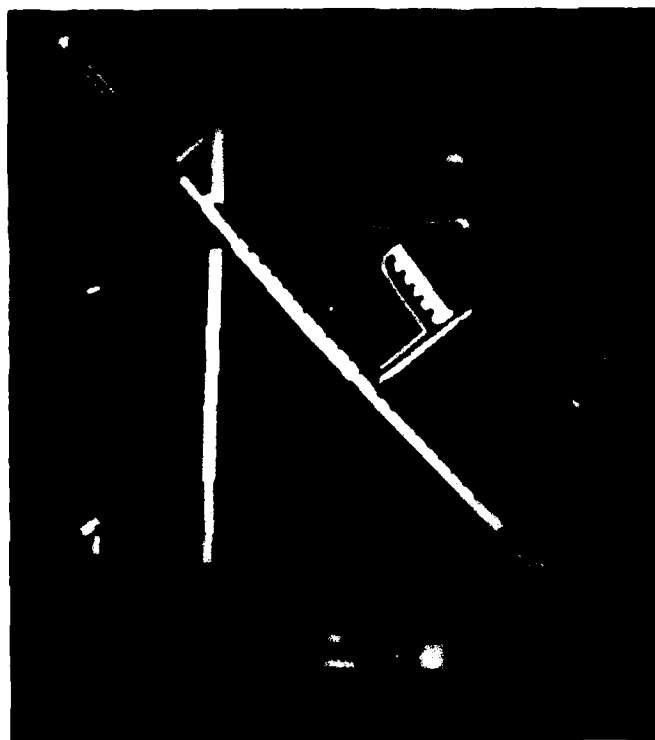
Figure 7.0-16 FALSE COLOR OF SCOTT AFB
(LEVEL X DATA BASE)

Figure 7.0-17   SAR IMAGE OF SCOTT AFB
(LEVEL X DATA BASE, 10-FOOT
RESOLUTION)
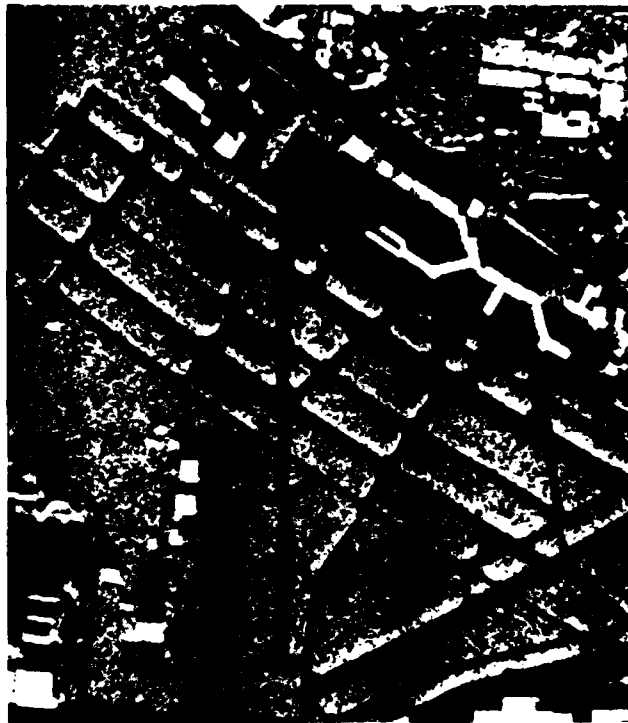
Figure 7.0-19 SAR IMAGE OF A BRIDGE, CHESTER,
ILLINOIS (LEVEL X DATA BASE)

8.0 CONCLUSIONS AND RECOMMENDATIONS

On the basis of this SAR Simulation Study and other extensive research on the subject, Link has reached the following conclusions and recommendations.

1) Currently existing digital landmass simulators are inadequate for effective simulation of synthetic aperture radar. SAR simulation requires higher accuracy (at least a five foot pixel and complex SAR signature generation, neither of which are available in present systems. However, the present state of the art in digital technology is adequate for building a SAR simulator.

2) Because all new radar systems will be controlled by powerful general purpose computers and because mode selection will be accomplished through these computers via programming, it is very likely that over the lifetime of the radar system a great number of significant operational changes will take place. In order to be cost-effective, the simulator will need to have a similar kind of organization; that is, to primarily be a programmable device rather than a hard-wired one. Only system operations that are part of radar physics and remain invariant, should be hard wired in the simulator.

3) The greatest problem in synthetic aperture radar simulation is due to inadequacies of data bases. In order to realistically simulate an area to ground truth accuracy, a Level X data base must exist. Because of the very high cost of mapping an area at Level X detail, it is extremely unlikely that large areas will be available at this level of detail.

    In order to achieve high fidelity simulation, Link recommends four approaches to alleviate the data base problem:

    a. When Level X detail is available in the vicinity of navigation checkpoints and target areas, this level should be used.

8-1

b. If Level X detail is not available and it is vitally important to have actual ground truth, manual enhancement of the data base should be used, as demonstrated by the photographs of the China Lake area (refer to Figures 7.0-1 through 7.0-15). If ground truth is not of great importance, Level I, II, or V data should be used, combined with synthetic signature generation that portrays radar signature of typical features.

c. Even with SAR signature generation, it would be obvious where the boundary of a high resolution area is from the roads, streams, and other features which terminate at the boundary. To make this boundary indiscernible, Link proposes that the data base outside the Level X area be augmented by artificial data. This artificial data would extend roads, streams, and selected features from the Level X area by using a random data base generation process similar to the one currently employed by Link in visual programs. The statistical characteristics of the artificial data would correspond to statistical data derived from the actual area.

d. The much higher resolution of SAR has shown anomalies in the Defense Mapping Agency terrain elevation data base. These anomalies may be due to problems in the algorithms used in the conversion of contour map data to grid elevation posts, or merely due to the fact that the elevation data has a least significant bit of one meter. This causes quantization effects which result in "embankments" or the appearance of terracing effects. A solution must be found either by the Defense Mapping Agency or by the simulation manufacturer to eliminate these spurious effects.

On the basis of studying radar photographs, Link concludes that a number of special effects and malfunctions should be simulated for realistic simulation of synthetic aperture radar. The following items should be included:

(1)   Azimuth and Range Direction Layover - Layover in both azimuth
        and range direction should be simulated. (Range direction
        layover applies equally to a real beam radar simulation.)

(2)   Moving Object Displacement - Moving objects on the ground are
        displaced in the azimuth direction due to the basic assumption
        in synthetic aperture radar that all ground objects are
        stationary. Simulation should include displacement of the
        object and the correct placement of the shadow.

(3)   Velocity Errors - Velocity errors must be simulated because the
        pilot should be trained in recognizing such errors and taking
        corrective action by recalibrating the inertial navigation
        system. A small velocity error would result in feature
        displacement in the azimuth direction. Large velocity errors
        can completely shift the ground map outside the area to be
        viewed. If this happens, the beam width of the radar may be
        insufficient to illuminate the desired area. This is called
        footprint error.

(4)   Incorrect Elevation - Simulation of incorrect assumed elevation
        is needed because the radar assumes that all objects on the
        ground are in a plane and the distance between the plane and
        the aircraft is known. Should these assumptions be untrue, the
        map will be distorted by effects similar to velocity errors.

(5)   Motion Compensation or Acceleration - Error due the flexing of
        the aircraft or the aircraft not flying in a straight line
        implies that the velocity at the inertial navigation system may
        not be identical to the velocity at the radar antenna.
        Depending on the particular radar, various methods may be used
        to correct this disparity. The failure of this correction
        should be simulated.

(6)   Antenna Side Lobe Effect - The antenna side lobe effect may produce an unwanted input with synthetic aperture radar. Features within this side lobe will be superimposed on the regular image. Also, in the range direction, the Barker code will produce an effect similar to that of the antenna side lobes. Typically, a strong signal will recur in the range direction at fixed intervals from the actual location of the return. The pilot should be trained to recognize the appearance of these effects.

(7)   Filter Broadening - Strong returns have a tendency to saturate the digital filter and certain features may appear to be larger than their actual size. Similarly, filter saturation may result in the repetition of a strong signal in the range direction.

(8)   Analog-to-Digital Overload - An overload in the analog-to-digital converter will produce harmonics. These harmonics manifest themselves as spurious returns on an image. The simulation of analog-to-digital overload should be implemented whenever such an overload can occur.

(9)   Glitter - The well known glitter of synthetic aperture radar can be caused by the coherent properties of the transmission and by objects on the ground (such as buildings) that act as corner reflectors. Glitter should be simulated to maintain high fidelity simulation so that pilots would not be trained on an idealized image. An idealized image (i.e., no glitter) could give the pilot a false impression of the correct appearance of the image and effect transfer of training.

(10) Multilook - With most synthetic aperture radar systems, several ground map returns are averaged under the control of the pilot to reduce glitter and noise. Unless the display equipment is actual aircraft hardware, the simulator must perform this multilook averaging function.

(11) Weather Simulation - Depending on the wavelength of the radar, clouds or moisture will generate strong returns and also cause absorption. Absorption will cause a loss of signal strength and a shadow in the area behind the cloud. Weather simulation may be necessary depending on the wavelength of the radar. Moving clouds should be displaced in a manner similar to moving objects on the ground.

The above list of effects are those that should be simulated for most synthetic aperture radars. Depending on the particular radar or the mission of the aircraft, all of these effects may not be required for effective training. Since SAR simulation is a new technology and consequently the requirements for a SAR simulator are full of uncertainties, Link recommends that the government procure a research SAR simulator.

The purpose of this simulator would be to develop methods for advanced senior simulation and to fully explore the specifications of new simulators. A secondary purpose of this research simulator would be to aid in the development of air-to-ground tactics.

APPENDIX A

REFERENCES

APPENDIX A

REFERENCES

Bracewell, Ron, The Fourier Transform and Its Applications, McGraw-Hill, 1965

Brigham, E. Oran, The Fast Fourier Transform, Prentice-Hall, 1974

Goodman, Joseph W., Introduction to Fourier Optics, McGraw-Hill, 1968

Hovanessian, S.A., Introduction to Synthetic Array and Imaging Radars, Artech House, 1980

Hovanessian, S.A., Radar Detection and Tracking Systems, Artech House, 1982

Hovanessian, S.A., Synthetic Array and Imaging Radars, Hughes, 1982

Kovaly, John J., Synthetic Aperture Radar, Artech, 1976

Long, Maurice W., Radar Reflectivity of Land and Sea, Lexington Books, D.C. Heath and Co., 1975

Mensa, Dean L., High Resolution Radar Imaging, Artech House, 1981

Nathanson, Fred E , Radar Design Principles, McGraw-Hill, 1969

O'Neill, Edward L., Introduction to Statistical Optics, Addison-Wesley, 1963

Radar School Staff, Massachusetts Institute of Technology, Second Edition, McGraw-Hill, 1946

Rihaczek, August W., Principles of High-Resolution Radar, McGraw-Hill, 1969

Skolnik, Merrill I., Introduction to Radar Systems, McGraw-Hill, 1962

Skolnik, Merrill I., (Editor in Chief), Radar Handbook, McGraw-Hill, 1970

Swiger, J.M., Principles of Synthetic Array Radar, Hughes Aircraft, 1978

Tylka, John, Jr., Evolving Technology Seminars, 1981

Weaver, H. Joseph, Applications of Discrete and Continuous Fourier Analysis, John Wiley and Sons, 1983

REFERENCES FROM PERIODICALS

AUSHERMAN, DALE A., "Digital Versus Optical Techniques in Synthetic Aperture Radar (SAR) Data Processing", Optical Engineering, March/April 1980, Vol. 19, No. 2

AVILA, PAUL G., Eric R. Keydel, Jerol E. Kronenfeld and Robert W. Pinto, "Real-Time SAR Simulation Analysis, Phase I, Volume I: Technical Analysis", April 1983, Prepared for Aeronautical Systems Division, Deputy for Simulators, Wright-Patterson AFB, Ohio

BEASLEY, A.R., "Synthetic Aperture Radar Signal Processing for Airborne Applications", Marconi Review, Vol. 45, No. 225, 2nd. Qtr., 1982

BOOTH, WILLIAM C., "Approaches to Radar Signal Processing", IEEE Transactions on Computers, June 1983

BUNKER, DR. W. MARVIN, "Training Effectiveness Versus Simulation Realism", 11th NTEC/Industry Conference Proceedings, 1978

CHEN, CHUNG-CHING and Harry C. Andrews, "Multifrequency Imaging of Radar Turntable Data", IEEE Transactions on Aerospace and Electronics Systems, Vol. AES-16, No. 1, January 1980

CUTRONA, LOUIS J., "Studies Directed Toward the Achievement of Wide Swathwidths in Synthetic Aperture Radar", University of California, San Diego, Applied Physics and Information Science Department, February 23, 1979

ELLIS, A.B.E., "The Processing of Synthetic Aperture Radar Signals", The Radio and Electronic Engineer, Vol. 53, No. 3, March 1983

FAINTICH, MARSHALL B., "Digital Sensor Simulation", 1980-1985 Proceedings of the 13th Annual Simulation Symposium, 1980

FAINTICH, MARSHALL B., "Digital Sensor Simulation at the Defense Mapping Agency Aerospace Center", St. Louis Air Force Station, MO., Proceedings of the National Aerospace and Electronics Conference (NAECON), Dayton, May 15-17, 1979

JACKSON, PHILIP L., "Radar Focused Doppler Spectra (RFD): A Transformation of SAR Signal Film for Radar Scattering Analysis", Environmental Research Institute of Michigan, Ann Arbor, Michigan

KIRK, JOHN C. JR., "A Discussion of Digital Processing in Synthetic Aperture Radar", IEEE Transactions on Aerospace and Electronic Systems, Vol. AES-11, No. 3, May 1975

MERSEREAU, RUSSELL M. and Alan V. Oppenheim, "Digital Reconstruction of Multidimensional Signals from Their Projections", Proceedings of the IEEE, Vol. 62, No. 10, October 1974

MUNSON, D.C. JR. and W.K. Jenkins, "A Common Framework for Spotlight Mode Synthetic Aperture Radar and Computer-Aided Tomography", Asilomar Conference on Circuits, Systems and Computers, 15th, 1981

MUNSON, DAVID C. JR., James Dennis O'Brien, and W. Kenneth Jenkins, "A Tomographic Formulation of Spotlight-Mode Synthetic Aperture Radar", Proceedings of the IEEE, Vol. 71, No. 8, August 1983

PORCELLO, LEONARD J., Normal G. Massey, Richard B. Innes and James M. Marks, "Speckle Reduction in Synthetic-Aperture Radars, J. Optical Society of America, Vol. 66, No. 11, November 1976

ROBINSON, ROGER, DMAAC Project Officer and others, "Test and Evaluation of USAF Project 1183 Digital Data Bases", The Defense Mapping Agency, Aerospace Center, February 1979

ROGERS, DAVID E. and Thomas H. Heimburger, "Synthetic Aperture Radar (SAR) Coordinate Processing System", SPIE Vol. 278 Electro-Optical Instrumentation for Resources Evaluation (1981)

TOMIYASU, KIYO, "Tutorial Review of Synthetic-Aperture Radar (SAR) With Applications to Imaging of the Ocean Surface", Proceedings of the IEEE, Vol. 66, No. 5, May 1978

ULABY, FAWWAZ T., "Radar Signatures of Terrain: Useful Monitors of Renewable Resources", Proceedings of the IEEE, Vol. 70, No. 12, December 1982

VAN DE LINDT, W.J., "Digital Technique for Generating Synthetic Aperture Radar Images", IBM Journal of Research and Development, Vol. 21, No. 5, September 1977

WALKER, JACK L., "Range-Doppler Imaging of Rotating Objects", IEEE Transactions on Aerospace and Electronics Systems, Vol. AES-16, No. 1, January 1980

SPECIFICATIONS

Defense Mapping Agency Product Specifications for a Prototype Data Base to Support High Resolution Sensor Simulation, First Edition December 1979, Stock No. SPECXVDB

Defense Mapping Agency Product Specifications for Digital Landmass System (DLMS) Data Base, Second Edition, April 1983, Prepared by Defense Mapping Agency, Aerospace Center, St. Louis AFS, Missouri

Defense Mapping Agency Prototype Product Specification to Support High Resolution Level X, First Edition, June 1983, Stock No. SPEC X HRD/LVX

Defense Mapping Agency Product Specification Supporting Prototype Level X for STRC, First Edition, January 1984, Stock No. SPEC X HRD/B1B, Draft

APPENDIX B

DEFINITIONS AND SYMBOLS

DEFINITION AND SYMBOLS

A Altitude

a One-half of aperture width

A_A $(R - \lambda K_P)$

A_{CC} Acceleration

A_L Aperture

A_M Amplitude

A_{RP} Altitude above the reference plane

A_{SP} Aspect

B_B Data collection distance

B_W Bandwidth

C Velocity of light

C_C Equal to range

cos   cosine

D_C Distance along flight path where data is collected

D_{FPT} Distance from point PT

E Elevation

e 2.7183

E_{Rf} Elevation above the reference plane

exp   Exponential to the base e

F Frequency

F_{DS} Doppler frequency

$f_{(Acc)}$ Acceleration function

F_R Received frequency

DEFINITION AND SYMBOLS

F_T Transmitted frequency

F_β Aperture function

G_C Gain function (due to gain control, weather, and atmospheric attenuation)

G_{RA} Receiver antenna gain

G_{TA} Transmitter antenna gain

H Height

i Imaginary constant $\sqrt{-1}$ (physics usage)

j Imaginary constant $\sqrt{-1}$ (electronic usage)

K Selectable constant

k Wave number

K_F Aperture modification factor

K_E Earth radius modification factor

K_K Selectable constant for SAR resolution

K_P Phase shift limit

K_R $\cos(\Theta_R)\cdot\cos(\phi_R)$

L_{ID} Isodoppler line

O Orientation

P Phase shift

P_{FR} Pattern factor along the receiving path

P_{FT} Pattern factor along the transmitting path

DEFINITION AND SYMBOLS

P_R	Received power
P_T	Transmitted power
R	Range for radar
R	Distance from aperture to image plane (physic usage)
R_{DB}	Data base resolution
R_{DS}	Aircraft display resolution
R_E	Earth radius
R_{EC}	Modified earth radius for atmospheric refraction
R_{FM}	Range forward mapping due to elevation
R_R	Range rate
R_{SAR}	Synthetic aperture radar resolution
R_{SL}	Slant range
$R_{SL(m)}$	Range coordinate
R_{t1}	Range at time t_1
R_{t2}	Range at time t_2
R_W	Range walk
R_1	Range at position one
R_2	Range at position two
R_{RES}	Resolution in length
R_{DG}	Delta ground in length
R_{SLT}	Slant range top of target
$\sin$	Sine
S_{AMT}	Received signal amplitude

DEFINITION AND SYMBOLS

S_E /shadow effect

S_{IP} In phase component of received signal

S_Q Quadrature component of received signal

S_R Received signal

S_{RF} Received signal in frequency

S_T Transmitted signal

$S_{(s)}$ Intensity spread function

t Time

tan Tangent

T_{CS} Target cross section

t_D Delta time

T_{REF} Target reflectance coefficient

u Dimension in the aperture

$u_{(s)}$ Complex amplitude distribution of a point

V_{AC} Aircraft velocity

V_C Closing velocity

V_{ERR} Velocity error

V_{GAC} Velocity from aircraft to ground

V_{GT} Velocity of ground target

V_P Velocity between the aircraft nadir point and a

point on the ground

DEFINITION AND SYMBOLS

V_{MP} Velocity between aircraft nadir point and a moving point on the ground

V_{TAC} Velocity between aircraft and target on ground

V_V Velocity vector

W Width

X Variable or dimension

$X_{(n)}$ Azimuth coordinate

Y Variable or dimension, reference along flight path, reference ground coordinate

$Y_{(m)}$ Point along flight path, ground coordinate

DISTRIBUTION LIST

Defense Technical Information Center
Cameron Station
Alexandria, VA 22314   12 copies

Technical Information Center
NAVTRAEQUIPCEN
Orlando, FL 32813   2 copies

Dr. Stan Collier
Office of Naval Technology
Room 504
800 North Quincy Street
Arlington, VA 22217   1 copy

Commander
Naval Air Systems Command
ATTN: Air 330J (CDR Tom Jones)
Washington DC 20361   1 copy

NAVTRAEQUIPCEN
Orlando, FL 32813   50 copies

END

FILMED

4-85

DTIC